POLYBENZIMIDAZOLES AS ION EXCHANGE MEMBRANES

by

Owen Thomas
Bachelor of Science, University of Victoria, 2007

THESIS SUBMITTED IN PARTIAL FULFILLMENT OF
THE REQUIREMENTS FOR THE DEGREE OF

MASTER OF SCIENCE

In the
Department of Chemistry

© Owen Thomas 2011

SIMON FRASER UNIVERSITY

Spring 2011

APPROVAL

Name: **Owen Thomas**

Degree: **M.Sc.**

Title of Thesis: **Polybenzimidazoles as Ion Exchange Membranes.**

Examining Committee:

Chair: **Dr. Erika Plettner**
Associate Professor, Department of Chemistry

Dr. Steven Holdcroft
Senior Supervisor
Professor, Department of Chemistry

Dr. Andrew J. Bennet
Supervisor
Professor, Department of Chemistry

Dr. Hua-Zhong (Hogan) Yu
Supervisor
Professor, Department of Chemistry

Dr. Barbara Frisken
Internal Examiner
Professor, Department of Physics

Date Defended/Approved: February 9, 2011

ABSTRACT

Two sets of soluble, benzimidazole-based polymers have been synthesized. One series containing sulfonic acid groups (sulfonated polybenzimidazole (SuPBI)) utilizes the basic character of polybenzimidazole to form acid-base cross-links that improve the mechanical integrity of proton conducting polymers. The other series shows how the benzimidazole segments in the polymer can be quaternized to produce a polymer (poly(1,3-dimethylbenzimidazolium) (PDMBI$^+$)) capable of transporting anions.

SuPBI membranes resist extensive swelling in water but have poor proton conductivity. When blended with high IEC sulfonated poly(ether ether ketone) (SPEEK), a polymer that has high proton conductivity but poor mechanical integrity, ionic cross-links form and reduce the extent of swelling. The effect of sulfonation of PBI on cross-linking in these blends was gauged through comparison with non-sulfonated analogues. Sulfonic acid groups present in SuPBI were expected to compensate for acid groups involved in cross-linking, thereby increasing IEC and proton conductivity of the membrane. When water uptake and proton conductivity were compared to the IEC of blends containing either sulfonated or non-sulfonated PBI, no noticeable distinction between PBI types could be made. Comparisons were also made between these blends and pure SPEEK membranes of similar IEC. Blend membranes exhibit slightly lower maximum proton conductivity than pure SPEEK membranes but had significantly

enhanced dimensional stability upon immersion in water, especially at elevated temperature. Elevated temperature measurements in humid environments show increased proton conductivity of the SuPBI membranes when compared to SPEEK-only membranes of similar IEC likely due to the increased stability of the blend.

In the second part of this thesis, PDMBI$^+$ membranes were synthesized and their ability to transport anions (I$^-$, Br$^-$, Cl$^-$, NO$_3^-$, HCO$_3^-$, and OH$^-$) was studied. The counter ions in the membrane were exchanged and the polymers produced, in large part, were very resistant to swelling while still having high IEC ($\geq$ 3 meq/g). Attempts to form hydroxide-containing membranes were unsuccessful due to a side reaction, which causes degradation of the polymer chain. Attempts to understand and minimize this problem are also discussed in this work.

DEDICATION

To everyone who has helped me along the way.

To Elena, my family, my friends and past teachers.

This one's for you, you've earned it.

ACKNOWLEDGEMENTS

TABLE OF CONTENTS

LIST OF FIGURES

x

LIST OF TABLES

GLOSSARY

AAEMFC   Alkali anion exchange membrane

ABS   Available basic sites

AEC   Anion exchange chromatography

AEM   Anion exchange membrane

DS   Degree of sulfonation

DMAc   N,N-Dimethylacetamide

DMSO   Dimethylsulfoxide

DVS   Dynamic vapour sorption

EAS   Electrophillic aromatic substitution

F   Faraday's constant (96485 $C \cdot mol^{-1}$)

FRA   Frequency response analyzer

FTIR   Fourier transform infrared

GPC   Gel permeation chromatography

HPLC   High performance liquid chromatography

IEC   Ion exchange capacity

IEM   Ion exchange membrane

IEMFC   Ion exchange membrane fuel cell

μ'_{H+} Effective proton mobility

μ'_{X-} Effective anion mobility

NMP   N-Methylpyrrolidone

NMR   Nuclear magnetic resonance

PBI	Poly(benzimidazole)
PDIPBI$^+$	Poly(diisopropylbenzimidazolium)
PDMBI$^+$	Poly(dimethylbenzimidazolium)
PEEK	Poly(ether ether ketone)
PEM	Proton exchange membrane
PEMFC	Proton exchange membrane fuel cell
PPA	Poly(phosphoric acid)
ppm	Parts per million
PTFE	Poly(tetrafluoroethylene)
RH	Relative humidity
SHE	Standard hydrogen electrode
σ'_{H+}	Proton conductivity
[-SO$_3$H]	Sulfonic acid group concentration
SPEEK	Sulfonated poly(ether ether ketone)
SuPBI	Sulfonated poly(benzimidazole)
σ'_{X-}	Anion conductivity
TBS	Total basic sites per gram
VU	Water uptake by volume
WU	Water uptake by mass
[X$^-$]	Anion concentration
X_v	Water volume fraction

1: INTRODUCTION

1.1 Hydrogen Fuel Cells

Fuel cells are devices used to convert chemical energy of fuels into electrical energy. These devices date back to their invention in 1839 by William Grove.[1,2] The device he created reacted hydrogen and oxygen electrochemically to form water while producing an electrical current. In this sense, the device he created operated as a galvanic cell, where a current flows due to the difference in electrochemical potentials of two different half-cells. Fuel cells, however, differ from conventional galvanic cells in that they can produce a continuous current without the need for recharging, as long as a supply of fuel is available.[3] The same principles apply today, which have made fuel cells an attractive alternative for the internal combustion engine in vehicles[4-7] and stationary power generation.[7]

The benefits of fuel cells that operate on hydrogen gas (H_2) is that they only produce water and heat as by-products. This technology is thought to be a source of clean energy, in that no carbon dioxide or harmful pollutants are emitted.[5] In addition, the lack of moving parts inside a fuel cell means that they should function quietly and require very little maintenance, allowing for uninterrupted power generation over extended periods.[3] These advantages were considered by NASA when they chose fuel cells for onboard power generation as far back as the Gemini and Apollo missions.[8-10]

All fuel cells consist of three main components: an anode, a cathode, and an electrolyte. The oxidant (O_2 or Air) is reduced at the cathode and the fuel (H_2) is oxidized at the anode. Ions move through the electrolyte and a current is produced in an external circuit that is used to power a device.

Currently, fuel cells are too expensive to be widely used and the hydrogen delivery infrastructure is insufficient to make them convenient.[11] However, the concern over the dwindling supplies of fossil fuels and greenhouse gas emissions have created a need for the development of clean, renewable energy sources.[12,13] In order for fuel cells to be a viable alternative, they must be able to generate power at a lower cost.[11,13,14] The main costs associated with current fuel cells come from three areas: the expensive catalysts, which are often precious metals, the polymer membranes used as electrolyte, and the cost of the fuel itself. Efforts to reduce the amount of precious metal catalyst needed, use of less expensive polymer electrolytes and improved overall efficiency are seen as pathways to lowering the cost of fuel cells.[11,14,15]

The following chapters will discuss two types of hydrogen fuel cells and detail experiments and systems based on new polymer electrolytes in the hope that the increased understanding of these systems can lead to future increases in fuel cell efficiency.

1.2 Ion exchange membrane fuel cells

Most fuel cells studied today use ion-conductive polymers as electrolytes. Ion exchange membrane fuel cells (IEMFCs) come in two main types: alkaline anion exchange membrane fuel cells (AAEMFCs) and proton exchange membrane fuel cells (PEMFCs). The distinction between these fuel cell types is the charge carrier transported between the electrodes. Hydroxide ions (OH^-) are transported in the AAEMFC system, whereas protons (H^+) are transported in the PEMFC.

These devices are made up of a polymer electrolyte (ionomer) membrane sandwiched between two electrodes (Figure 1a).[9,16] The electrodes consist of a layer of finely divided platinum particles supported on carbon held together with a ion conducting ionomer (Figure 1b).[9] These layers play an important role in fuel cell operation as they are responsible for adsorbing gases, conducting electrons and providing or removing ions. This requires contact to be kept between the catalyst sites and the ionomer, gas channels and the electrically conductive carbon electrode.[9] Any catalyst particles that do not have contact with any of these phases will not contribute to the fuel cell reactions. Investigations into reducing the amount of platinum found at the non-active sites could result in a reduction in the platinum needed without affecting fuel cell performance.[15,17] In addition, there is a push for alternative catalyst materials (i.e., non-precious metals), which could also lower costs.[9]

The next part of the introduction will focus on PEMFCs; a discussion on AAEMFCs will be left to Chapter 3.
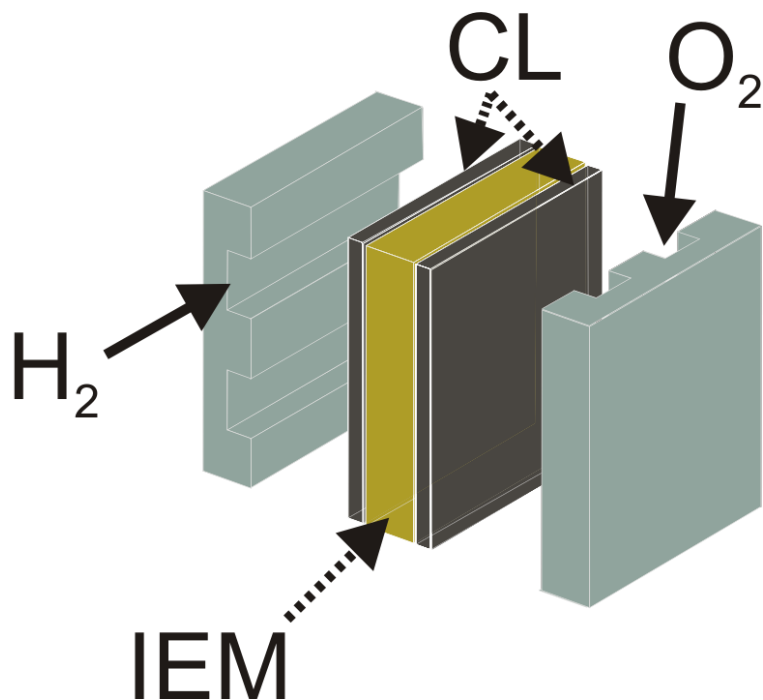
Figure 1: **Expanded diagram of an IEMFC showing the ion exchange membrane (IEM) the catalyst layers (CL) and reactant and product inlet and outlets.**

1.3 Proton Exchange Membrane Fuel Cells (PEMFC)

PEMFCs are one of the most studied fuel cell formats. These devices, like other hydrogen fuel cells, harness the current produced from the oxidation of hydrogen to produce water. The reaction (shown below) is spontaneous and produces a voltage of 1.299 V.[9,16,18,19]

Anode	$2H_2 \rightarrow 4H^+ + 4e^-$	$E^0 = 0$ V
Cathode	$4H^+ + O_2 + 4e^- \rightarrow 2H_2O$	$E^0 = 1.229$ V
Overall	$2H_2 + O_2 \rightarrow 2H_2O$	$E^0 = 1.229$ V
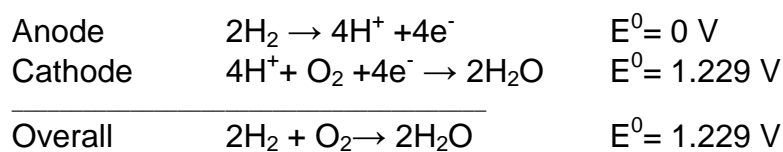
At the anodic side of the fuel cell, a flow of H_2 comes in contact with the catalyst layer. At this interface, the hydrogen is converted into protons (H^+) and

electrons (e⁻). The electrons move from the anode to the cathode via an external circuit, meanwhile the protons travel to the cathode through the proton exchange membrane (PEM). The oxygen then reacts with protons and electrons at the cathode to form water. Kinetically, the reaction at the cathode is much slower[20-23] and as a result, platinum loading of the catalyst layer for the cathode must be much higher than for the anode.[9]

At the centre of the fuel cell is the PEM, a polymer membrane that facilitates the movement of protons between the anode and cathode (Figure 2). The concentration gradient formed by the production of protons at the anode and their consumption at the cathode is the driving force for the movement of cations toward the cathode in these systems. Increased understanding of PEMs and how they function can lead to improvements in fuel cell performance in the future.
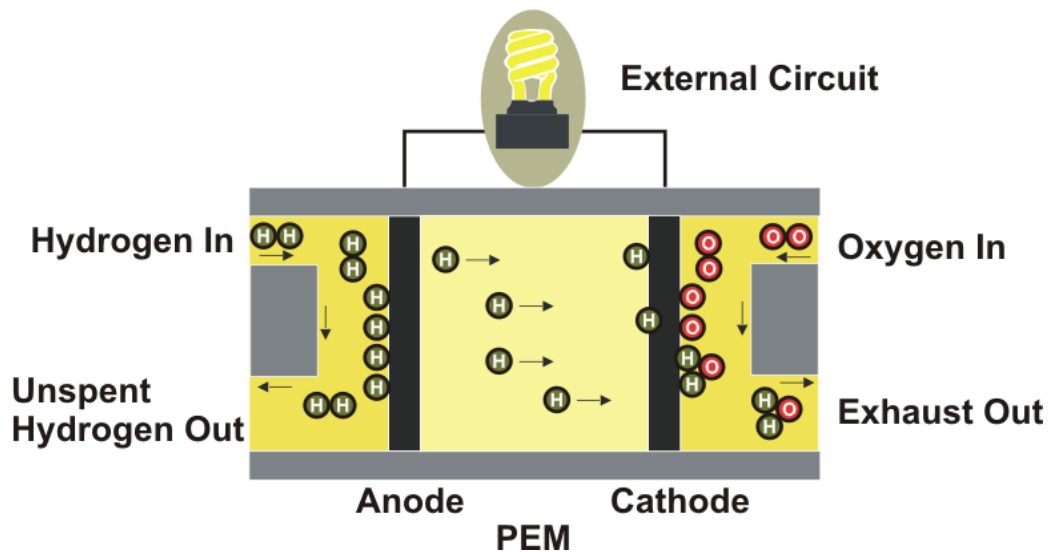
Figure 2:   **Diagram illustrating the function of a PEMFC.**

1.4 Proton Exchange Membranes

PEMs are usually made from polymers containing sulfonic acid groups. The differences in polarity between the sulfonic acid groups and the non-polar backbone result in the formation of segregated domains within the polymer. In the dry state, these domains are often isolated from each other and thus incapable of proton transport through the membrane. However, when the membrane is hydrated, the polar domains swell and begin to connect.[24-26] At this point, called the percolation threshold, interconnected ionic channels begin to form within the polymer (Figure 3).[24,25] It is through this network that proton transport is possible.
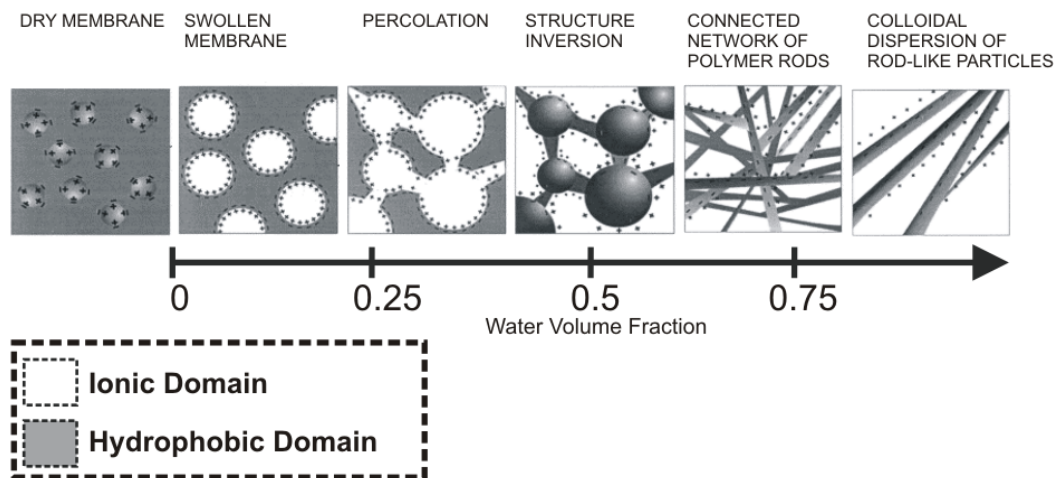
Figure 3:   **Diagram illustrating the interconection of segregated domains as water content increases in Nafion®, a commonly used PEM. [24]**

(Reprinted from Polymer, Vol 40 / 15, Gebel, G., Structural Evolution of water swollen perfluorosulfonated ionomers from dry membrane to solution, 5829-5838, Copyright (2000), with permission from Elsevier)

The mechanism for proton transport through the water channels is dependent on the amount of water present (Figure 4).[25] At low hydration levels,

proton transport is limited and whatever movement of protons there is happens through a surface mediated mechanism, where the protons move from acid group to acid group (Figure 4a). At slightly higher hydration levels, the protons, now likely part of a hydrated ion (e.g., H_3O^+, $H_5O_2^+$, $H_9O_4^+$), can move on their own through the channels (Figure 4b). This vehicular mechanism is possible as the hydration increases but its relative contribution becomes less due to a third, more effective method.[25] When the ratio of water molecules to acidic protons is high, water molecules aid in the transport of protons through a Grotthus-type mechanism.[25,27] In this, the rotation of water molecules (and hydrated ions) and reordering of O-H bonds can result in the movement of charge through the system (Figure 4c).[25,28] This mechanism is very effective at moving protons through water and is the cause of the high conductivity found for protons in bulk water.[28]
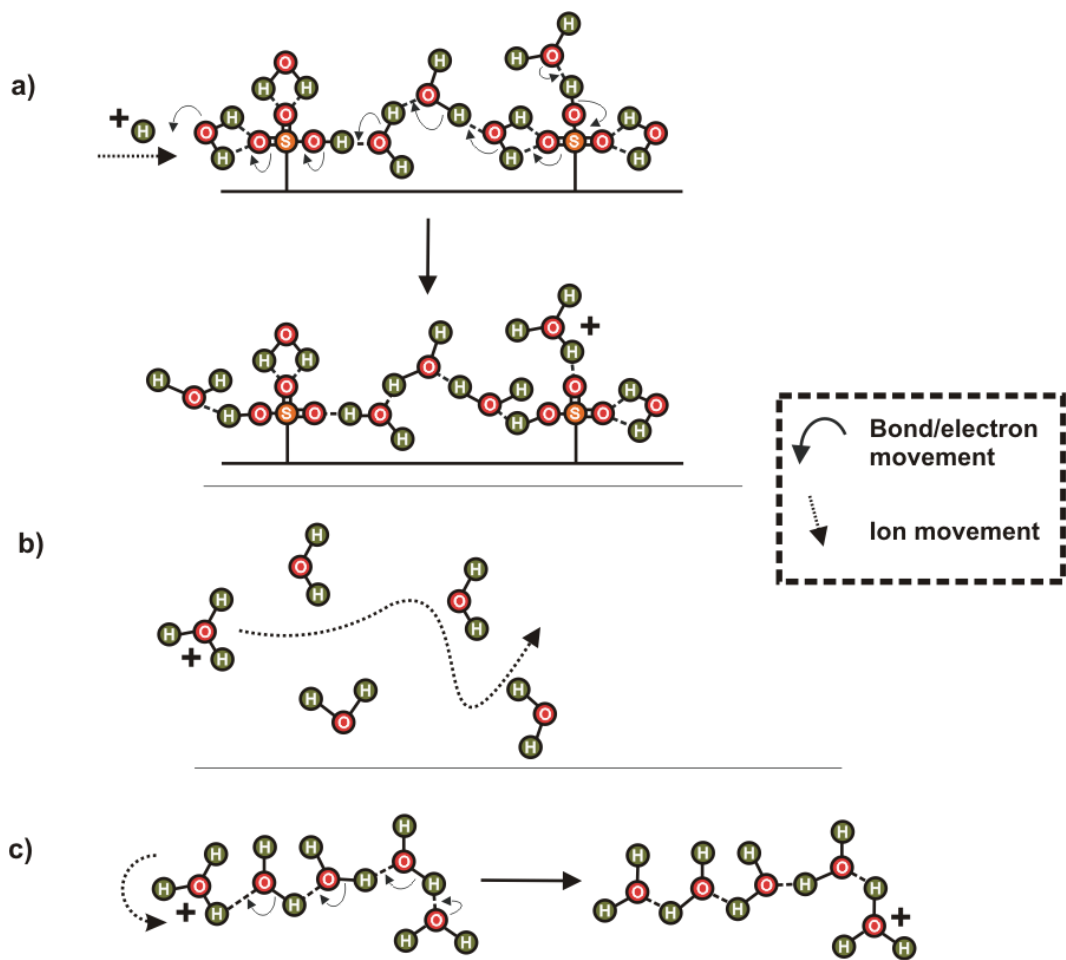
Figure 4: Illustrations showing mechanisms for proton transport through water. a) Surface-mediated mechanism. b) Vehicular mechanism. c) Simplified Grotthus-type mechanism.

There are certain attributes associated with a polymer that would make it suitable for use as a PEM.[18,29] Firstly, the polymer needs to have acidic sites to transport the protons. Next it needs to form connected hydrophilic domains when hydrated while still being mechanically stable (it cannot absorb too much water as that would cause the membrane to swell excessively). Thirdly, the membrane needs to be chemically stable in order to survive the harsh conditions found inside a fuel cell (both strongly oxidizing and strongly reducing).[30]

Besides transporting protons from the anode to the cathode, the PEM also serves to separate the two chambers of the fuel cell so that there is no mixing of the reactant gases. This mixing of gases, called gas crossover, lowers the efficiency of the system by diluting the reactant gases on either side of the membrane.[31] As well, the PEMs need to be electrically insulating, which prevents short-circuiting between the anode and cathode. This short-circuiting would reduce the current available to power an external device.

Over the past 50 years, many materials have been developed for use as PEMs. Over this time, none has been as successful as Nafion®, created in the late 1960's at DuPont.

1.4.1 Nafion®

Nafion®, originally developed for the chlor-alkali industry, has become the most widely used PEM material.[19,32] Nafion® is a perfluorinated polymer consisting of an alkane backbone with ether side-chains terminated with a sulfonic acid group (Figure 5).[33] The reason that Nafion® is so successful has to do with its high proton conductivity and high resistance to the harsh conditions inside a fuel cell.
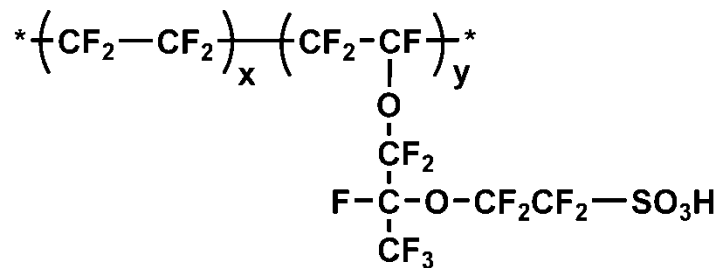
Figure 5: **Structure of Nafion®.**

The C-F bonds in the Nafion® backbone are resistant to cleaving, and as such, make for a robust membrane that is able to withstand the harsh conditions inside a fuel cell. As well, this high degree of fluorination in the polymer renders it strongly hydrophobic, which along with the hydrophilic pendant sulfonic acid groups, allows distinct hydrophobic and hydrophilic domains to form; a morphology that is beneficial to proton transport. In addition, the highly hydrophobic backbone allows Nafion® to resist swelling in the moist conditions in a fuel cell. Mechanical stability is important inside a fuel cell where excessive swelling is detrimental.

Nafion®, however, does have some drawbacks. Due to its high number of C-F bonds, the polymer is expensive to prepare and process.[34] It has limited solubility in most solvents, which makes fabricating the membranes a challenge. This lack of solubility also poses an additional problem for recovery of the platinum from the catalyst layer when the membrane reaches the end of its functioning life. Compounding this is the difficulty in recovering the platinum through burning. Burning of Nafion® results in the production of hydrogen fluoride (HF), which can attack the platinum and human exposure to the fumes has been linked to flu-like conditions.[35]

Another drawback arises from the dependence of water channels for proton transport in Nafion®. As a result, these membranes often perform poorly in conditions where there is little liquid water available (i.e., at low relative humidity or temperatures near or above 100 °C). This is an important limitation as studies

suggest higher fuel cell efficiencies are possible as temperatures increase due to improved O_2 reduction kinetics.[9] In addition, fuel cells operating at temperatures above 120 ^{o}C are less susceptible to carbon monoxide poisoning, which can occupy catalyst sites.[36] Because of these drawbacks, an opportunity for Nafion$^®$ alternatives has arisen for membranes that offer solutions for these challenges.[18,19,37-40]

1.4.2 Hydrocarbon membranes

Hydrocarbon membranes offer solutions to many of the problems found with Nafion$^®$. They are free of fluorine so they can be burned without creating HF gas. In addition, particularly with polyvinyl- or polystyrene-based polymers, they are soluble in commonly-available solvents. These both allow for easier recovery of the catalyst, through either burning or dissolution of the polymer. Another advantage of hydrocarbon membranes is that, since they do not have a multitude of C-F bonds, they can be produced easily and inexpensively.

The first PEMFCs manufactured and used on the Gemini space missions used hydrocarbon membranes based on sulfonated polystyrene.[8] These membranes, however, were found to degrade badly over time and as a result were replaced by another technology on subsequent missions. Membrane degradation is a common problem for hydrocarbon polymers in fuel cells. The degradation is often a result of radical species attacking the polymer chain, which in turn can cause chain cleavage.[30] Continual degradation of the polymer chain results in the lowering of the polymers molecular weight, leading to lower mechanical stability and portions of the polymer chain becoming soluble and

11

washing away. Hydrocarbon polymers containing vinyl or styrene-based chains are particularly susceptible due to a cleavage reaction whereby an OH· attacks the polymer forming a radical on the polymer chain.[41] This radical can cause the polymer to undergo chain scission (Figure 6) in a process opposite to polymerization.
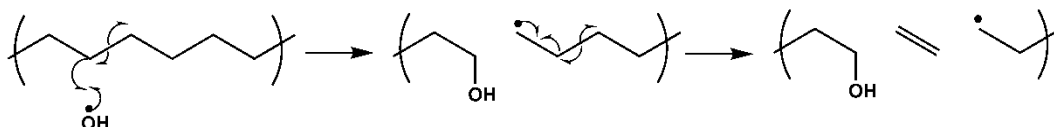
Figure 6: Mechanism for chain scission in hydrocarbon polymer (polyethylene).

Today most hydrocarbon membranes intended for PEM applications utilize so-called "high performance" polymers (e.g., aramids, polybenzimidazoles, polysulfones, etc.) (Figure 7), which are more resistant to degradation.
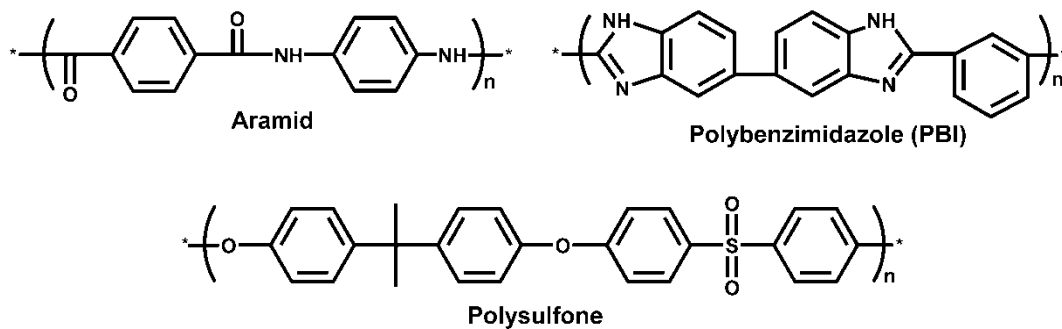
Figure 7: Chemical structure of high performance polymer backbones considered for use as PEMs.

The polymer structures shown in Figure 7 do not undergo this type of chain scission due to the lack of adjacent sp^3 carbons in which to form double bonds. However, radical degradation still occurs in these polymers, but the

12

depolymerisation chain reaction mechanisms are not available, resulting in a lower degree of degradation.

As with Nafion[®] membranes, operation of poorly hydrated hydrocarbon membranes is an ongoing challenge. Attempts to increase conductivity in low water content systems include the use of water-retention additives, or hydrophilic inorganic materials (e.g., SiO_2, $ZrPO_4$, etc.)[42,43] that hold water within the membrane even at elevated temperatures. As well, the inclusion of nitrogen heterocycles (e.g., imidazole),[16,25,44] which can transport protons in low water conditions, is being examined. Furthermore, there has been a lot of interest in polymer membranes imbibed with phosphoric acid.[16,25,45-50] These additives serve to replace water in the membranes, which allows for Grotthus-type proton movement and because of their higher boiling points are capable of higher operating temperatures.[50]

Each of the methods mentioned to improve high temperature proton conductivity includes the incorporation of an additive to the membrane. This is problematic because in a fuel cell, where H_2O is produced and liquid water can be present during warming up and cooling down, additives can be leached out, reducing the performance of the membrane.

Another strategy has been to prepare polymers with high ion exchange capacity (IEC),[25,51-54] which means that they have a high number of ionic sites per gram of polymer. In these polymers, the acid groups (usually sulfonic acid) are covalently bound to the polymer ensuring none is leached away. These high IEC polymers have a shorter distance between sulfonic acid groups, which

facilitates movement of the proton from acid group to acid group via the surface mechanism (Figure 4a).[55] This mechanism is the main method of proton transport at low water content, so by increasing its effectiveness it is thought that proton conduction at high temperature and low relative humidity (RH) should improve. However, the high numbers of sulfonic acid groups, which has benefits at low water content, can result in significant swelling when liquid water is present (Figure 8). This leads to poorer mechanical properties and, possibly, dissolution during the hydration cycles common in fuel cell operation.[51,53,56,57]
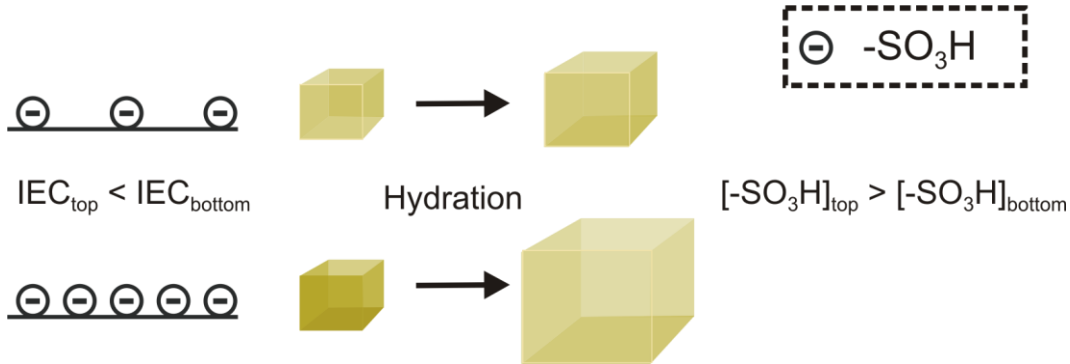
Figure 8: **Illustration showing how the swelling can increase as acid concentration increases.**

In addition to reducing mechanical stability, increased swelling can actually reduce the concentration of acid groups in the membrane. This is due to a dilution effect that arises from the increased water uptake of the membrane when the acid content is high, resulting in a drop in acid concentration (Figure 8). Proton conductivity (σ'_{H^+}) in a membrane is shown by Equation 1:

$$\sigma'_{H^+} = F[-SO_3H]\mu'_{H^+} \quad (1)$$

Where: F= Faraday's Constant

[-SO$_3$H] = Concentration of sulfonic acid groups

μ'_{H^+} = Effective proton mobility

As this shows, the σ'_{H^+} of a membrane is due, in part, to its acid concentration, which is used as an approximation of the proton concentration in the membrane.[58] The result of this is, if the acid groups are severely diluted due to high water content, the membranes ability to conduct protons will be hindered. As a result, there is an increased need for high IEC polymers that resist swelling.

1.4.3 Cross-linked membrane systems

Covalent cross-linking has been examined as a potential method to control the degree of swelling in high acid content membranes.[59-61] These systems usually involve a sulfonated polymer modified to contain potentially cross-linkable groups. After this polymer is cast, it is then treated either chemically or thermally to form a cross-linked membrane (Figure 9).[62,63] This results in a material that is resistant to swelling; however attempts to cross-link high acid content polymers have resulted in membranes that are brittle upon drying.[37] Again, this reduces the membranes ability to withstand typical fuel cell hydration-dehydration cycles. Furthermore, covalent cross-linking increases the complexity of membrane manufacture by necessitating the synthesis of monomers containing a cross-linkable functionality.[37] These factors may impede the usefulness of covalently

cross-linked membranes in fuel cell applications, especially those with high acid content.
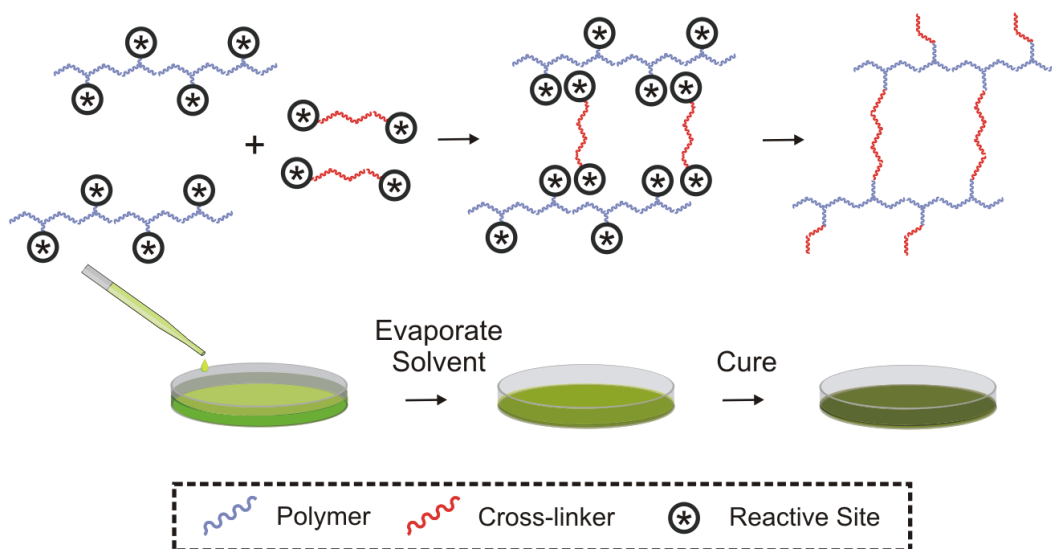
Figure 9: **Illustration of the synthesis/fabrication of covalently cross-linked PEMs.**

To circumvent this, ionic cross-linkers[37,64,65] and blends of polymeric acids and bases[66-69] are being investigated. It can be argued that ionically cross-linked polymers are also easier to prepare than covalently crosslinked PEMs as they do not require the synthesis of cross-linkable monomers[70] while still exhibiting equal or improved fuel cell performance.[71,72]

Systems utilizing basic polymers to form ionic cross-links with acidic polymers have been studied in depth.[18,66,70,73-75] Cross-links can form in these membranes through hydrogen bonding interactions between the acidic proton and basic site, interactions between positive and negative charges brought about by the protonation of the basic site and deprotonation of the acidic site, or some combination of the two (Figure 10).[18,72] Membranes made in this way have good

mechanical integrity but low proton content, which is a common drawback for these types of membranes as the basic sites used in cross-linking attracts protons that would otherwise be used in transport.[76]
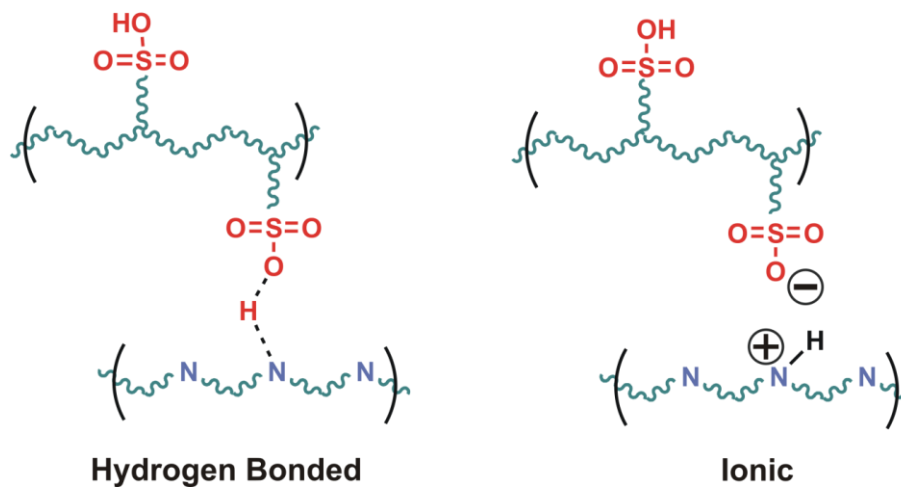
Figure 10:   Illustration showing hydrogen bonded and ionic cross-linking between acidic and basic polymers.

In an attempt to increase the proton concentration in these cross-linked systems, polymer blends have been made using acidic polymers mixed with cross-linking polymers that have both acidic and basic functionalities. These amphiphilic polymers are thought to replace protons that are used in cross-linking and thereby increase the IEC of the blend, which can lead to improved proton conductivity (Figure 11).
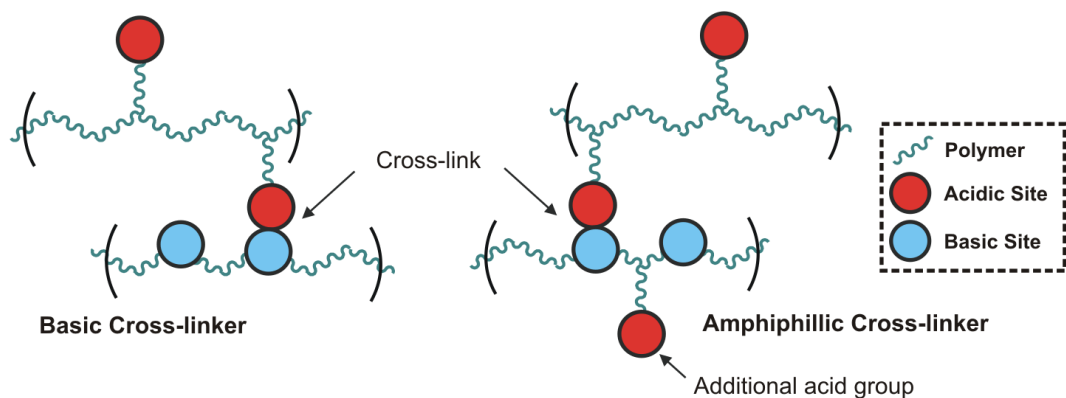
Figure 11: **Illustration of basic and amphiphilic polymers used for cross-linking.**

These systems have shown good conductivity results when using lower IEC systems (IEC = 1-1.5 meq/g),[66] but little information is available on use of these cross-linkers at IECs greater than 1.5 meq/g when the membrane is more susceptible to swelling and cross-linking is therefore desirable.

1.5 Design and Synthesis of Polymers for use as PEM

In order to design a new PEM system there are a few important factors to consider. Chemical stability is a concern and as a result most current hydrocarbon PEM polymers contain aromatic ring systems to increase chemical stability. As well, the polymer needs acidic groups in order to transport protons.

1.5.1 Polymerization

There are two fundamental methods of polymerization used to make PEMs: chain-growth and step-growth. Chain-growth polymerizations rely on the creation of radicals or ions that form bonds to unsaturated molecules while reforming the active centre. This results in the propagation of the reaction to form a long chain of many repeat units (Figure 12a). This type of polymerization is

capable of producing polymers with very high molecular weights in short periods. However, these types of polymers usually have polyethylene-type backbones, which, in hydrocarbon polymers, are prone to degradation under fuel cell conditions. Nafion® is synthesized using a chain-growth technique, but is resistant to degradation due to its lack of C-H bonds (Figure 5).
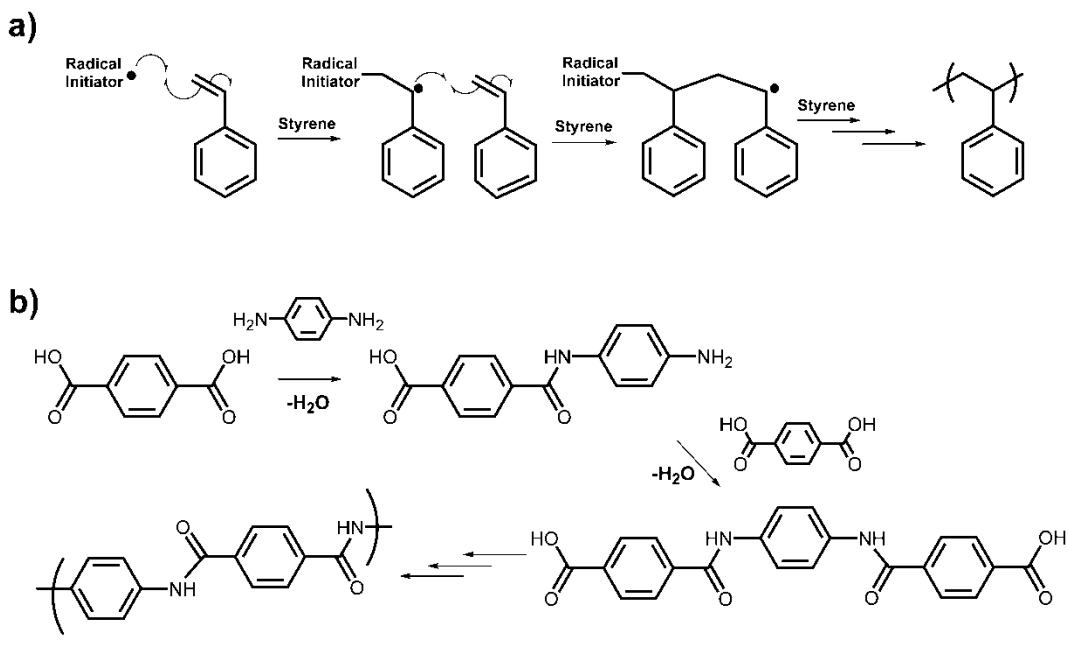
Figure 12: Schemes showing a) the chain-growth propagation of a radical reaction leading to the formation of polystyrene, and b) reactions showing the step-growth development of an aramid polymer.

The other type of polymerization is known as step-growth or condensation polymerization and relies on reactions between functional groups in the monomers (Figure 12b). The resulting reactions are able to take place throughout the system (c.f. chain-growth mechanism where reaction only takes place at the active sites). Initially this creates a large number of dimers and oligomers. High molecular weights are only achieved when the polymerization is close to completion (i.e., most of the reactive sites are used up).[77]

Most polymers capable of withstanding the conditions inside a fuel cell are made using the step-growth mechanism (with the exception of perfluorinated polymers).[18] This type of synthesis allows for polymers to be created that have aromatic systems in the polymer backbone, making them highly stable (i.e., resistant to chain scission (Figure 6)). Challenges associated with this type of polymerization are that the reaction times are usually long and often high temperatures are needed to obtain high molecular weight materials.[77]

1.5.2 Sulfonation

Most aromatic proton-conducting polymers contain sulfonic acid groups and attachment of these sulfonated groups is usually done in one of two ways. The first is a method called post-sulfonation, whereby the polymer is treated with a sulfonation reagent (e.g., concentrated sulfuric acid, oleum, etc.) to attach a sulfonic acid group to an aromatic ring. The mechanism is illustrated in Figure 13 and is the result of an electrophilic aromatic substitution (AES). As such, it directs the reaction to the ortho/para positions if the ring has substituents that are electron donating and to the meta positions if they are electron withdrawing.
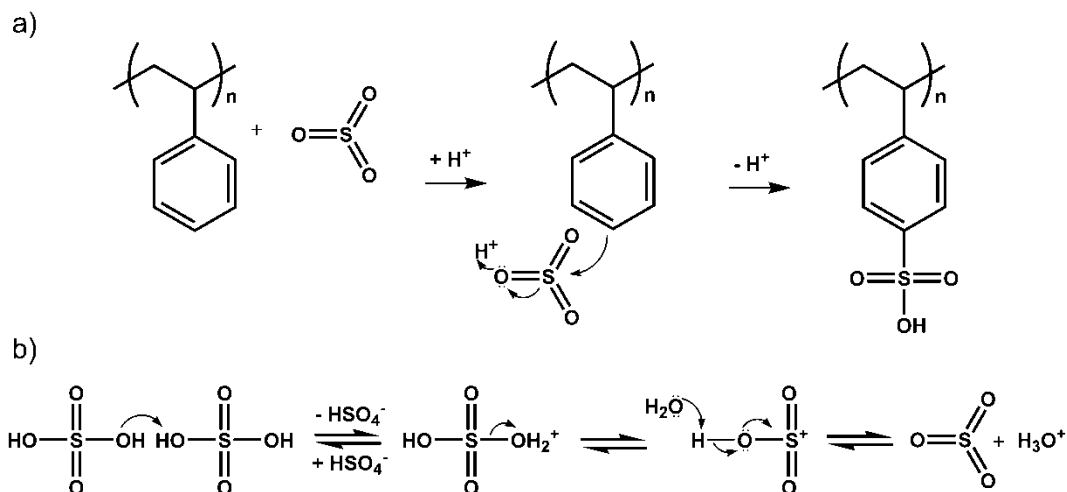
Figure 13: Scheme showing the a) sulfonation of polystyrene[78] with sulfur trioxide and b) the equilibrium between sulfuric acid and sulfur trioxide in concentrated sulfuric acid.

This type of sulfonation is often the least difficult to perform, as it can be done by dissolving the polymer (often available commercially) in sulfuric acid and applying heat. The degree of sulfonation can be controlled somewhat, by varying the temperature and reaction time. Problems with this type of synthesis can arise if the unsulfonated polymer is not stable in concentrated sulfuric acid, or if the most activated (electron-rich) sites in the polymer are different than the desired sulfonation sites (e.g., sulfonation needed at meta position relative to electron donating group).[18]

The second method to synthesize sulfonated polymers is through the polymerization of already sulfonated monomers (Figure 14).[78,79] These monomers contain sulfonate groups ($-SO_3^-M^+$) as well as polymerizable groups. This type of synthesis, although more challenging, can provide much greater control of degree of sulfonation and location of those sulfonic acid groups. By mixing sulfonated and non-sulfonated monomers, the degree of sulfonation of the

final polymer can be controlled much more precisely than in post sulfonation, where slight differences in time and temperature can result in noticeable differences in degree of sulfonation. In addition, the location of the sulfonic acid groups is ensured by using monomers with the sulfonic acid in the desired position.
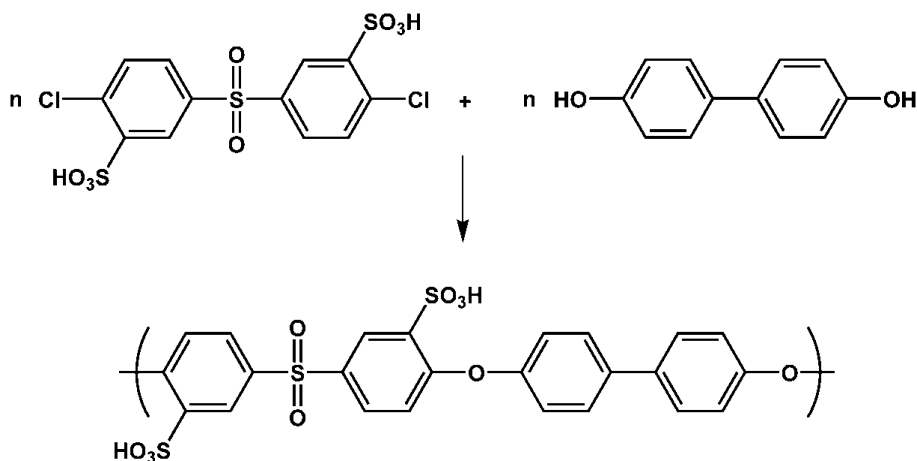
Figure 14: **Scheme showing the preparation of sulfonated poly(aryl ether sulfone) using a sulfonated monomer.**[79]

Both of these sulfonation methods will be used in the synthesis of the polymer blends discussed in this work.

1.5.3 Basic sites

Polymers used in acid-base blended systems described above, usually incorporate their basic sites done through adding amine or imine nitrogen sites. Like acidic sites, they can be added before or after polymerization (Figure 15).[72,80,81]
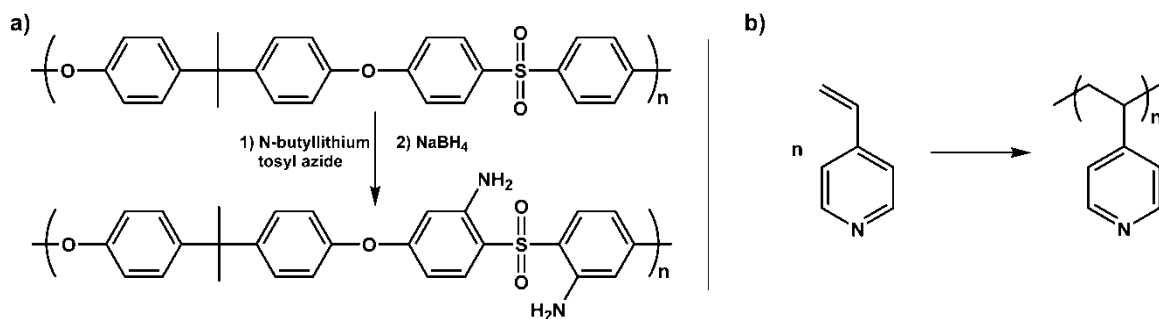
Figure 15: Schemes showing a) the preparation of post-aminated polysulfone using an azide substitution[80] and b) the polymerization of basic vinylpyridine monomer to become polyvinylpyridine.

1.5.3.1 Poly(benzimidazole)s (PBIs)

Poly(benzimidazole)s are a class of compounds containing repeating benzimidazole units. PBIs are usually highly stable and are resistant to high temperatures. The imine nitrogen in the benzimidazole ring is basic, making this polymer a suitable choice for acid-base blends. Much of their strength comes from the interactions between the amine protons and the imine nitrogens in the benzimidazole rings (Figure 16).
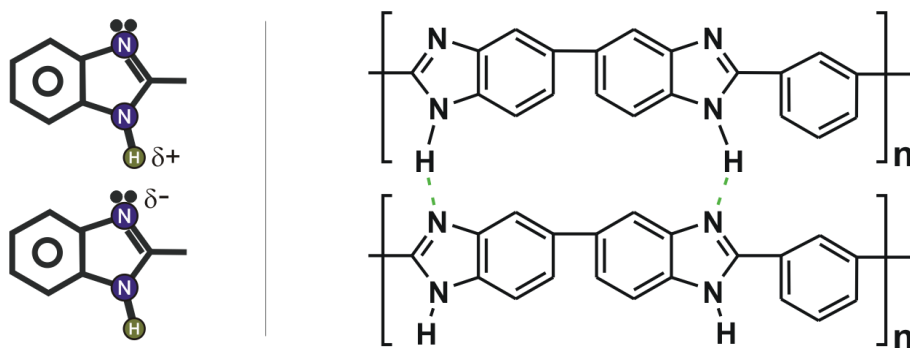
Figure 16: Illustration of the attractive interaction between benzimidazole units and how these interactions repeat through the polymer.

The synthesis of these polymers is usually performed by reacting a dicarboxylic acid with a tetraamine (Figure 17).[82] The resulting polymer structure

depends on the dicarboxylic acids and tetraamines used allowing for the design of a large number of polymer variations.
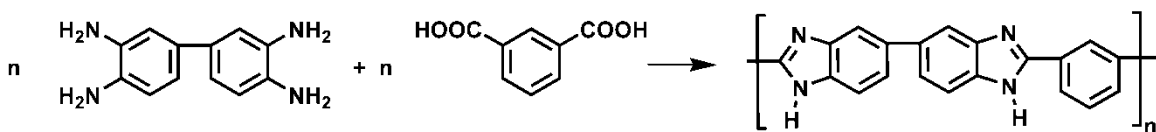
Figure 17: Scheme showing a general PBI synthesis (example shown for poly(2,2'-(m-phenylene)-5,5'-dibenzimidazole)).

Chapter 2 will detail the design and results of a high IEC, hydrocarbon, proton exchange membrane that is cross-linked using an amphiphilic polymer to reduce swelling.

1.6 Research objectives

The purpose of this work was to investigate PBI for use as ion exchange membranes for both proton and ion exchange applications. As reported in the literature,[18,66,70,73-75] PBI can be used to increase mechanical stability of acid-containing polymer chains through the formation of cross-links. The goal of this project was to synthesize a PBI material containing sulfonic acid groups for use as a proton exchange membrane, both alone and in blends with acid containing polymers. Through characterization of the membranes' mechanical properties, and proton conductivity over a range of conditions, a greater understanding of these materials advantages and disadvantages can be found.

To further develop our understanding of PBI, a polymer was synthesized containing cationic sites in the polymer backbone for use as an anion exchange membrane. This would be a novel use for these types of polymers and through

the investigation of the anion conductivity and mechanical and chemical stability

of these materials, more conductive and stable systems can be realized.

2: POLYBENZIMIDAZOLES AS PROTON EXCHANGE MEMBRANES AND ACID-BASE CROSS-LINKERS

2.1 Overview

This section details a series of proton exchange membrane systems based on high IEC sulfonated poly(ether ether ketone) cross-linked with sulfonated polybenzimidazole. The properties of these cross-linkers were compared to non-sulfonated analogues. The methods used in this study are described in Experimental Section 2.5. The materials used for this research can be found in the Appendix, Table A1.

2.2 Materials used in this work

2.2.1 Poly(ether ether ketone) (PEEK)

The acidic polymers used for this study were based on poly(ether ether ketone) (PEEK) (**1**). PEEK is an aromatic polymer consisting of aryl rings connected together through ether or ketone linkages. The polymer is synthesized through the reaction of 4,4'-difluorobenzophenone and the sodium salt of hydroquinone (Figure 18). The resulting polymer is hydrophobic, resistant to most solvents and has high thermal stability.
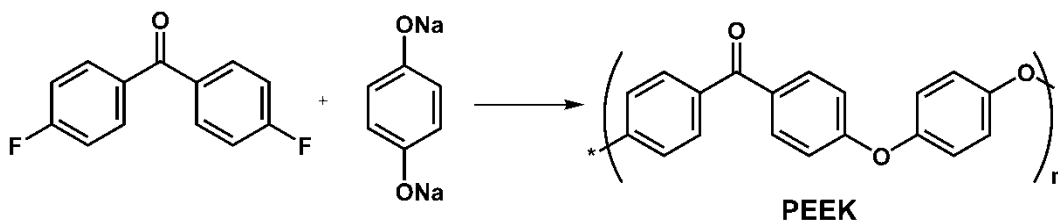
Figure 18: Schemes showing the synthesis of poly(ether ether ketone) (PEEK) (**1**).

Sulfonation of this polymer was done through post sulfonation. The resulting polymer (Figure 19) sulfonates preferentially at the aryl ring attached to two ether groups as these substituents activate the ring. The resulting polymer, sulfonated PEEK (SPEEK) (**2**), can be made to varying degrees of sulfonation (DS) depending on reaction conditions.
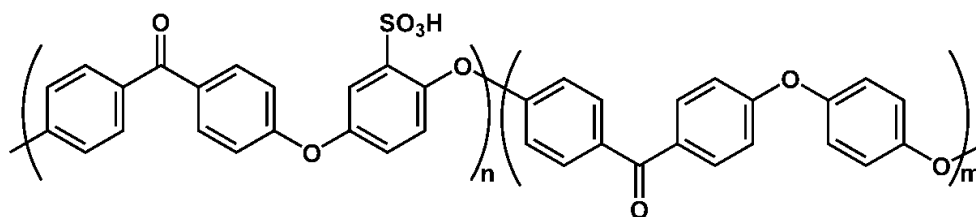
Figure 19: Structure of sulfonated poly(ether ether ketone) (SPEEK) (**2**).

2.2.2 Sulfonated poly(benzimidazoles) (SuPBI)

The basic and amphoteric polymers used in this study were based on a PBI structure (Figure 17). These polymers can be pre-sulfonated or post-sulfonated using a variety of sulfonation reagents. However, sulfonation using sulfuric acid requires ring systems that are next to electron donating groups (Figure 20a). This requires that special monomers are selected. Polymerization using sulfonated monomers (Figure 20b) creates a pre-sulfonated polymer in which the degree of sulfonation can be precisely controlled.
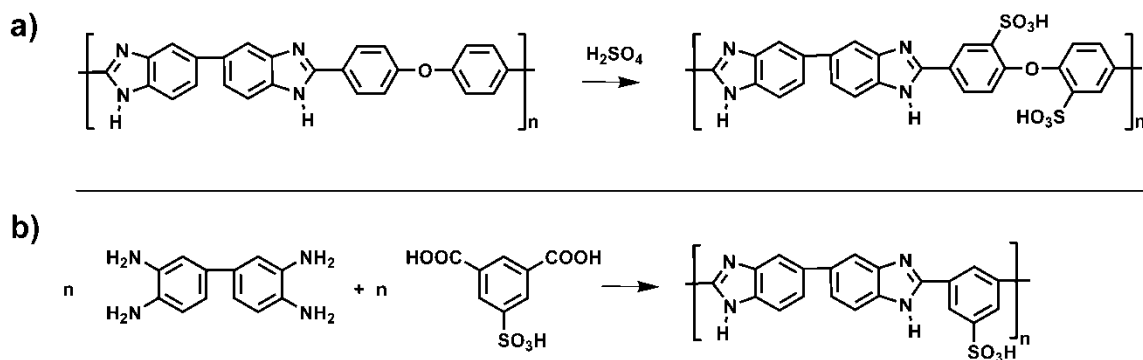
Figure 20: Schemes showing a) the post-sulfonation of a PBI and b) the synthesis of a pre-sulfonated PBI using a sulfonated monomer.

Highly sulfonated PBI materials often have low solubility in most solvents even in the neutralized form ($-SO_3^- M^+$). Solubility can be improved by adding a percentage of hydrophobic groups to the polymer backbone. These groups increase the hydrophobicity of the polymer. In addition, they can cause kinks in the chain, which facilitates dissolution by hindering polymer packing.

A range of PBIs with varying degree of sulfonation was made for this study (**3a-d**) (Figure 21). Sulfonation was performed using sulfonated monomers and the degree of sulfonation was controlled by varying the ratio of sulfonated to non-sulfonated dicarboxylic acid monomers in the reaction mixture. The polymers contained a percentage of a biphenyl hexafluoropropylene unit added to aid in solubility.

These polymers were compared to non-sulfonated analogues (**4**, **5**) to examine the effect of sulfonation on the mechanical and ion conduction properties of these materials.

3(a - d): R=SO₃H
4: R=H, n=70, m=30
5: m=100
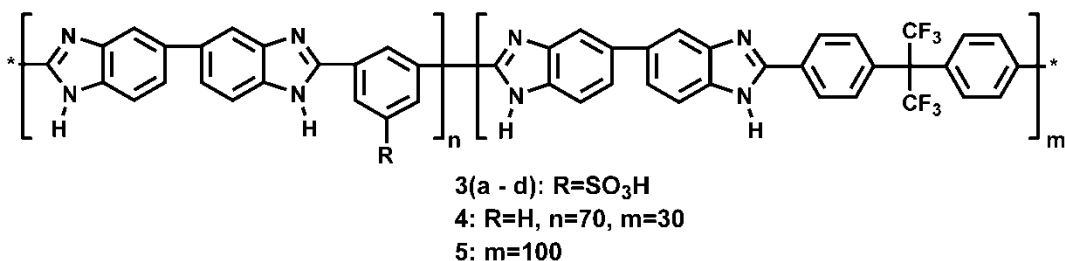
Figure 21: Structures of PBI polymers synthesized in this study (3a: n=50, m=50. 3b: n=60, m=40. 3c: n=70, m=30. 3d: n=80, m=20).

2.2.3 PBI:SPEEK Blends

Blends of the PBI polymers were made with high IEC SPEEK and the mechanical and proton conduction properties were examined. By varying the ratio of PBI to SPEEK, a range of membranes was produced with differing IEC. Three sets of blend membranes were assembled, each using a different PBI (i.e., for **3c**, **4** and **5**). This would allow for the effect of the sulfonation of the cross-linker to be determined over a range of IEC. In addition, a series of SPEEK only membranes was produced with varying degree of sulfonation (and thus IEC), which when compared to the blend membranes would gauge the effect of the cross-linking in general.

2.3 Results and Discussion

2.3.1 Polymer Synthesis

Using the polycondensation reaction reported in the literature,[82-84] a series of sulfonated polybenzimidazoles (**3a-d**) was synthesized according to Figure 22. By adjusting the molar feed ratios of sulfonated (**7**) to non-sulfonated dicarboxylic acid monomers (**9**), it was possible to prepare copolymers with varying acid group content. Two other PBIs were synthesized: polymer **4**, which is the

unsulfonated analogue of **3c** and polymer **5,** prepared from only monomers **6** and **9**. The molecular weight of the polymers was determined using gel permeation chromatography (GPC) to be ~4x10^4 Da against polystyrene standards.
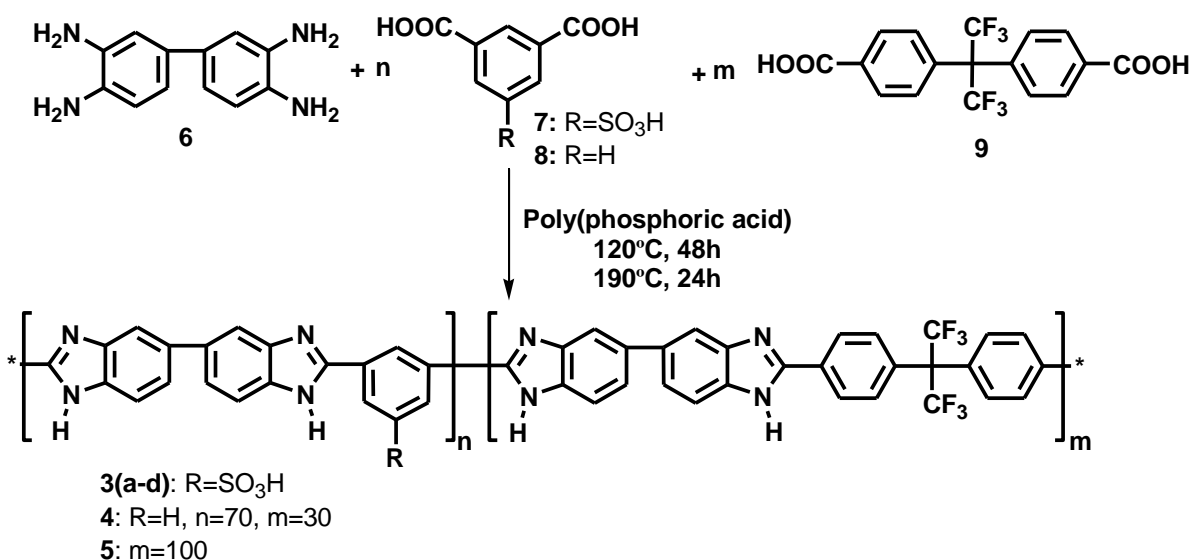
Figure 22:   **Scheme detailing the synthesis of polymers 3(a-d), 4 and 5.**

^{1}H NMR spectra obtained for the synthesized polymers were consistent with the those found in the literature for similar materials. The spectra exhibited for the different compositions of **3** are similar except for the relative integrals of the peaks (Figure 23a). **4** contains an additional aromatic hydrogen peak (Figure 23b) due to the proton (H_h) at the position occupied by the sulfonate group in **3**. Also, the peak corresponding to H_d in **3c** is downfield from H_d in **4** due to its proximity to the sulfonate group. When comparing the spectra of either **3** or **4** to **5**, the peaks corresponding to protons H_e and H_d are not present in **5**. Ratios of

repeat groups present in the polymer were also determined using ^{1}H NMR spectroscopy. Using compound **3** as an example, by integrating a peak (H$_a$) in the benzimidazole rings, a structure common to both repeat groups, and a peak observed only in the sulfonated repeat unit (e.g., H$_d$), the ratio of sulfonated units to the total number of repeat units was determined. The ratio found for **4** was similarly determined except peak H$_e$ was used and the integral was multiplied by 2 to account for the different ratio of those protons in the structure. The compositions of the polymers produced are presented in Table 2.

a)

5: n=0 m=100   3b n=58, m=42   3d n=81, m=19
3a n=49, m=51   3c n=68, m=32

b)

3c n=68, m=32, R=SO₃Na
4: n=66, m=34, R=H
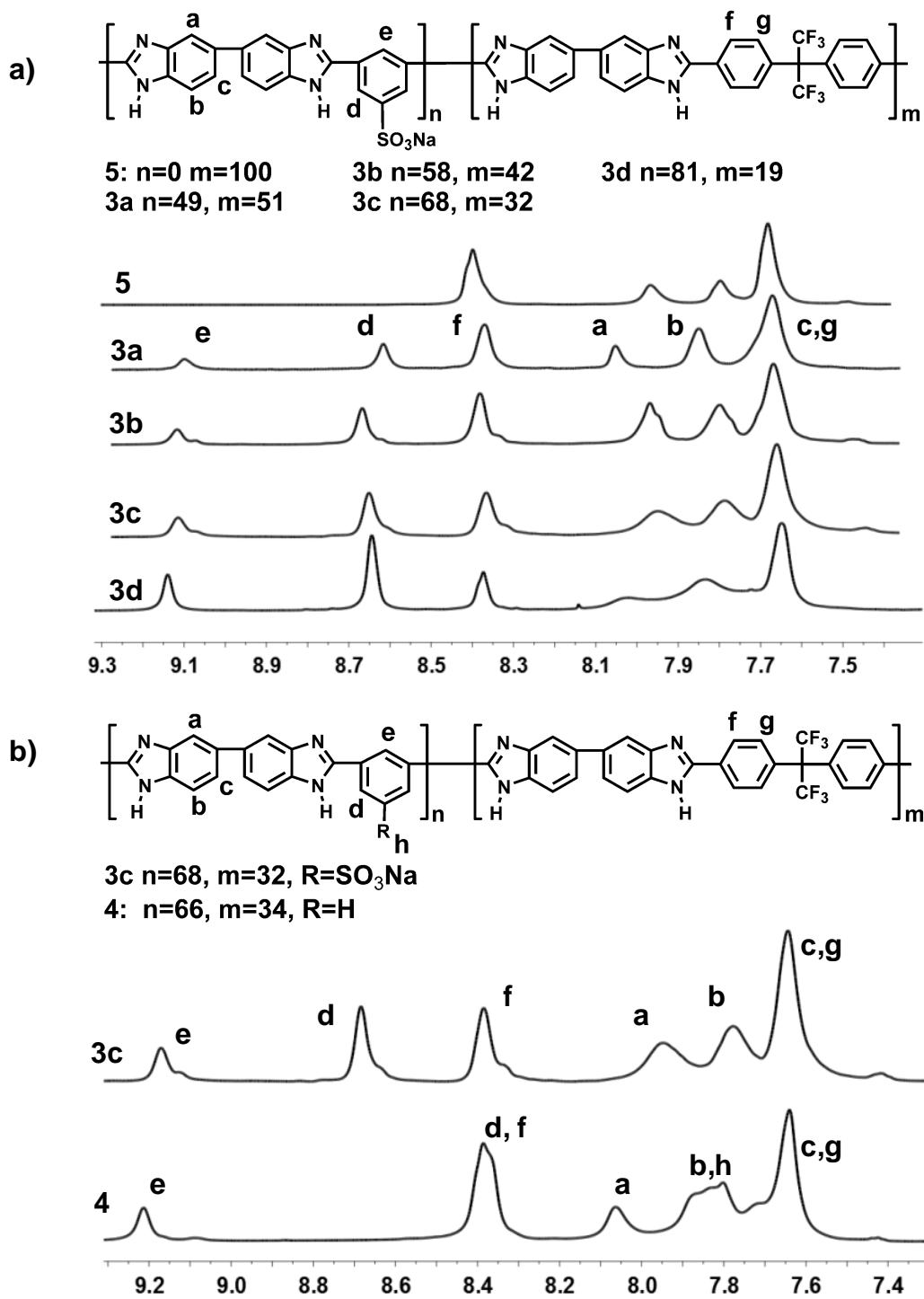
Figure 23:   a) ¹H NMR spectra of (a) **3a** - **d**, and **5**; (b) **3c** and **4**.

32

The FTIR spectra (Figure 24) confirmed that polymers **3**, **4** and **5** all contained C=N/C=C groups (~1620 cm^{-1}) and exhibited an in-plane deformation of the benzimidazole ring (~1440 cm^{-1}). However, only compound **3** showed peaks at 1044 cm^{-1} (S-O symmetric stretch) and 626 cm^{-1} (C-S bend), which provides additional evidence for the presence of sulfonate groups.
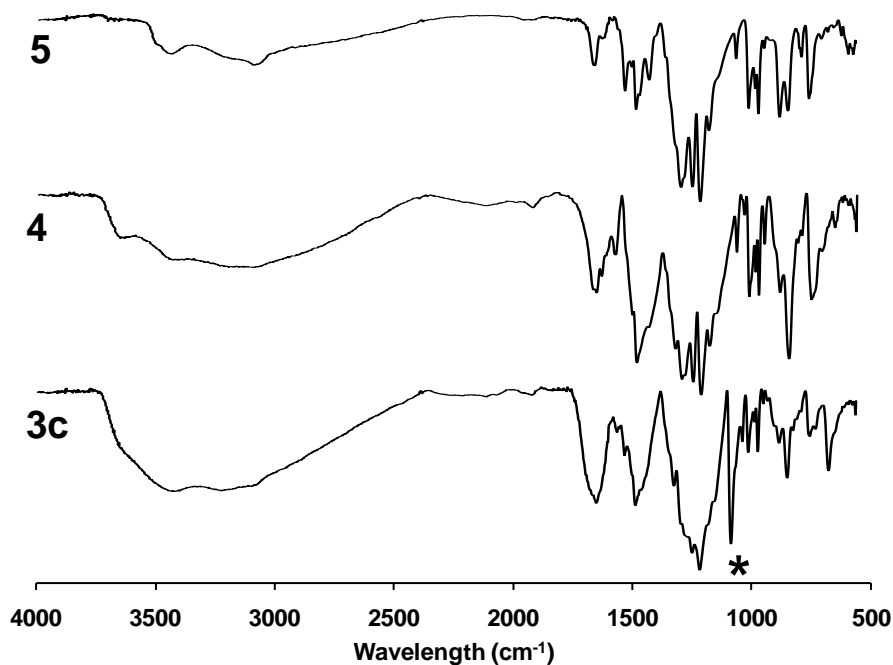
Figure 24: FTIR spectra of **3c**, **4** and **5** (*= symmetric stretch for S-O).

2.3.2 SPEEK Membrane Properties

Membranes of polymer **2**(**a**-**e**) were prepared and the IEC and water uptake were measured. The IEC measured for the membranes increased with the length of time spent reacting in concentrated sulfuric acid (Table 1). The IECs found through titration agreed well with the IECs determined by NMR (± 5%). The

water uptakes of these membranes increased with IEC and highly sulfonated

membranes swelled dramatically and in some cases dissolved (**2d,e**).
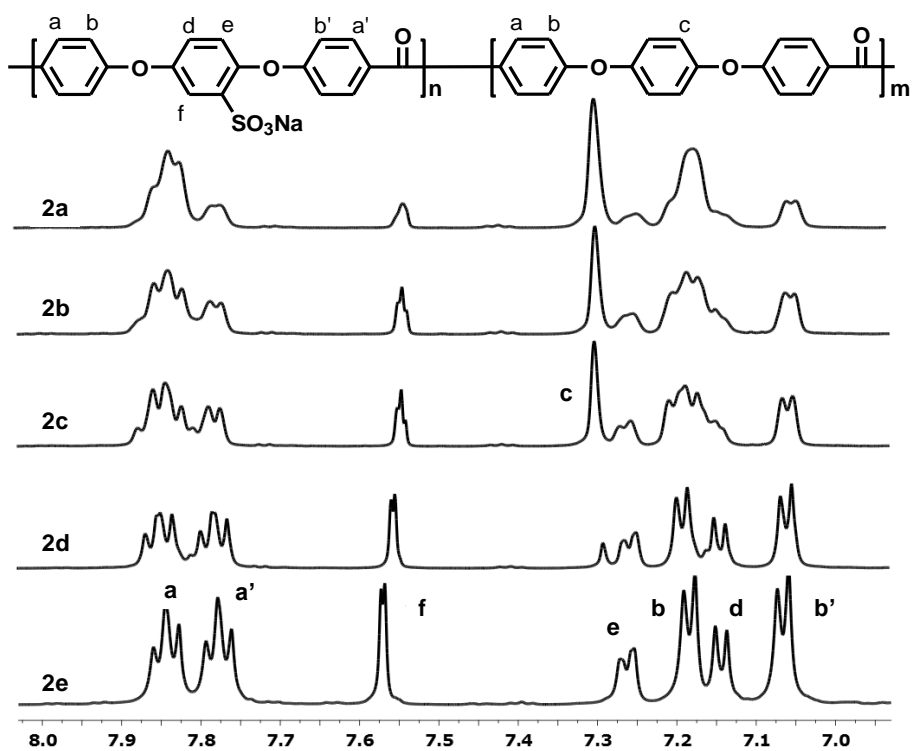
Figure 25:   ¹H NMR spectra of **2(a-e)**.

Table 1: IEC data for SPEEK polymer series **2(a-e)**.

Polymer	Reaction Time (min) [a]	Degree of Sulfonation (%)	IEC from ^{1}H NMR (meq·g^{-1})	Titrated IEC (meq·g^{-1})	Water Uptake[b,d] (%)	σ_{H+}[c,d] (S·cm^{-1})
2a	0[a]	36	1.13	1.19	23	0.015
2b	30	56	1.68	1.66	29	0.038
2c	60	64	1.90	1.94	122	0.074
2d	120	86	2.42	2.40	478	0.038
2e	240	94	2.58	2.54	-[e]/12800[f]	0.005[e]

-Details of these measurements are found in Experimental Section 2.5.3

[a] Reaction time t =0 defined as the time the polymer completely dissolved in solution (See Section 2.5.2.6).

[b] Water uptake percent by weight (See Section 2.5.3.1).

[c] Proton conductivity measured using Impedance Spectroscopy (See Section 2.5.3.9).

[d] Measurements taken after immersion in water for 24 h.

[e] Soluble when soaked for full 24 h.

[f] Soaked in water for 3 h only due to solubility concerns.

The proton conductivity of the SPEEK membranes achieved a maximum of $0.074 \text{S} \cdot \text{cm}^{-1}$ at IEC of 1.94 $\text{meq} \cdot \text{g}^{-1}$ (**2c**). Membranes at lower IEC lacked either the proton concentration or the proton mobility to conduct protons efficiently, while the higher IEC membranes suffered from excessive swelling that lowered the proton concentration of the system through dilution. This is a common occurrence for PEMs as there is a balance needed in order to ensure high proton concentration and high mobility. The large amount of swelling associated with these highly sulfonated membranes impacts their ability to conduct protons. In order for these materials to be useful in fuel cell applications, measures need to be taken to reduce the swelling of the membranes in water.

2.3.3 Properties of SuPBI Membranes

In order to cast membranes of **3**, it was necessary to dissolve the polymer in the salt form, as the protonated form was insoluble due to intermolecular interactions. Once cast, membranes of **3** were converted to the acid form by treatment with $\text{HCl}_{(aq)}$. The sulfonic acid protonates the imine nitrogen of the benzimidazole creating a positive charge on the polymer backbone, and is electrostatically balanced by the sulfonate as illustrated in Figure 26. The membranes produced are brittle and require care when handling.

Table 2: Composition and IEC data for PBI polymers **3(a-d), 4, 5**.

Polymer	Monomer feed ratio **7**:**8**:**9**[a]	Polymer ratio from ^{1}H NMR	Calculated IEC[b] (meq·g^{-1})	Calculated ABS[c] (meq·g^{-1})	Titrated IEC[d] (meq·g^{-1})
3a	50:0:50	49:0:51	1.08	3.26	0.04
3b	60:0:40	58:0:42	1.29	3.16	0.04
3c	70:0:30	68:0:32	1.56	3.03	0.05
3d	80:0:20	81:0:19	1.98	2.86	0.08
4	0:70:30	0:66:34	0	5.25	< 0.01
5	0:0:100	0:0:100	0	3.74	< 0.01

[a] Refer to Figure 22.

[b] IEC calculated from ^{1}H NMR (See Section 2.5.3.5).

[c] ABS- Available Basic Sites found in the polymer. (See Section 2.5.3.6).

[d] Ion Exchange Capacity determined by titration (See Section 2.5.3.4, Equation 5).

The IEC of **4** and **5** were found to be negligible (Table 2) due to the absence of sulfonic acid groups in their structure. In the case of **3,** the IECs found by titration were close to zero. This result was in contrast to the IEC calculated from the number of $-SO_3H$ groups estimated by ^1H NMR, which was between 1 and 2 meq·g^{-1}. The reason for this discrepancy is self-neutralization of the acidic protons by the basic sites in the benzimidazole backbone (see Figure 26). Comparable small molecules show pK_a of $-$ 2.7[85,86] for benzenesulfonic acid and a pK_a protonated benzimidazole $pK_a = 5.4$[87]. The titration method employed in this work to determine IEC values of these polymers consisted of soaking the membranes in an aqueous NaCl solution. Back titration methods have been employed by other groups for similar acid-base polymer systems. However, for the purposes of this study, ^1H NMR analysis was sufficient to determine the ratio of sulfonated:unsulfonated groups on the polymer. Furthermore, the direct titration method also provides a measure of the number of dissociated protons available to participate in proton conduction. It was found that the number of basic sites available in these polymers was sufficient to neutralize all of the sulfonic acids attached.
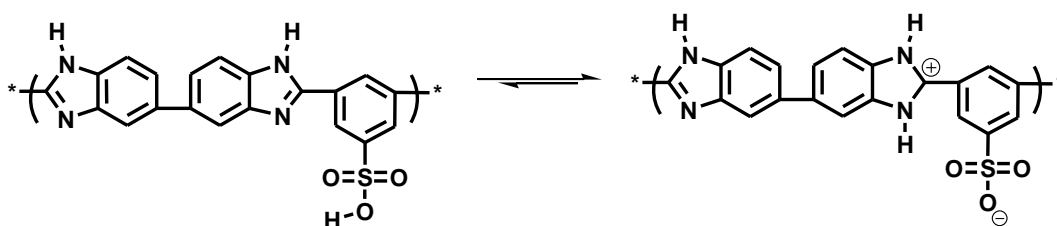
Figure 26:   Diagram illustrating the self-neutralization of polymer 3.

All of the PBI membranes, including sulfonated derivatives, showed conductivity values less than 10^{-6} S·cm^{-1} (Table 3). Each of these membranes possessed a sufficient number of sulfonic acid groups (0.99 M-1.56 M), as determined by ^{1}H NMR, yet was unable to yield significant proton conductivity. This is due to the low effective proton mobility, which is calculated to be ~10^{-6} cm^2·V^{-1}·s^{-1}, and a direct consequence of the association of protons with basic sites in the benzimidazole rings (pK$_a$ of the conjugate acid = 6),[88] which hinders their movement through the membrane.

Table 3:   **Conductivity data for sulfonated polybenzimidazole series 3a-d.**

Polymer	$\sigma_{H}+$ [a] (S·cm^{-1})	[-SO$_3$H] [b] (M)	$\mu'_{H}+$ [c] (cm^2·V^{-1}·s^{-1})	λ [d] (H$_2$O/-SO$_3$H)
3a	1.4x10^{-7}	0.99	1.4x10^{-6}	6
3b	3.7x10^{-7}	1.07	3.5x10^{-6}	10
3c	3.2x10^{-7}	1.37	2.4x10^{-6}	6
3d	3.2x10^{-7}	1.56	2.1x10^{-6}	8

[a] Proton conductivity measured using Impedance Spectroscopy (See Section 2.5.3.9).

[b] Sulfonic acid group concentration (See Section 2.5.3.10).

[c] Proton mobility calculated from conductivity and concentration data (See Section 2.5.3.10).

[d] Number of water molecules per sulfonic acid group (See Section 2.5.3.8).

2.3.4 Properties of SPEEK:PBI Blend membranes

SPEEK:PBI blend membranes were cast with different weight ratios (see Table 4), and their properties were subsequently examined. Polymer **3c** was selected as the representative sulfonated PBI due to its good compromise between high acid content and solubility in DMAc.

Table 4: IEC values for blend membranes.

| SPEEK[a]: PBI | PBI, **3c** | | PBI, **4** | | PBI, **5** | |
	Calculated IEC[b] (meq·g^{-1})	Titrated IEC[c] (meq·g^{-1})	Calculated IEC (meq·g^{-1})	Titrated IEC (meq·g^{-1})	Calculated IEC (meq·g^{-1})	Titrated IEC (meq·g^{-1})
95:5	2.28	2.33	2.17	2.12	2.25	2.14
92:8	2.11	2.11	1.94	1.94	2.07	2.04
85:15	1.72	1.73	1.36	1.41	1.62	1.57
75:25	1.16	1.25	0.61	0.73	0.99	0.99
68:32	0.77	0.69	0.06	0.26	0.54	0.40

[a] SPEEK, IEC = 2.54 meq·g^{-1}, Sample **2e**. Ratios of SPEEK to PBI by weight.

[b] Calculated IEC using IEC of SPEEK and ABS of PBI (See Section 2.5.3.7).

[c] IEC determined by titration (See Section 2.5.3.4).

IEC values of the blend membranes measured by titration closely matched the IEC values calculated by subtracting the available basic sites per gram (ABS) of PBI from the IEC of the SPEEK. These values decreased with increasing PBI content due to the increase in ABS (from 2.28 to 0.77 $meq \cdot g^{-1}$ for blends of SPEEK:**3c** from 95:5 to 68:32). It was also found that the blends prepared using **3c** exhibited higher IEC than those made with **4** or **5** (cf. 0.77 for **3c** with 0.07 and 0.54 for **4** and **5,** respectively, for 68:32 SPEEK:PBI blends) due to the additional sulfonic acid groups present in **3c**.

The effect of the PBI content on the room temperature water uptake of the blend membranes is shown in Figure 27. In general, increasing the PBI content decreases the water uptake in the membrane due to the increase in the degree of acid-base cross-linking between chains, which restricts membrane swelling. Additionally, the PBI lowers the overall IEC of the polymer blend, which in turn reduces the hydrophilicity of the material. For low PBI contents (< 5 wt. %) i.e., high acid content, a sharp increase in water uptake is observed, which is common for high IEC membranes.
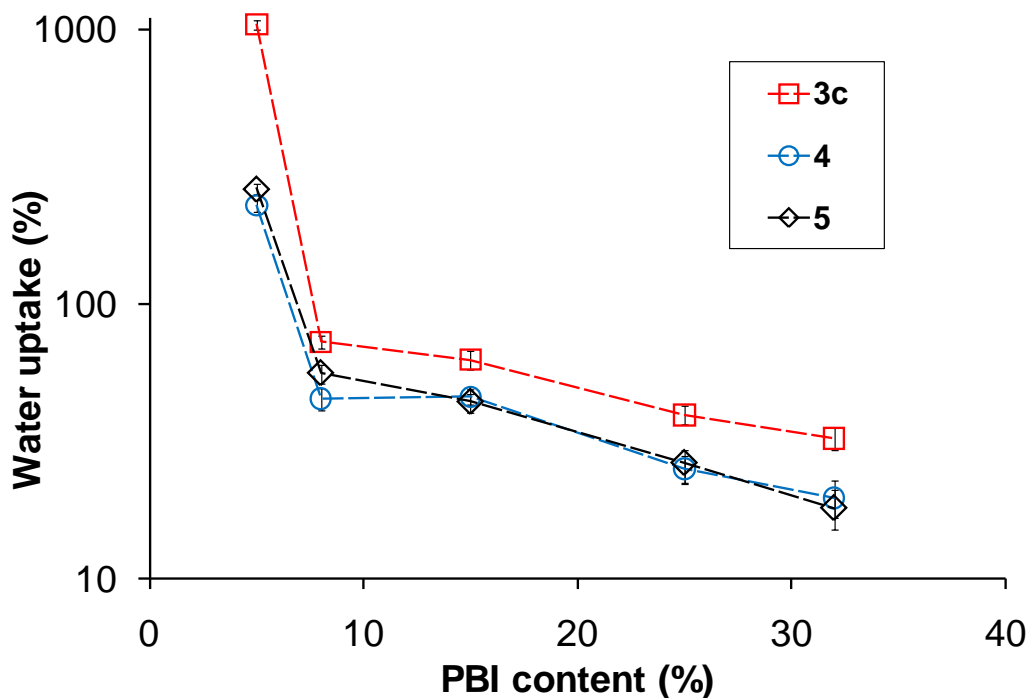
Figure 27: Water uptake (wt. %) as a function of PBI content (wt. %) for SPEEK:PBI blends at room temperature. Note: water uptake for membranes made using the high IEC SPEEK **2e** was 12800% after only 3 h (See Table 1).

For a given PBI content, the water content in the blends increases in the sequence: **4** < **5** < **3c** due to the increase in acid content. Indeed, for a SPEEK:PBI ratio of 92:8, IEC values for **4**, **5**, and **3c** are 1.94, 2.07 and 2.11 meq·g^{-1} respectively, with corresponding water uptakes of 45, 56, and 72 wt. %.

The dimensional stability of the SPEEK:PBI blend membranes along with pure SPEEK membranes, for comparative purposes (IEC values for all membranes ~2 meq·g^{-1}), were measured in water at 20, 50, and 80 °C (see Table 5). The blend membranes exhibited a greater resistance to swelling, especially at higher temperature (80 °C). At 50 °C, the blend membranes swelled but retained sufficient structural strength to determine their dimensions. The

SPEEK membranes on the other hand were too gelatinous to measure. Increasing the temperature to 80 °C caused the SPEEK-only membranes to dissolve completely; the blend membranes incorporating **3c** remained intact but were fragile. The blend membranes incorporating either **4** or **5** retained some mechanical strength despite water volume increases of 715 and 900 %, respectively. The increase in the amount of water taken up by membranes containing **3c,** compared to those using the non-sulfonated PBIs (**4** and **5**), may be due to its slightly higher IEC but also to the lower number of basic sites available to form inter-chain ionic cross-links, since a fraction may be neutralized by sulfonic acid groups attached to the PBI.

Table 5: Dimensional stability of SPEEK:PBI blends.

SPEEK:PBI	PBI	IEC_{titr} (meq·g^{-1})	Water volume uptake[a] (%)		
			20°C	50°C	80°C
92[b]:8	**3c**	2.11	72	350	-[d]
92[b]:8	**4**	1.94	45	140	715
92[b]:8	**5**	2.07	56	250	900
100[c]:0	-	1.94	70	-[d]	-[e]

[a] Water volume uptake determined using Equation 3 (See Section 2.5.3.2).

[b] IEC = 2.54 meq·g^{-1} for SPEEK used in blends, Sample **2e**.

[c] IEC = 1.94 meq·g^{-1} for SPEEK used alone, Sample **2c**.

[d] Gelatinous.

[e] Membrane dissolved.

The proton conductivity (σ_{H+}) values of the blend membranes (see Table 6) are compared to pure SPEEK membranes (see Table 7). A plot of IEC vs. σ_{H+} (Figure 28a) shows there is little difference in the evolution of the proton conductivity of the blend membranes with increasing IEC. In the moderately swollen membranes (i.e., in membranes where IEC< 1.7 meq·g^{-1}), there is little difference in the conductivity in the blends when compared to the SPEEK-only membranes. However at IEC ~2.0 meq·g^{-1}, significantly higher σ_{H+} were recorded for the SPEEK-only membranes (cf. 0.074 for **2** with 0.059 for blends using **3c**), before dropping rapidly with further increases in IEC. When conductivity is plotted against λ (Figure 28b), a sharp loss of conductivity is noticed for **2** at $\lambda >$ 30 whereas the blends are much less susceptible to increases in λ in this dilution regime. For instance, the blend incorporating **3c** does not show a significant reduction in σ_{H+} even when λ is ~250. A reduction in conductivity for high IEC membranes is usually due to a dilution of protons caused by a disproportionate increase in water uptake with increasing IEC. It is shown in Figure 28c that the calculated acid concentration for membranes with IEC > 2 meq·g^{-1} falls rapidly.

Table 6:   Conductivity data for blend membranes.

PBI	SPEEK[a]: PBI	$\sigma_{H}+$ [b] $(S \cdot cm^{-1})$	$[-SO_3H]$ [c] (M)	$\mu'_{H}+$ [d] $[\mu \times 10^3]$ $(cm^2 \cdot V^{-1} \cdot s^{-1})$	λ [e] $(H_2O/-SO_3H)$
3c	95:5	0.054	0.20	2.74	248
	92:8	0.058	1.25	0.49	19
	85:15	0.033	1.09	0.32	20
	75:25	0.007	0.92	0.08	17
	68:32	0.003	0.54	0.07	26
4	95:5	0.057	0.60	0.90	68
	92:8	0.049	1.44	0.40	12
	85:15	0.009	1.12	0.10	15
	75:25	0.001	0.81	0.02	15
	68:32	0.002	0.35	0.09	25
5	95:5	0.057	0.65	0.99	60
	92:8	0.055	1.27	0.40	16
	85:15	0.022	0.99	0.21	18
	75:25	0.004	0.60	0.06	19
	68:32	0.003	0.22	0.09	42

[a] IEC = 2.54 meq·g^{-1} for SPEEK used in blends.

[b] Proton conductivity measured using Impedance Spectroscopy (See Section 2.5.3.9).

[c] Sulfonic acid group concentration (See Section 2.5.3.10).

[d] Proton mobility calculated from conductivity and concentration data (See Section 2.5.3.10).

[e] Number of water molecules per sulfonic acid group (See Section 2.5.3.8).

Table 7: Conductivity data for pure SPEEK membranes.

SPEEK	IEC (meq·g^{-1})	σ_H+ [a] (S·cm^{-1})	[-SO$_3$H] [b] (M)	μ'_H+ [c] [μ x 10^3] (cm^2·V^{-1}·s^{-1})	λ [d] (H$_2$O/-SO$_3$H)
2a	1.19	0.008	1.00	0.08	10
2b	1.66	0.018	1.32	0.14	10
2c	1.94	0.074	1.17	0.66	20
2d	2.40	0.038	0.42	0.94	110
2e [e]	2.54	0.005	0.02	7.74	2820

[a] Proton conductivity measured using Impedance Spectroscopy (See Section 2.5.3.9).

[b] Sulfonic acid group concentration (See Section 2.5.3.10).

[c] Proton mobility calculated from conductivity and concentration data (See Section 2.5.3.10).

[d] Number of water molecules per sulfonic acid group (See Section 2.5.3.8).

[e] Soaked in water for 3 h only due to solubility concerns.
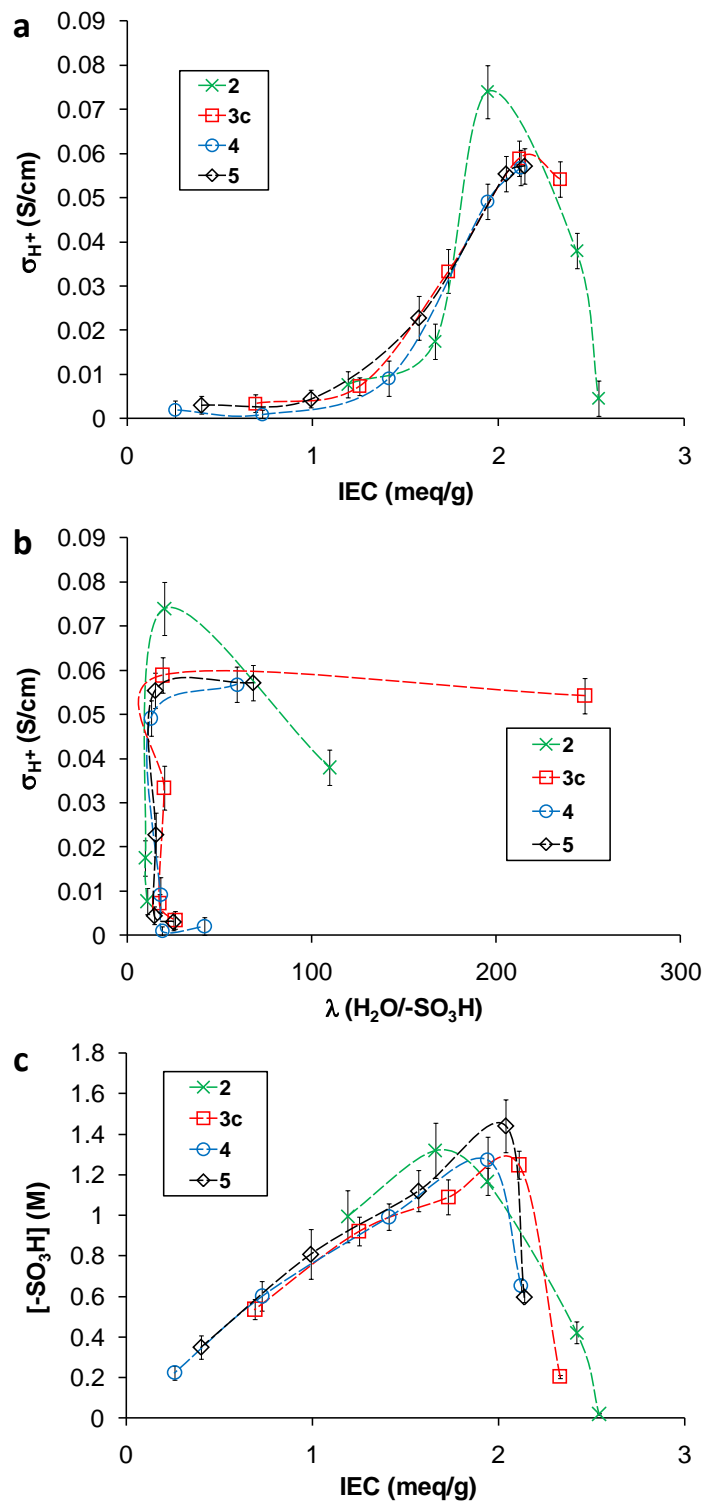
Figure 28: Proton conductivity of **2** and blends containing **3c**, **4** and **5** as a function of (a) IEC and (b) λ (**2e** omitted from chart). (c) Proton concentration of the same membranes compared to IEC.

The difference in σ_{H+} found between the blends and pure SPEEK membranes at ~2 meq·g^{-1} (cf. 0.074 S·cm^{-1} for **2** with ~0.058 S·cm^{-1} for the blends) suggests higher μ'_{H+} and/or [-SO$_3$H] (refer to Equation 12) for the SPEEK-only system. Looking more deeply into Figure 28c, the plot of [-SO$_3$H] against IEC shows similar curves for all membranes, with a slightly lower acid concentration at an IEC of ~2 meq·g^{-1} for the SPEEK-only membrane (1.17 M for **2** compared to 1.24-1.44 M for the blends). This lower value found for acid concentration of the SPEEK-only membranes suggests that higher proton conductivity observed at this IEC is a result of a higher effective proton mobility. Comparisons of μ'_{H+} (Figure 29a) show higher mobility at IEC ~2 meq·g^{-1} for **2** than the blends (c.f. 0.65x10^{-3} cm^2/V·s for **2c** with 0.39x10^{-2} cm^2/V·s for 8% blend of **3c**).
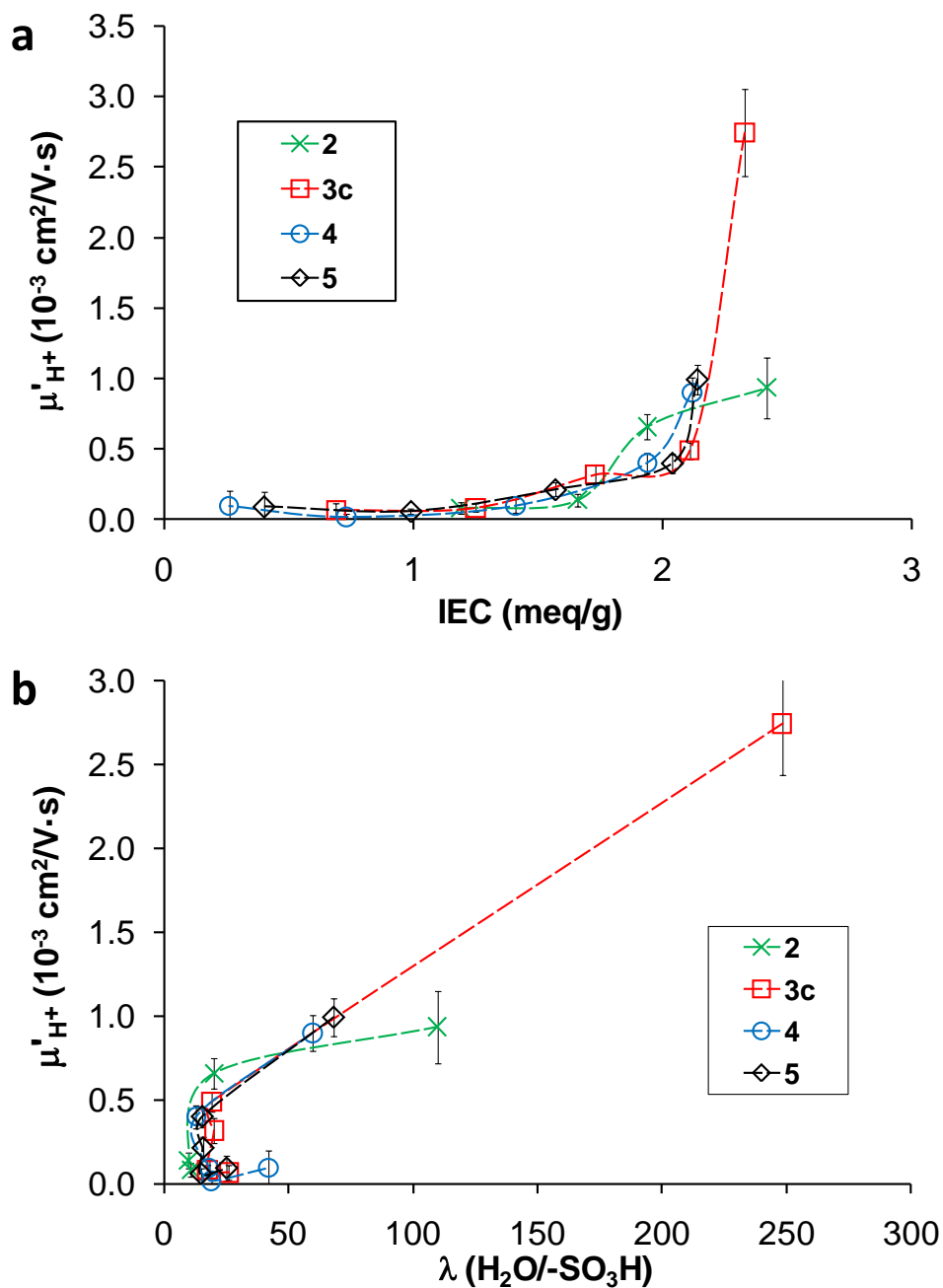
Figure 29: Proton mobility of **2** and blends containing **3c, 4** and **5** compared to a) IEC and b) λ.

As proton mobility in these membranes is closely related to water content (λ), these two values are plotted in Figure 29b. The SPEEK-only membranes exhibited a higher proton mobility compared to the blend membranes at λ ~20

(0.66×10^{-3} cm^2/V·s for **2** compared with 0.39×10^{-3} cm^2/V·s for blends using **3c**). The lower mobility for the blends may be due to the ionic cross-links formed between the polymers, resulting in a narrowing or blocking of the water channels or reduced flexibility of the polymer chains. When $\lambda > 50$, the effective proton mobility of the blend membranes exceeds that of pure SPEEK membranes, and approaches that of protons in water (3.62×10^{-3} cm^2/V·s) when lambda is very large. This compensates for the drop in acid concentration and causes proton conductivity to remain high for the blends in the high IEC regime (see

Figure 28b).

Conductivity values for the 8 wt. % blends of **3c**, **4** and **5** with SPEEK along with pure SPEEK (**2c**) are found to increase with increasing relative humidity (RH) (Figure 30a) at 80 ºC. In the region of low RH (≤ 50%), there is no observable difference amongst the membranes, which would be expected due to the low water contents preventing complete dissociation of the acid groups and hence leading to low levels of proton mobility. However, at RH = 90%, the conductivity of the **3c**-containing blend (54 mS/cm) is significantly higher than any of the other membranes, including **2c** (42 mS/cm).
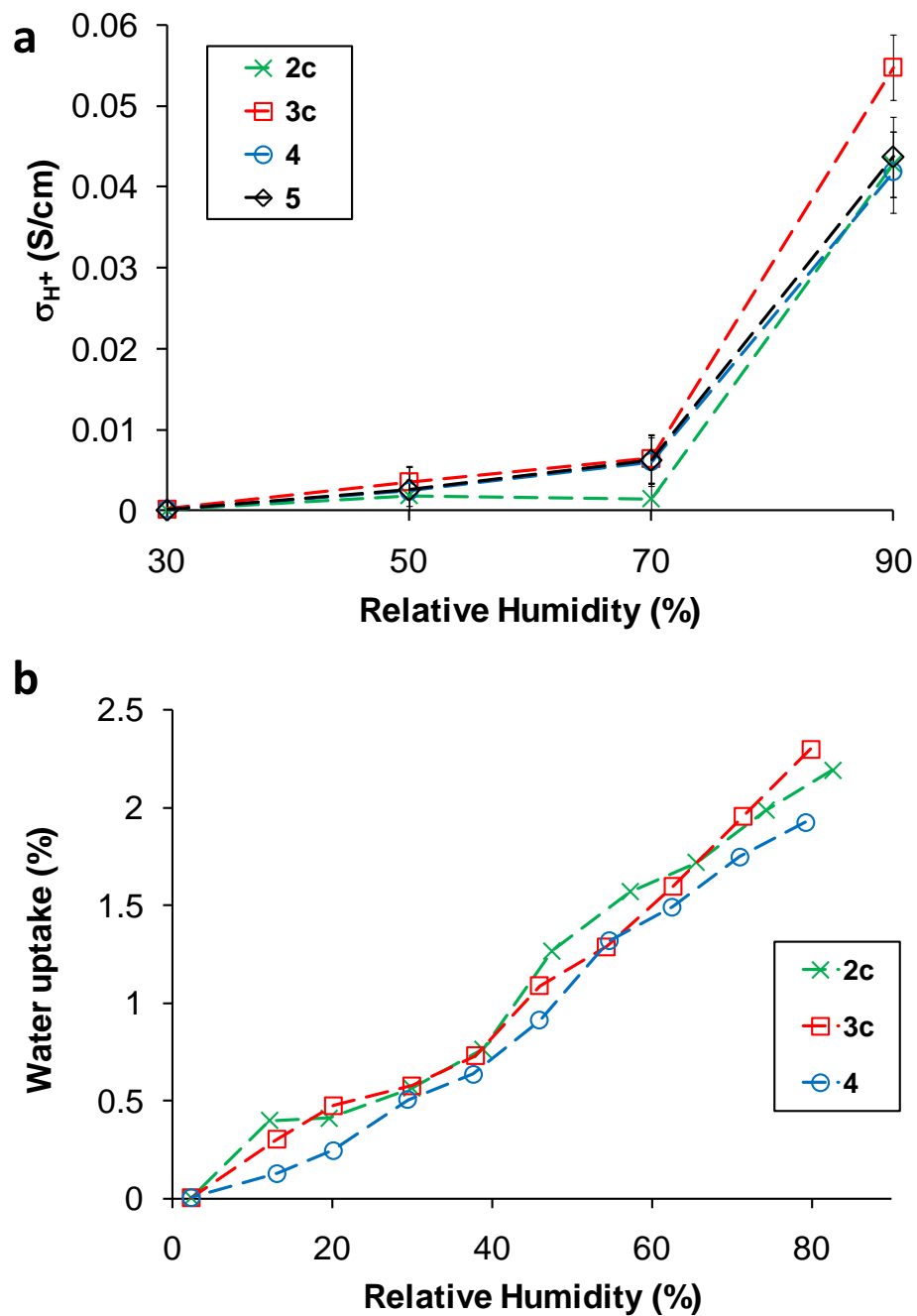
Figure 30: a) Proton conductivity of **2** and blends containing **3c**, **4** and **5** at varying relative humidity at 80 °C and b) water uptake of those membranes at 80 °C, data shown for one representative sample of each membrane.

Examination of the water contents over this RH range using the dynamic vapour sorption (DVS) instruments shows no significant difference for the **3c**-containing blend in comparison to **2c** or the blend containing a non-sulfonated cross-linker (**4**) (Figure 30b). It is interesting to note that **2c** actually exhibits higher acid concentration (Figure 31a) than the **3c**-containing blend. Therefore, it appears that the higher value of conductivity at RH = 90% for the latter is due to higher effective proton mobility in comparison to that of **2c** (Figure 31b).
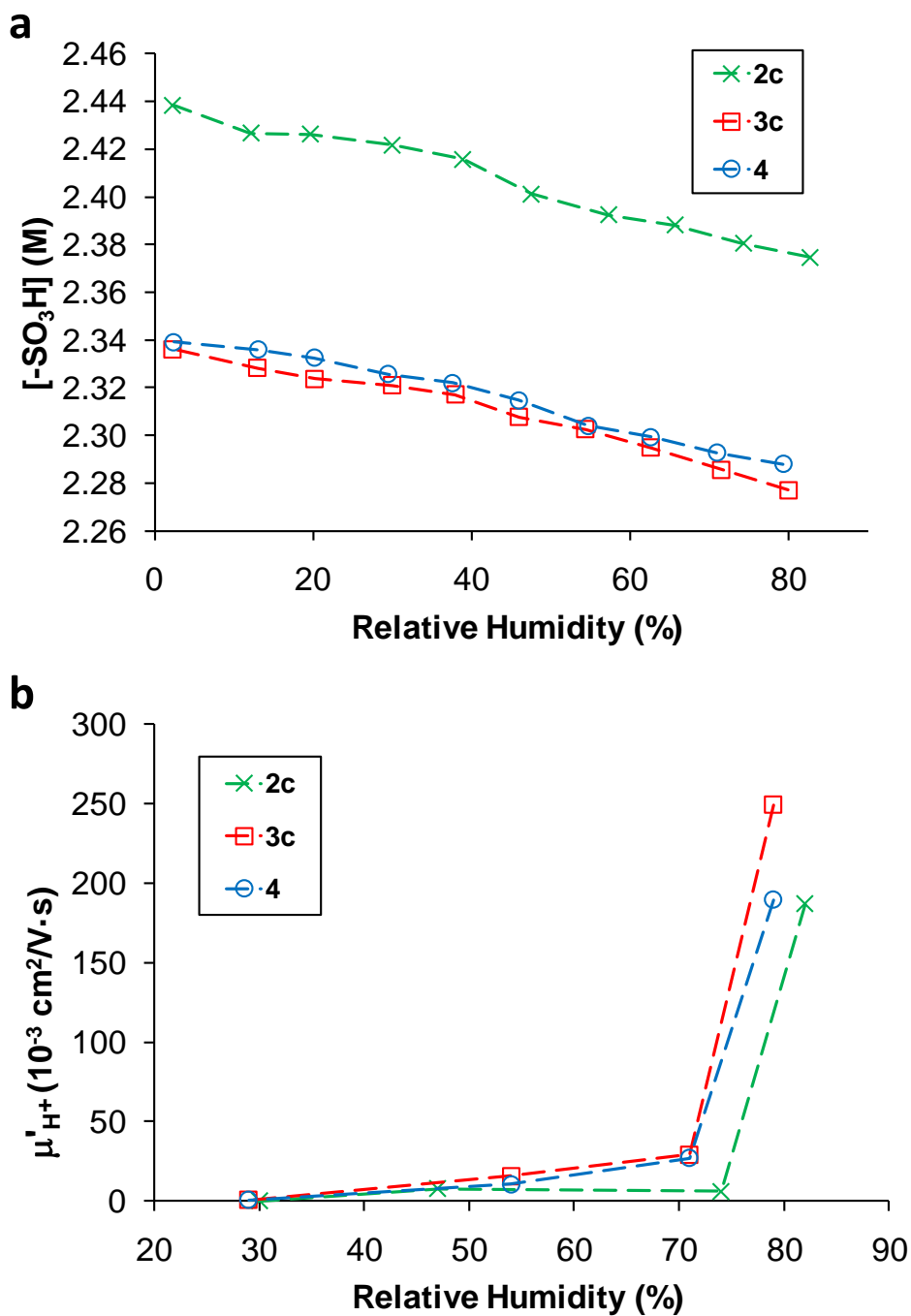
Figure 31: a) Sulfonic acid concentration of membranes of **2c** and blends using **3c** and **4** at varying relative humidity at 80 °C. b) Proton mobility of the same membranes at varying humidity at 80 °C. These parameters calculated using Equations 15 and 16, Section 2.5.3.10.

However, it has also been visually observed that when the conductivity of **2c** is measured at 80 ⁰C, RH = 90%, the membrane undergoes a deformation due to the constraints of the conductivity measurement cell (Figure 32a, cell design shown in Figure 38). This deformation is not as noticeable for the blend membranes (Figure 32b,c).   Furthermore, the conductivity of **2c** drops significantly over time when the membrane is exposed to 80 ⁰C, RH = 90% (Figure 33). The expected cause of the decrease in conductivity for **2c** is the mechanical deformation, which could cause cracks or voids in the membrane and has been shown to affect conductivity in other systems.[89]
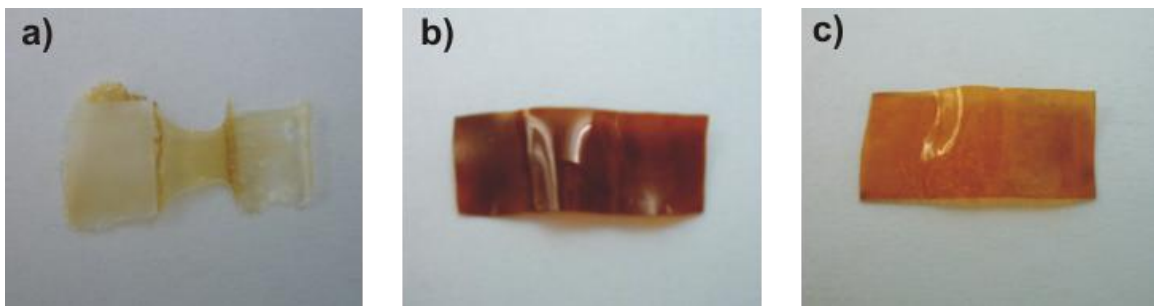
Figure 32: Photographs showing the mechanical degradation of a) pure SPEEK 2c compared to SPEEK:PBI blends of b) 3c and c) 4.
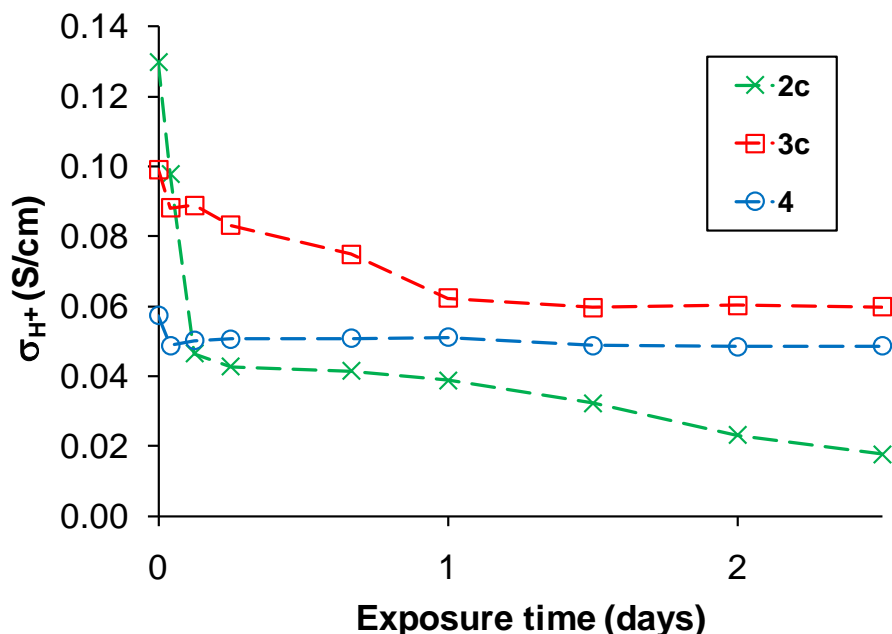
Figure 33: Chart showing the decrease in proton conductivity over time for membranes of **2c** and blends using **3c**, and **4**. Data shown for one representative sample.

2.4 Conclusion and Future Work

The series of sulfonated polybenzimidazole polymers prepared in this work were much more resistant to swelling than many other classes of sulfonated polymer. However, they lacked significant proton conductivity, even at their most sulfonated, due to acid-base, intermolecular interactions between the sulfonic acid groups and the benzimidazole, which reduced effective proton mobility. When blended with high IEC SPEEK, they improve the mechanical stability of these otherwise highly swellable polymers. The impact of the acid-base cross-linking on reducing swelling of the membranes was most noticable at elevated temperature where pure SPEEK membranes completely dissolve.

Comparisons of sulfonated to non-sulfonated PBIs in SPEEK:PBI blends revealed an increase in conductivity and water uptake for the sulfonated form

when plotted against PBI content due to the marginally higher IEC. However, when examined against the IEC alone, no advantage of the sulfonated form was observed; in fact, pure SPEEK membranes possessed the highest proton conductivity of all the membranes studied in this work. This is because PBI/SuPBI present in the membranes lowers the effective mobility of the protons.

At elevated temperature (80 ºC) and relative humidity (90%), a blend containing the sulfonated cross-linker (**3c**) exhibits a significantly higher level of proton conductivity than **2c**, as well as blends using **4** and **5**. This is in contrast to the values seen at room temperature for water-soaked membranes. The higher conductivity level may be due to greater effective proton mobility for the blend containing **3c** under these conditions. It has also been observed, however, that the **2c** membrane deforms significantly when exposed to this environment whereas the blend membranes do not.

Future work in these systems can be directed toward understanding why the blends using the sulfonated PBI show increased proton conductivity at elevated temperatures compared to the blends using non-sulfonated PBI of comparable IEC. One theory that may have interesting implications, is that the sulfonate group on the phenylene ring reduces the basicity of the imine nitrogen by withdrawing electrons from the benzimidazole ring. This would allow a larger number of protons to be involved in transport and could be responsible for the higher conductivity found for the sulfonated PBI blends. An example of this reduction in basicity has been shown for substituted benzimidazoles (Figure 34) where an electron-withdrawing group is added to the C2 position. At higher

temperature, this effect may be enhanced (c.f. increase in pH of water as temperatures increase), which could result in the differences in conductivity found for the blends using sulfonated and non-sulfonated PBI.

$pK_{BH+} = 4.68$ $pK_{BH+} = 5.41$ $pK_{BH+} = 6.10$
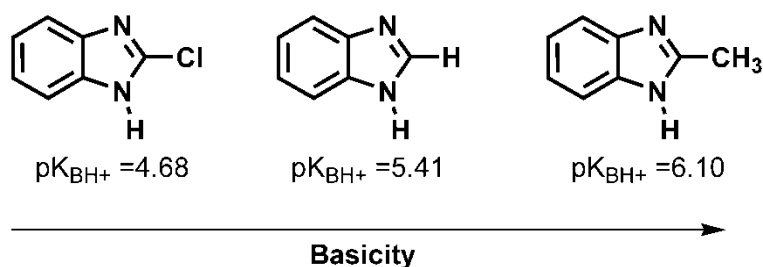
Basicity

Figure 34: **Structures and pK_{BH+} illustrating the effect of electron withdrawing (-Cl) or donating (-CH$_3$) groups on the basicity of the imine nitrogens in 2-substituted benzimidazoles.[87,90]**

This effect could be studied further by examining the differences in conductivity between PBI synthesized using a meta sulfonated dicarboxylic acid (as done in this work, compound **7**) and using an ortho sulfonated dicarboxylic acid (2-sulfoisophthalic acid). In the polymer, the position ortho to the sulfonic acid would be the most affected by its electron withdrawing effect and may result in a less basic imine nitrogen.
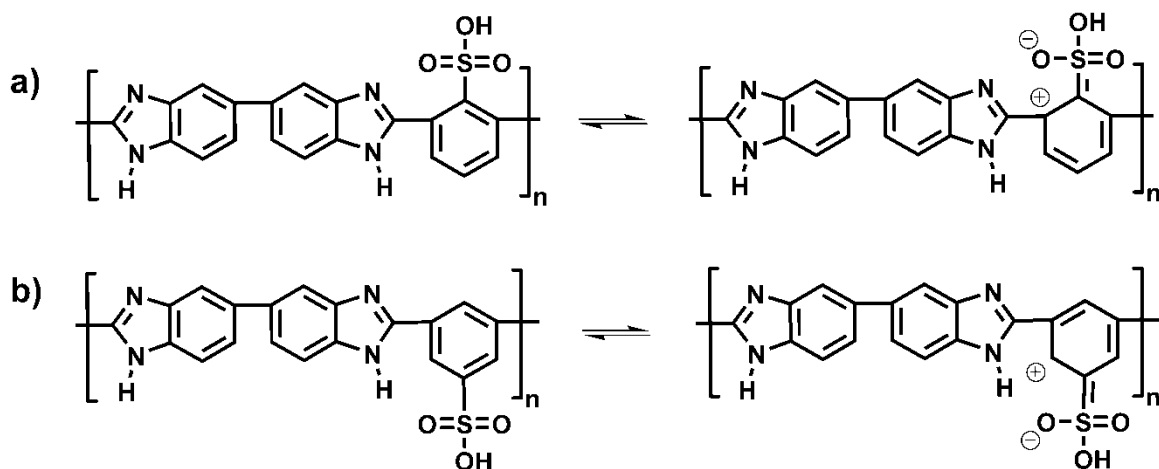
Figure 35: Illustration showing the increased positive character of carbon closest to benzimidazole ring for ortho-sulfonated (a) m-phenylene unit compared to meta-sufonated (b).

Interestingly, at higher water content, the sulfonic acid groups would be deprotonated, lessening their electron withdrawing effect. This would result in an increase in the basicity of the imine and strengthen the cross-linking, possibly allowing this system a means of controlling swelling at high water content, while maximizing free proton concentration when water is scarce.

2.5 Experimental

2.5.1 Synthesis

2.5.1.1 Materials

All chemicals were obtained from Sigma-Aldrich Canada Ltd. unless stated otherwise. Concentrated sulfuric acid, 2,2-bis(4-carboxyphenyl)-hexafluoropropane and poly(ether ether ketone) were obtained from Anachemia, TCI America and Victrex, respectively. All chemicals were used as-received.

Deionized H_2O was purified using a Millipore Gradient Milli-Q® water purification system to a resistance of 18 MΩ.

2.5.2 Instrumentation

2.5.2.1 Nuclear Magnetic Resonance (NMR)

^{1}H NMR spectra were obtained on a Varian Unity Spectrometer operating at 500 MHz. The compounds were dissolved in deuterated dimethylsulfoxide (DMSO-d$_6$) at a concentration of ~30 mg/mL. For sulfonated PBI and SPEEK, the potassium or sodium salts were used due to its higher solubility compared to the acid form.

2.5.2.2 Fourier Transform Infrared Spectroscopy (FTIR)

Fourier transform infrared spectroscopy (FTIR) was performed on a Bomem® FTLA2000-154 FTIR system. Sulfonated PBIs (potassium form) were drop-cast from a dimethylacetamide (DMAc) solution on a NaCl disk and dried under vacuum at 80 °C for 2 h prior to measurements.

2.5.2.3 Molecular Weight Determination

Molecular weight determinations were done using a Waters® gel permeation chromatograph in dimethylformamide (DMF) at 80 ºC and an elution rate of 1.0 mL/min. The columns were calibrated with polystyrene standards.

2.5.2.4 Elemental Analysis

Elemental analyses were performed by Mr. Frank Haftbaradaran using a Carlo Erba model 1106 CHN analyzer.

2.5.2.5 Vapour Sorption

Vapour sorption data of the IEC~ 2.0 meq/g were collected using a Surface Measurement Systems DVS Advantage dynamic vapor sorption (DVS) analyzer. Data collected from this instrument is reported without error bars, as it is the result of one representative measurement for each sample. In addition, due to the length of time required to perform these measurements and the similarity in structure and properties found for the blends containing **4** and **5**, no blend of **5** was tested.

2.5.2.6 Synthesis of SPEEK (2a-e)

The sulfonation of PEEK was performed according to literature procedures.[52,91] 10.0 g of PEEK was dissolved in stirred concentrated sulfuric acid at 45 ºC. Once dissolved, a sample was taken and the temperature was raised to 80 ºC. The initial time (t = 0) for the reaction was defined as the time at which all of the PEEK was dissolved in the sulfuric acid. Samples were removed periodically as the sulfonation progressed with the last sample being taken 4 h after the polymer dissolved (see Table 1). The dissolved polymer was precipitated into deionized water and filtered, followed by a thorough washing of the solid with additional deionized water. Conversion to the Na^+ form of the polymer was achieved by stirring in an aqueous NaOH solution for 24 h. Polymer **2e**: ^{1}H NMR (Figure 25) (500 MHz, DMSO-d_6) of **2e-Na$^+$**: δ 7.84 ($H_{A'}$, t, 9.1Hz, 2.1H), 7.77(H_A, t, 9.1Hz, 2.1H), 7.53(H_F, d, 3.0Hz, 1.0H), 7.24(H_E, dd, 3.1Hz, 9.0Hz, 1.1H), 7.18 ($H_{B'}$, d, 8.5Hz, 2.1H), 7.13 (H_D, d, 8.7Hz, 1.0H), 7.04 (H_B, d, 8.7Hz, 2.1H). FTIR (DMAc solution cast onto NaCl plate): 3069 (Ar-H stretch),

1646 (C=O stretch), 1598 (C=C stretch), 1472 (C=C stretch), 1225 (C-O stretch), 1029 (S-O stretch), 626 (C-S stretch)

2.5.2.7 Synthesis of PBI Polymers (3 – 5)

A typical polymerization procedure is described for **3c**: 3,3'-diaminobenzidine **(6)** (0.1246 g, 0.582 mmol), 5-sulfoisophthalic acid **(7)** (0.0931 g, 0.407 mmol), 2,2-bis(4-carboxyphenyl)-hexafluoropropane **(9)** (0.1362 g, 0.174 mmol) and poly(phosphoric acid) (4 mL) were placed in a 50 mL flask. The flask was placed under vacuum and then refilled with N_2. After this process was repeated three times, the contents of the flask were heated to 120 $^{\circ}$C for 48 h and then to 190 $^{\circ}$C for 24 h. The hot solution was poured into Millipore water in order to precipitate the polymer. The product (brown solid) was filtered, washed repeatedly with deionized water and dried under vacuum. Yield: 0.2401g (90%) of a brown solid. Conversion to the K^+ form of the polymer was achieved by stirring in an aqueous K_2CO_3 (2 M) solution for 48 h followed by filtering and washing with deionized water to remove any residual K_2CO_3.

Polymer **3c**: ^{1}H NMR (Figure 23a) (500 Hz, DMSO-d_6) of **3c-K$^+$**: δ 13.33 (1.92H, s, br, amine proton), 9.18 (0.68H, s, H_E), 8.69 (1.26H, s, H_D), 8.39 (1.16H, s, H_F), 8.03 (1.00H, s, H_A), 7.83 (1.36H, s, H_B), 7.64 (2.61H, s, $H_{C,G}$). FTIR (DMAc solution cast onto NaCl plate): 3200 v.br (N-H stretch), 1606 (C=N stretch), 1440 (benzimidazole ring deformation), 1044 (S=O symmetric stretch). Elemental analysis: Calc'd (**3**·2H_2O): C 58.31, H 3.53, N 11.99. Found: C 57.70, H 3.50, N 11.62. Molecular weight (GPC) M_n= 4.4 x10^4 Da, M_w/M_n= 1.1.

Polymer **4**: ^{1}H NMR (Figure 23b) (500 Hz, DMSO-d$_6$) of **4-K$^+$**: δ 13.40 (1.83H, s, br, amine proton), 9.22 (0.67H, s, H$_E$), 8.39 (1.79H, s, H$_{D,F}$), 8.07 (1.00H, s, H$_A$), 7.80 (1.76H, s, H$_{B,H}$), 7.64 (2.57H, s, H$_{C,G}$) FTIR (DMAc solution cast onto NaCl plate): 3200 v.br (N-H stretch), 1610 (C=N stretch), 1438 (benzimidazole ring deformation). Elemental analysis: Calc'd (**4**·2H$_2$O): C 65.75, H 4.13, N 13.30. Found: C 68.19, H 3.89, N 13.65. Molecular weight (GPC) M$_n$= 3.9x10^4 Da, M$_w$/M$_n$= 1.5.

Polymer **5**: ^{1}H NMR (Figure 2a) (500 Hz, DMSO-d$_6$) of **5-K$^+$**: δ13.14 (1.90H, s, br, amine proton), 8.37 (2.10H, s, H$_F$), 7.92 (1.00H, s, H$_A$) 7.74 (1.08H, s, H$_B$), 7.62 (3.13H, s, H$_{C,G}$). FTIR (DMAc solution cast onto NaCl plate): 3200 v.br (N-H stretch), 1616 (C=N stretch), 1442 (benzimidazole ring deformation). Elemental analysis: Calc'd (**5**·2H$_2$O): C 61.05, H 3.51, N 9.82. Found: C 61.91, H 3.39, N 10.01. Molecular weight (GPC) M$_n$= 4.0 x10^4 Da, M$_w$/M$_n$= 1.9.

2.5.2.8 Membrane Preparation

Membranes of **3-K$^+$** and **2-Na$^+$** were cast from 3.5 wt. % and 6.5 wt. % polymer in N,N-dimethylacetamide (DMAc) solutions into flat bottom Petri dishes, heated at 80 °C overnight and then under vacuum at 50 °C for 2 h. The films were removed from the slides by brief immersion in water. Conversion to the acid form was achieved by soaking the films in 2 M HCl overnight at room temperature. Membranes were then washed with deionized water and dried again under vacuum to remove residual HCl. Blended membranes of **2e-Na$^+$** and **3c-K$^+$**, **4-K$^+$** or **5-K$^+$** were obtained by combining appropriate amounts of 6.5 wt. % of **2e-Na$^+$** in DMAc and 3.5 wt. % of the corresponding PBI polymer in DMAc.

Acid conversion and film casting were as per the procedure for the pure membranes.
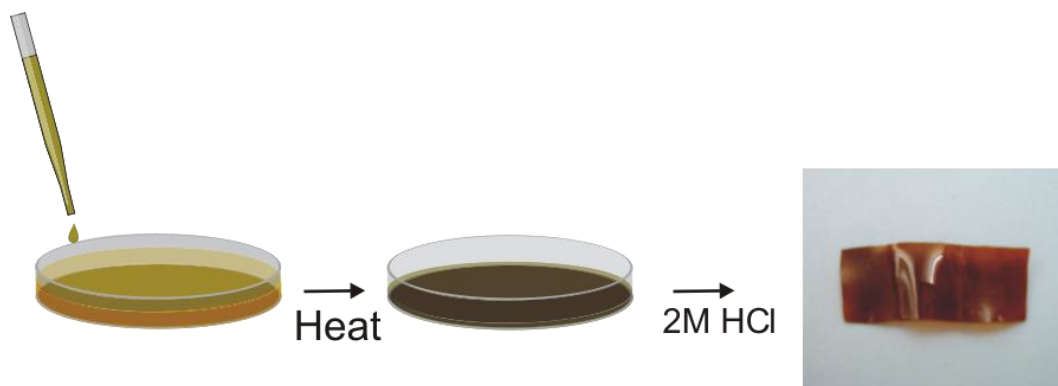
Figure 36:   Scheme detailing membrane casting and cross-linking procedure.

2.5.3 Characterization Procedures

The data obtained by the methods shown below were determined, where possible, by calculating the average of three samples from the same cast membrane of each type.

2.5.3.1 Membrane water weight uptake (WU)

After casting, membranes were soaked in 2 M HCl for 24 h, then rinsed and soaked for 2 h at room temperature in deionized H_2O. The membranes were dried in a vacuum oven at 80 °C for 24 h.   The dry membranes were then weighed, soaked again in deionized H_2O for 24 h, and weighed again.   Water uptake is reported as a percentage and determined by taking the weight difference between the wet and dry films ($W_{wet} - W_{dry}$) and dividing it by the dry film weight (W_{dry}).   The equation is given below:

$$WU = \frac{w_{wet} - w_{dry}}{w_{dry}} \times 100\% \qquad (2)$$

2.5.3.2 Membrane water volume uptake (VU)

The acidified membranes were dried under vacuum at 80 °C for 24 h and then measured twice for each membrane, once after drying and then again after soaking in Millipore water for 24 h at room temperature. Similar membranes were then soaked in 50 °C or 80 °C water for 8 h to examine their stability at higher temperatures. Membrane thickness was measured with Series 293 Mitutoyo Quickmike Series calipers while length and width were measured with Series 500 Mitutoyo Digimatic Calipers. VU was calculated using equation 3:

$$VU = \frac{V_{wet} - V_{dry}}{V_{dry}} \times 100\% \qquad (3)$$

2.5.3.3 Membrane water volume fraction (X_v)

The membrane water volume fraction was calculated according to the following equation:

$$X_v = \frac{V_{water}}{V_{wet}} \qquad (4)$$

where $V_{water} = (w_{wet} - w_{dry})/\rho_{water}$. The density of water was assumed to be 1 g·mL^{-1}.

2.5.3.4 Ion exchange capacity from titration (IEC$_{Titr}$)

Polymers in the acid form were dried overnight at 80 °C under vacuum, weighed and then immersed in 2 M NaCl for 1 h. Titrations were carried out using 3 mM NaOH as a titrant (standardized against dry potassium hydrogen phthalate) and phenolphthalein as indicator. The reported titrated ion exchange capacities are the average of three separate titrated samples. Equation 5 was

used to calculate the ion exchange capacity. The volume of NaOH used to reach the end point (V_{NaOH}), the concentration of the NaOH solution used ([NaOH]) and the dry weight of the membrane (w_{dry}) were needed to calculate the ion exchange capacity.

$$IEC_{titr} = \frac{V_{NaOH} \times [NaOH]}{w_{dry}} \qquad (5)$$

2.5.3.5   Ion exchange capacity from ¹H NMR (IEC$_{NMR}$)

¹H NMR was used to confirm the polymer structure[92] and to determine the ion exchange capacity (IEC$_{NMR}$) and compare the results with the titration method (IEC$_{Titr}$).

For SPEEK, **2**(**a-e**), we determined the degree of sulfonation (DS) by comparing the area of the H_F peak with the H_A and $H_{A'}$ peaks (Figure 25). DS was calculated from Equation 6.

$$DS = \frac{\text{Integral } H_F}{\frac{1}{4}(\text{Integral } H_A + H_{A'})} \qquad (6)$$

The IEC can then be determined from the molecular weights of the polymer repeat units and the DS using equation 7.

$$IEC_{SPEEK} = \frac{DS}{DS(\text{MW of sulfonated}) + (1\text{-}DS)(\text{MW of unsulfonated})} \qquad (7)$$

For polybenzimidazoles, **3**(**a-d**), **4**, **5**, we determined the percentage of segment n (A) in the polymer by dividing the integral of H_D (Figure 23) the integral of H_A .

$$A = \frac{\text{Integration } H_D}{\text{Integration } H_A} \qquad (8)$$

The percentage of the segment m (B) becomes

$$B=1-A \qquad (9)$$

Then IEC_{PBI} is calculated using Equation 10:

$$IEC_{PBI}=\frac{A(\text{\# of } SO_3H \text{ in n})+B(\text{\# of } SO_3H \text{ in m})}{(A)MW_n+(B)MW_m} \qquad (10)$$

Where MW_n is the molecular weight of segment n, MW_m is the molecular weight of segment m (Figure 37).
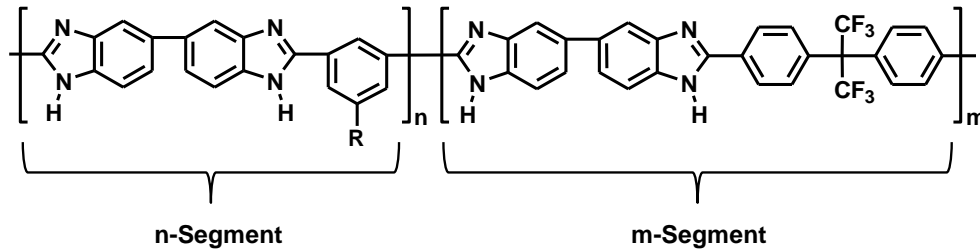
n-Segment   **m-Segment**

Figure 37:   Diagram defining the 'n' and 'm' segments.

2.5.3.6 Available basic sites of PBI (ABS)

Due to the basic nature of PBI, the conventional method of calculating IEC is not effective. For a more accurate prediction of the IEC of blended systems, the available basic sites per gram are calculated. ABS is calculated using equation 11:

$$ABS=\frac{A[(TBS)-(\text{\# of } SO_3H \text{ in n})]+B(TBS)}{MW_n+MW_m} \qquad (11)$$

Where TBS is the total number of basic sites in each repeat unit, note that there are no sulfonic acid groups in segment m.

2.5.3.7 Calculated IEC of the blend systems (IEC$_{BLEND}$)

The IEC values of the blended membranes were calculated from the IEC value of the particular SPEEK used in the blend, the ABS of the PBI and the percentage of the two in the blend.

$$IEC_{BLEND}=\%_{SPEEK}(IEC_{SPEEK})-\%_{PBI}(ABS) \qquad (12)$$

2.5.3.8 Lambda (λ)

The Lambda value represents the average number of H_2O molecules per sulfonic acid group. These were calculated using water uptake data (WU), the molecular weight of water (MW$_{water}$), and the IEC$_{Titr}$ using Equation 13:

$$\lambda=10\frac{WU}{(MW_{water})(IEC_{titr})} \qquad (13)$$

The multiplier 10 takes into account the fact that WU is a percentage and IEC is in meq·g^{-1}.

2.5.3.9 Proton conductivity

Proton conductivity was measured using AC impedance spectroscopy with a Solartron 1260 frequency response analyzer (FRA) employing a transverse two-electrode configuration. Acidified membrane samples were soaked in deionized water overnight and were cut to the required dimensions (0.5 cm ×1.5 cm). These were then laid across two Pt electrodes (0.5 × 1 cm) 0.5 cm apart fixed in place by adhering them to a PTFE block. Another block was placed on top and two clamps were used to hold the assembly together during measurement (Figure 38). Both PTFE blocks were vented with rectangular cut-

aways to allow for membrane hydration. Membranes were kept hydrated by periodically wetting them with Millipore water.
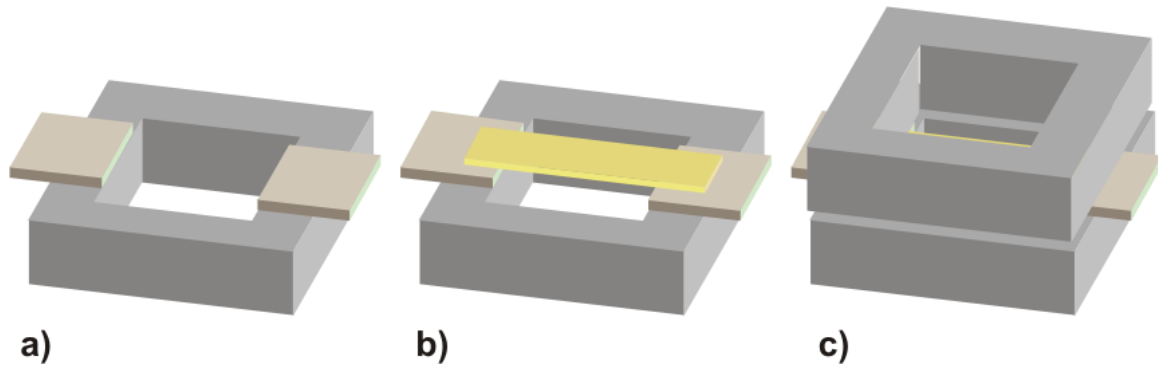
Figure 38: **Electrode apparatus for membrane impedance measurements. a) PTFE block with platinum contacts, b) same block with membrane, c) membrane held in place with second PTFE block.**

Two wires fitted with alligator clips connected the probe to the frequency response analyzer and ionic resistance was measured by applying a 100 mV sinusoidal AC voltage between the two platinum electrodes over 10 MHz – 100 Hz frequency range and measuring the AC resistance (*i.e.*, impedance). Measurements were collected every half hour during equilibration until constant ionic resistance was obtained. Data was analyzed using Zplot software (Scribner).

Ionic resistance was extracted from the impedance data and fitting was performed by non-linear least squares regression to a standard Randles equivalent circuit model. The data collected for a typical measurement is shown in Figure 39. The ionic resistance was used to calculate proton conductivity, σ_{H^+}, according to the following relationship (Equation 14):

$$\sigma_{H^+} = \frac{L}{R_m A} \qquad (14)$$

where L is the spacing between the Pt electrodes (1.0 cm), A is the cross sectional area of the membrane (w × h), and R_m is the ionic resistance of the membrane.
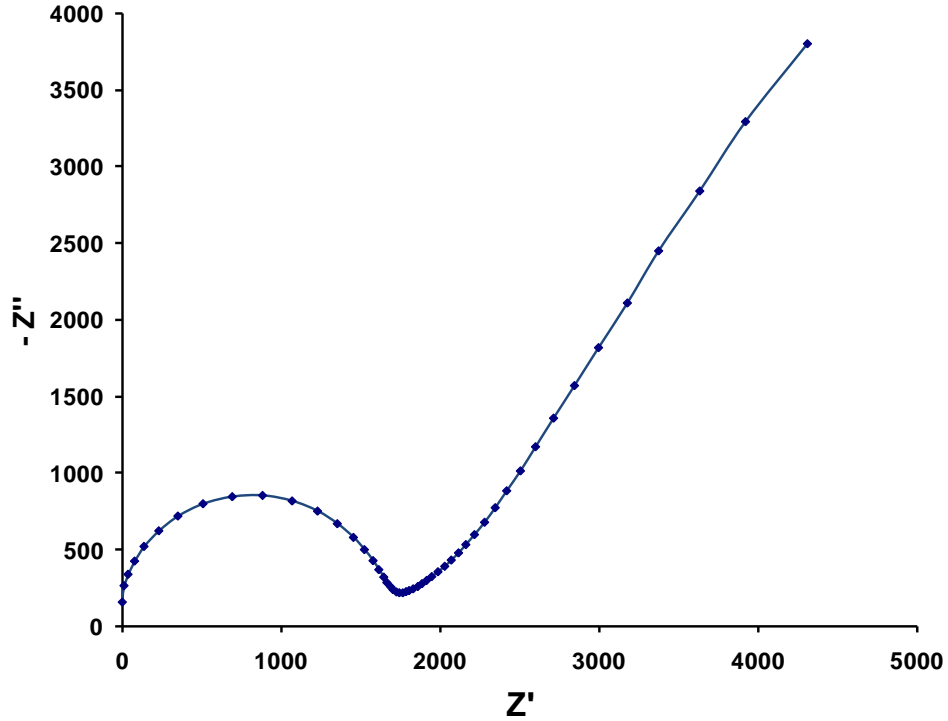
Figure 39: Typical Nyquist plot for AC impedance spectroscopy measurement of an membrane containing an 8 wt.% blend of **3c** in SPEEK (**2c**).

2.5.3.10 Acid Concentration ([-SO₃H]) and Effective Proton Mobility (μ'ₕ₊)

Acid concentrations for the membranes were determined according to Equation 15:

$$[-SO_3H] = \frac{IEC_{titr} \times w_{dry}}{V_{wet}} \qquad (15)$$

The effective proton mobility was then calculated from Equation 16:

$$\mu'_{H^+} = \frac{\sigma_{H^+}}{F[-SO_3H]} \qquad (16)$$

where F is Faraday's constant.

3: MODIFIED PBI FOR USE IN ANION EXCHANGE MEMBRANES

3.1 Overview

This section describes an anion exchange material based on poly(benzimidazole) and its stability in alkaline environments. The methods used in this study are described in Experimental Section 3.5. The materials used for this research are tabulated in Appendix Table A2.

3.2 Introduction

Anion exchange membranes (AEMs) are a class of materials that allows for the transport of anions through their structure. These materials contain bound cationic sites with mobile negatively-charged counter ions (Figure 40).
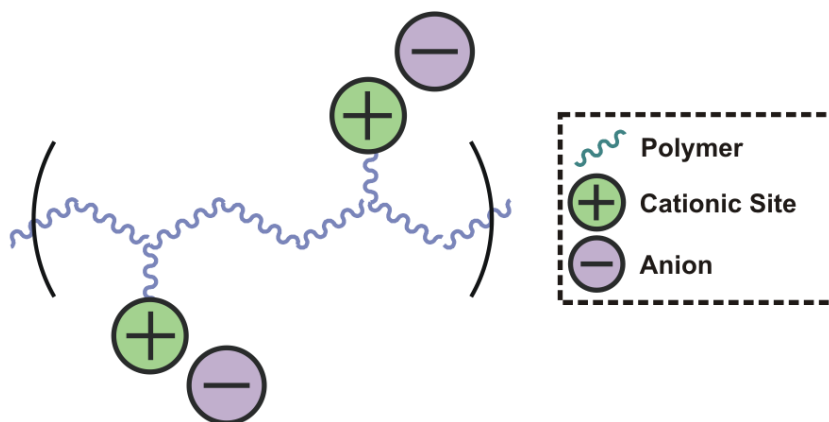
Figure 40:   Illustration depicting bound cationic sites and mobile anions in an AEM.

AEMs have found use in many fields, such as electrodialysis, ion chromatography and alkaline anion exchange membrane fuel cells (AAEMFC).

3.2.1 Electrodialysis

Electrodialysis is a method of purifying water that relies on a series of chambers separated with an alternating arrangement of anion and cation exchange membranes (Figure 41).[93] An ion containing solution, such as sea water, is used as the electrolyte and current is applied to the cell through two electrodes found in the outer chambers. Operation of this cell results in water being reduced at the cathode to form H_2 and OH^-, and O_2 and H^+ being formed at the anode. The charge balance in the chamber nearest the cathode becomes too negative and an anion moves out of this chamber through the AEM in order to balance the charge. Now the second chamber is unbalanced and draws a cation from the third chamber through the cation exchange membrane. Meanwhile, a similar process takes place at the anode where protons are produced and cations are transported out of the chamber. This results in some chambers having increased concentration of ions and others with decreased concentrations. Through this process, purified water can be collected from the diluted chamber (Figure 41).

Anion exchange membranes used for electrodialysis need to be resistant to swelling as anionic selectivity drops as water uptake rises. If cations are allowed to move through the anion exchange membrane, the driving force for the anion movement is reduced, resulting in a less efficient system and less pure product. Most electrodialysis cells operate with a cation exchange membrane nearest to the anode and an anion exchange membrane nearest the cathode (as depicted in Figure 41). This allows for the transport of the more mobile H^+ and

OH$^-$ ions (Figure 4c and Figure 42 respectively) from the outside chambers, resulting in operation that is more efficient. This however, requires the AEMs used to be stable in high pH environments, as they will be exposed to hydroxide containing solutions.[93]
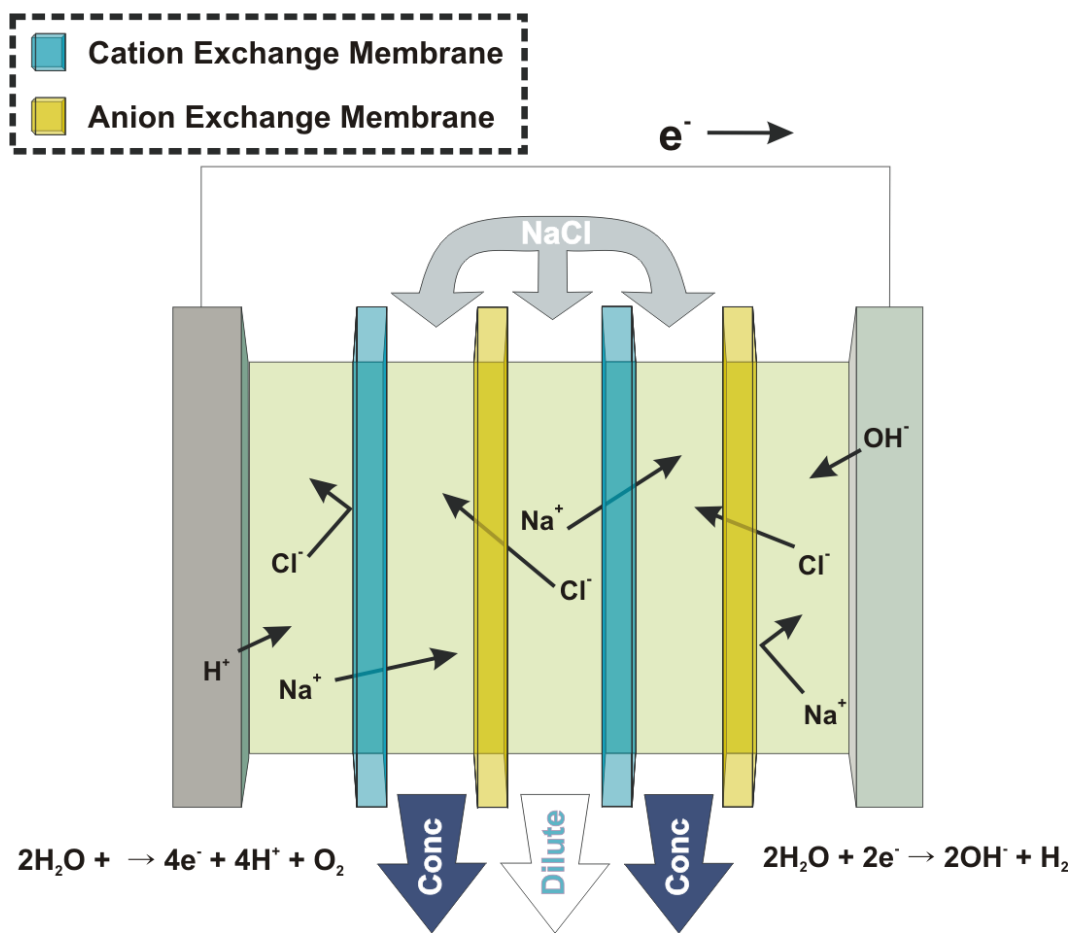
Figure 41: Illustration of an electrodialysis cell used to purify saline water.

3.2.2 Ion chromatography

AEMs are also finding use as the stationary phase in anion exchange chromatography (AEC), a variant of high performance liquid chromatography (HPLC). In AEC, the stationary phase is composed of a porous matrix of an anion exchange resin. The mobile phase is usually an aqueous salt solution (MX) that

flows through the matrix. Before the analysis, the positively charged sites in the anion exchange membrane are all balanced by X^- anions from the eluent. Upon addition of the sample, which contains analyte anions (Y^-), some of the X^- in the stationary phase is exchanged with Y^-. This exchange is reversible and the affinity of Y^- for the stationary phase will control how long it stays bound to the resin. Like other types of chromatography, this attraction to the stationary phase increases the retention time of the analyte. Due to different affinities to the stationary phase for different analytes, the species present in the sample can be separated and analyzed individually.

3.2.3 Alkali Anion Exchange Membrane Fuel Cells

Alkaline anion exchange membrane fuel cells (AAEMFC) function in a similar fashion to PEMFCs discussed in Chapter 1. They harness the electrical current produced from the oxidation of hydrogen to produce water. They differ from PEMFCs in that they transport negatively charged hydroxide ions through the membranes.

Hydroxide ions (OH^-) show high conductivity in water when compared to other anions. This is due to a mechanism similar to the Grotthus mechanism for protons, which allows the negative charge to move through the solution by reorganization of the covalent and hydrogen bonds in water (Figure 42).[94]
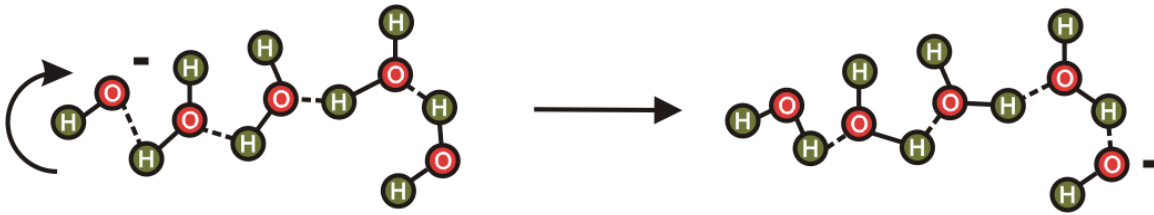
Figure 42: Illustration showing a simplified Grotthus-type mechanism responsible for hydroxide transport in bulk water.

The overall reaction in this system is the same as seen for the PEMFC and as a result is capable of the same potential.[9] The half-cell equations are shown below:

Anode	$4OH^- + 2H_2 \rightarrow 4H_2O + 4e^-$	$E^0 = 0.828$ V
Cathode	$2H_2O + O_2 + 4e^- \rightarrow 4OH^-$	$E^0 = 0.40$ V
Overall	$2H_2 + O_2 \rightarrow 2H_2O$	$E^0 = 1.23$ V
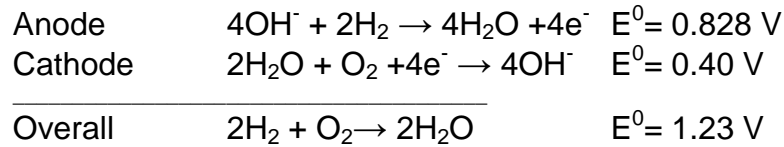
The reaction in the AAEMFC produces hydroxide ions at the cathode, which move through the anion exchange membrane (AEM) to the anode (Figure 43). Electrons move from the anode to the cathode through the external circuit, which balances the charge of the system. At the anode, protons are formed from H_2 and react with the hydroxide from the cathode to form water (c.f. PEMFC, where the cathode is the site of water production).
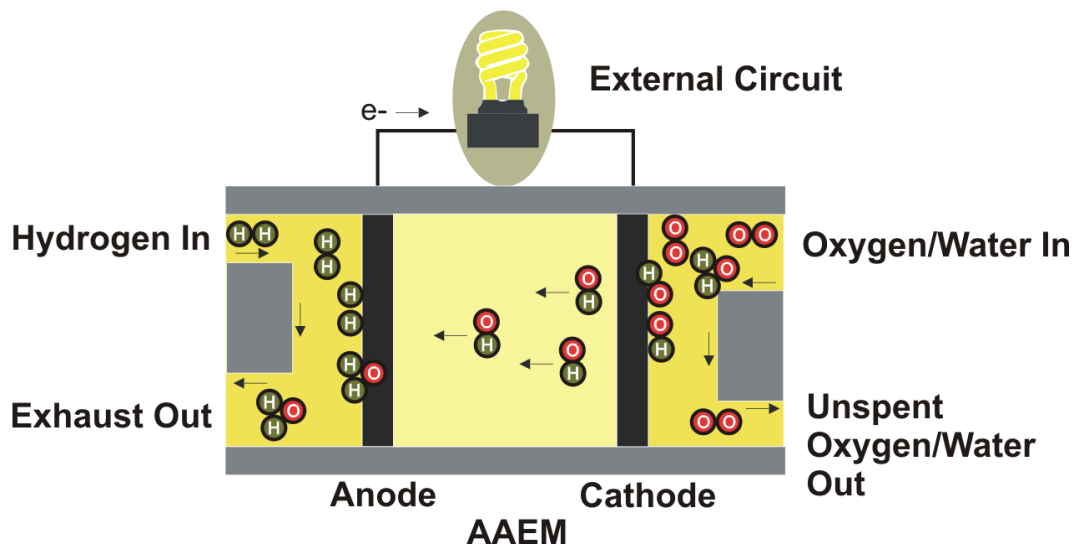
Figure 43: Diagram illustrating the function of an AAEMFC.

AEM for use in these type of fuel cells must be stable in hydroxide. In addition, the membranes must be resistant to swelling because the ability of these membranes to transport ions depends, in large part, on concentration of mobile ions. As was the case in the PEMFCs, membranes that are prone to a high degree of swelling[95] can result in a reduction in overall ion concentration.

3.2.4 Structure and stability

The cationic sites in the polymer are usually quaternized nitrogen groups,[96,97] and often these are formed by the reaction of a chloro group in the polymer with a tertiary amine (Figure 44).
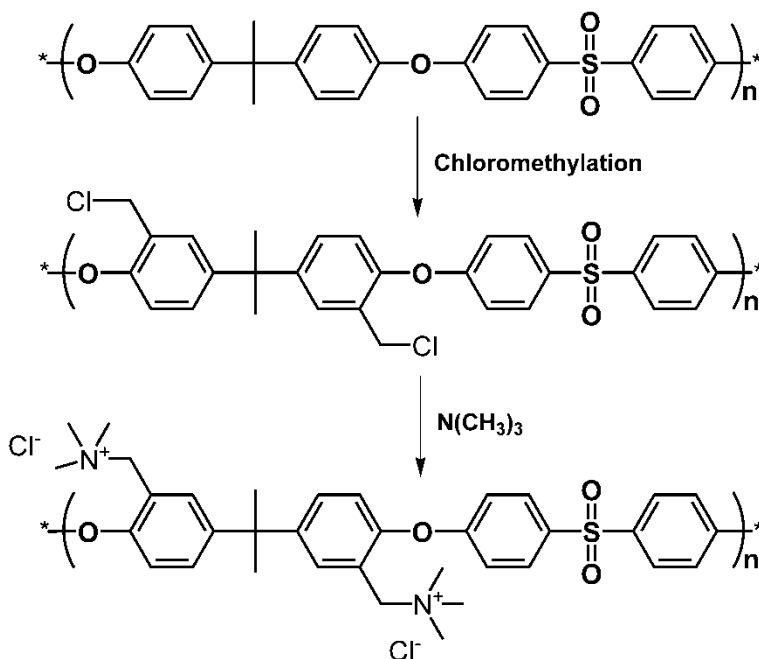
Figure 44: Scheme describing the general method for the formation of quaternized nitrogen groups for use as AEMs.[98]

As mentioned above, AEMs often need to be stable in the presence of hydroxide containing solutions. Unfortunately, the quaternary nitrogen sites found in most anion exchange membranes are attacked by hydroxide ions in a number of ways resulting in elimination of one of the substituents and loss of positive charge.[98,99] The quaternary amines can undergo direct nucleophilic attack by OH⁻, which extracts an alkyl group (Figure 45a), resulting in a bound tertiary amine and an alcohol.[100] In addition, quaternary amines can be degraded through the Hoffmann Elimination, where a β-hydrogen (if present) is removed, resulting in the formation of a double bond and the elimination of a tertiary amine (Figure 45b).[100] As a result, there has been considerable effort to develop hydroxide resistant AEMs.[101-104]
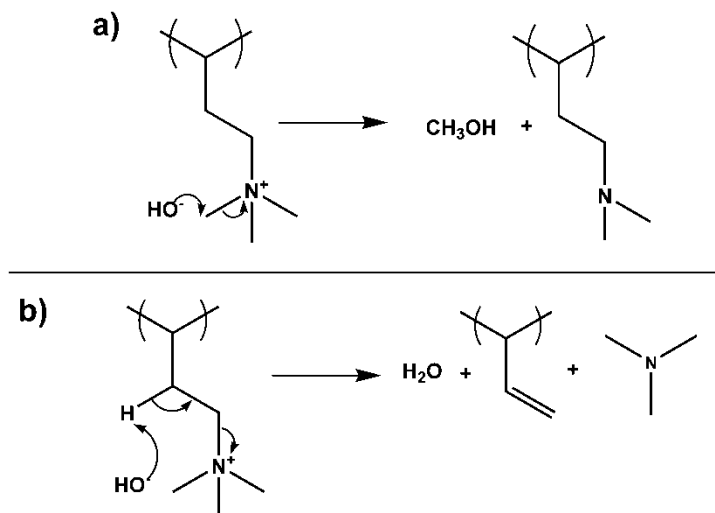
Figure 45: Mechanisms for removal of quaternary nitrogen sites through nucleophilic attack of the a) alkyl groups attached to the hydrogen and b) the β-hydrogen resulting in a Hoffmann Elimination.

3.2.5 Anion exchange membrane material developed for this work

In this work, an anion exchange polymer based on poly(benzimidazole) was synthesized. Unmodified PBI is known to be a chemically and thermally stable material which is resistant to swelling. In this work, cationic sites were imparted to this polymer in a different way: the benzimidazole rings were methylated at both of the nitrogen sites in the imidazole ring,[105] resulting in a benzimidazolium cation and corresponding anion. The resulting polymer, poly(1,3-dimethylbenzimidazolium) (P(DMBI⁺I⁻)) (**11-I⁻**) (Figure 46) had been synthesized previously by Hu et al.[105] as a means to improve the solubility of PBI. However, the anion transport properties of this material were not the focus of the work and were not reported. In addition, we propose a means of increasing the stability of the polymer to hydroxide solutions based on a study of small molecule analogues. A table detailing the numbered compounds used in this work is found in Appendix Table A2.
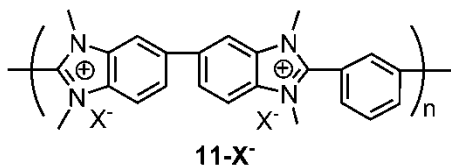
Figure 46: Poly(1,3-dimethylbenzimidazolium) (P(DMBI⁺I⁻)) (**11-I⁻**).

3.3 Results and Discussion

3.3.1 Synthesis and characterization of poly(2,2'-(m-phenylene)-5,5'-dibenzimidazole)) (**10**)

Polymer **10** was synthesised using the method described by Iwakura.[82,84] ^{1}H NMR spectra (Figure 47) obtained for the synthesized polymers were consistent with those found in the literature for similar materials. The peak found at δ13.30 ppm is due to imidazole N-H protons and is in appropriate ratio with the aromatic region in the spectrum (i.e., integral of 2 H for the peak at δ13.30 ppm and 10 H for the aromatic region from δ9.17 - 7.70 ppm).
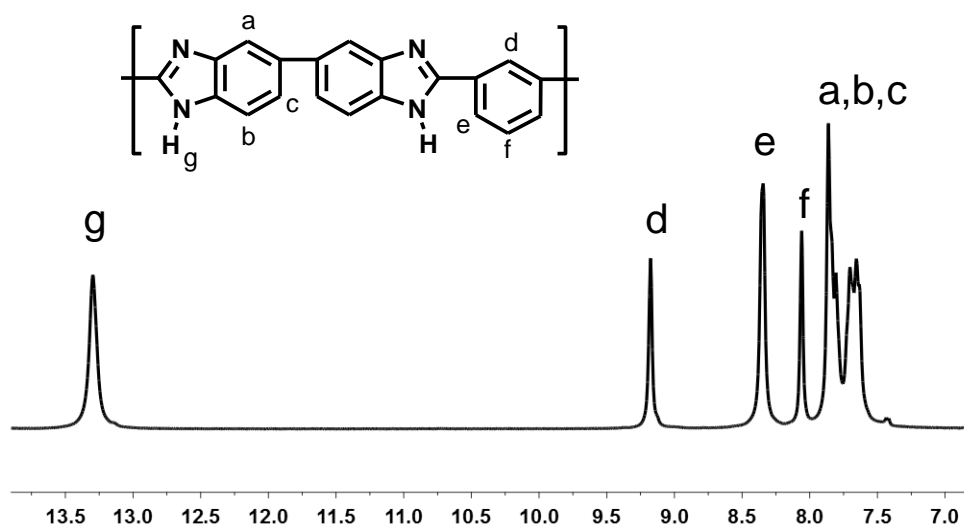
Figure 47: ^{1}H NMR spectrum of **10** showing proton assignments.

80

The FTIR spectrum for **10** (Figure 50a) shows good agreement with results found in the literature. For example, there is a broad absorbance at 2400-3600 cm^{-1}, which correlates to C-H and N-H stretching frequencies. As well, there is a characteristic poly(benzimidazole) peak at 1287 cm^{-1} due to the imidazole ring breathing frequency.

3.3.2 Synthesis and characterization of 11-I⁻
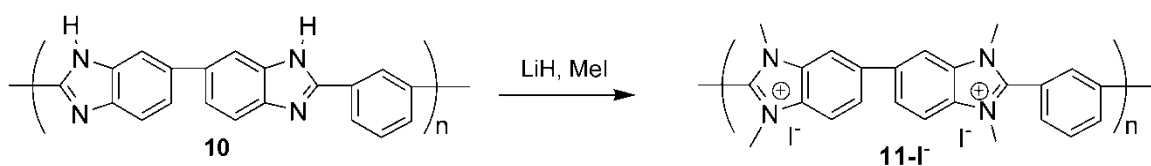
Figure 48:   **Scheme showing the synthesis of poly(dimethylbenzimidazolium iodide) (11-I⁻) from PBI (10).**

Polymer **11-I⁻** was synthesised using the method described by Hu et al.[105] (Figure 48). ^{1}H NMR spectra (Figure 49) for **11-I⁻** were consistent with those found in the literature. The peaks found at δ13.30 ppm in polymer **10** were absent in polymer **11-I⁻**, signalling the removal of these protons. In addition, the spectrum had two new peaks at δ 4.23 and δ 4.15 ppm, which are a result of the methylation. The degree of methylation was determined by the ratio between the methyl peaks (δ 4.23 and δ 4.15 ppm) and the aromatic peaks (δ 8.84 - 8.26 ppm). The resulting degree of methylation was found to be 0.95 methyl groups per nitrogen or 95% methylated.
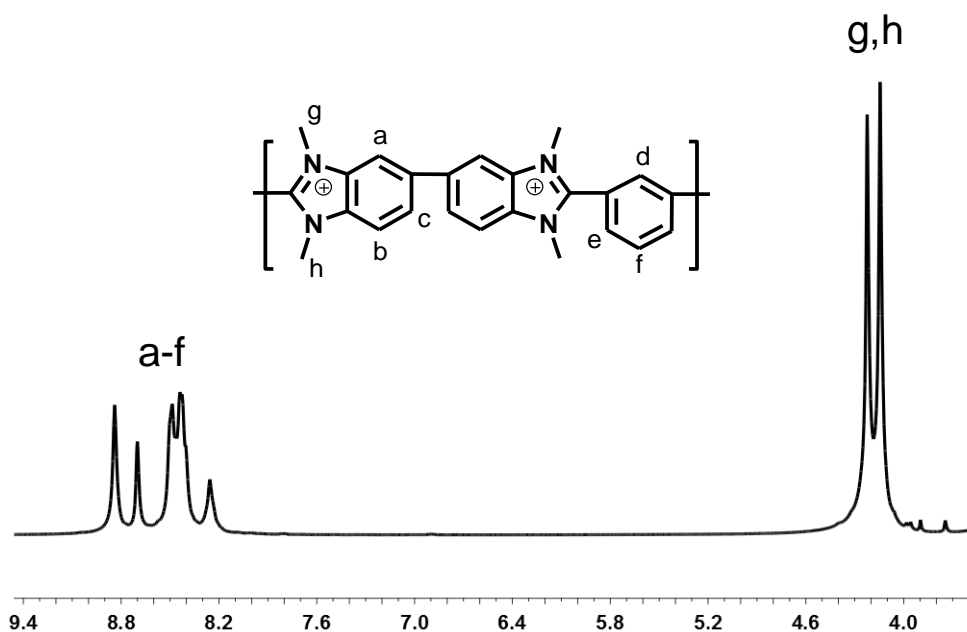
Figure 49: ¹H NMR spectrum of **11-I⁻** showing proton assignments.

Additional investigation was done using FTIR (Figure 50b) which showed a decrease in absorbance around 3200 cm⁻¹, indicative of a reduction in N-H bonds. Corresponding peaks at ~1200 cm⁻¹ were also found in the spectrum for **11-I⁻** due to an increase in C-N bonds.
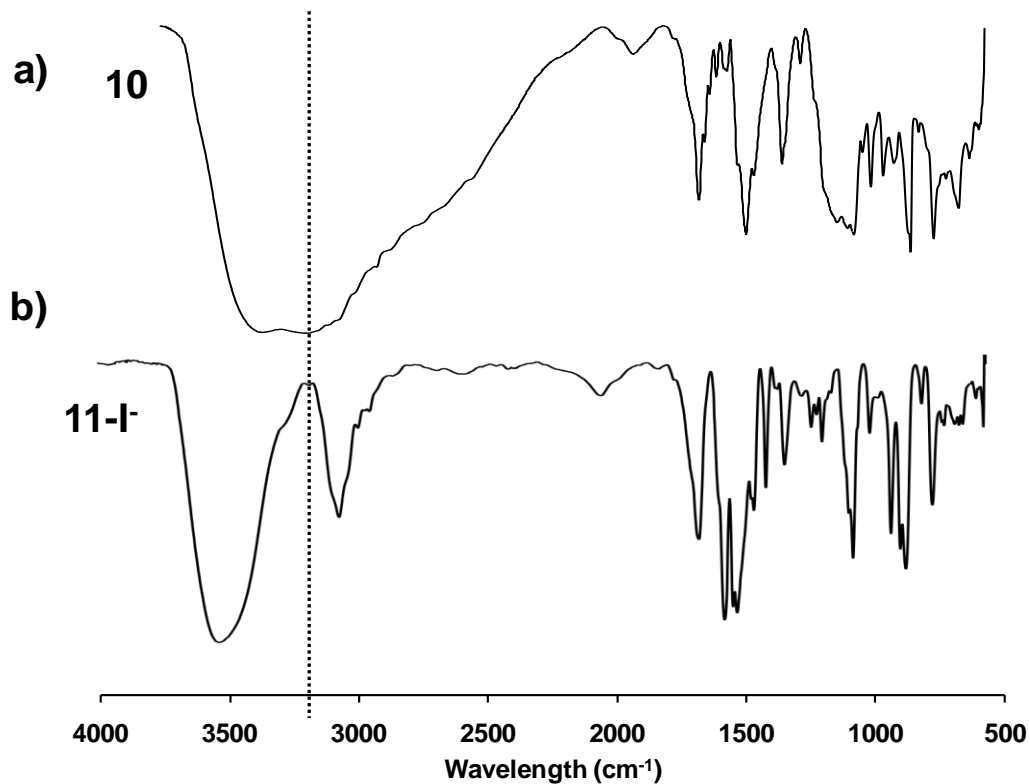
Figure 50: FTIR of a) **10** and b) **11-I⁻** highlighting the decrease in N-H stretching (~3200 cm⁻¹) and an increase in C-N stretching (~1200 cm⁻¹) resulting from the methylation.

3.3.3 Conductivity and water uptake of **11-X⁻**

By exchanging the counter ions in **11-I⁻** through soaking membranes of **11-I⁻** in aqueous potassium salt solutions (KX, where X= Br, Cl, NO_3, HCO_3 or OH), a series of polymer membranes was produced each containing a different counter ion. The water uptake of these membranes varied according to the anion present (Table 8).

Table 8: Anion conductivity of poly(dimethylbenzimidazolium) (**11-X⁻**) membranes.

X⁻	IEC[a] (meq·g⁻¹)	σ_{X^-}[b] [$\sigma \times 10^3$] (10^{-3} S·cm⁻¹)	[X][c] (M)	μ'_{X^-}[d] [$\mu \times 10^5$] (cm²·V⁻¹·s⁻¹)	λ[e] (H₂O/N⁺)
Cl⁻	4.16[f]	7.6±1.1	0.32	24.76	167
Br⁻	3.48[f]	3.2±0.4	4.32	0.72	2
I⁻	2.97	3.3±0.4	4.31	0.72	2
NO₃⁻	3.72[f]	4.9±0.4	4.96	1.02	3
HCO₃⁻	3.74[f]	8.5±0.5	3.68	2.40	5
OH⁻	4.51[f,g]	-[g]	-[g]	-[g]	-[g]

[a] Ion exchange capacity determined by ¹H NMR, based on 92% methylation of nitrogen groups (See Section 3.5.2.7).

[b] Anion conductivity determined using impedance spectroscopy (See Section 3.5.2.11).

[c] Anion concentration (See Section 3.5.2.9).

[d] Anion mobility calculated from conductivity and concentration data (See Section 3.5.2.12).

[e] Number of water molecules per quaternary cationic site (See Section 3.5.2.8).

[f] Based on 100% anion exchange.

[g] Membrane became brittle after exposure to KOH solution.

Water content (λ) and anion conductivity (σ'_{X^-}) were measured andused to calculate lambda values, which ranged from 2 for the iodide and bromide forms to 167 for the chloride. It is thought that anionic size plays a role in the water content; however no consistent trend could be observed. Conductivity of these membranes was in the range of 3.3 to 8.5 mS·cm⁻¹, with the chloride and bicarbonate membrane showing the highest values. Based on mobilites for ions

in bulk water (c.f. 206.4 x 10^{-5} $cm^2 \cdot V^{-1} \cdot s^{-1}$, for OH$^-$ to 79.1 x 10^{-5} $cm^2 \cdot V^{-1} \cdot s^{-1}$ for Cl$^-$),[106] hydroxide containing membranes should give high conductivities. However, attempts to convert this polymer to the hydroxide form were unsuccessful due to the instability of the polymer in alkaline solutions.

3.3.4 Exposure of 11-I$^-$ to hydroxide solution

Conversion of **11-I$^-$** to **11-OH$^-$** by soaking in basic solution results in the decomposition of the polymer resulting in a very brittle material. A possible pathway to this decomposition is illustrated in Figure 51. Reactions of this type have been observed in small molecule benzimidazolium species[107-109] and result from the slightly positive character at the C2 carbon.[107]
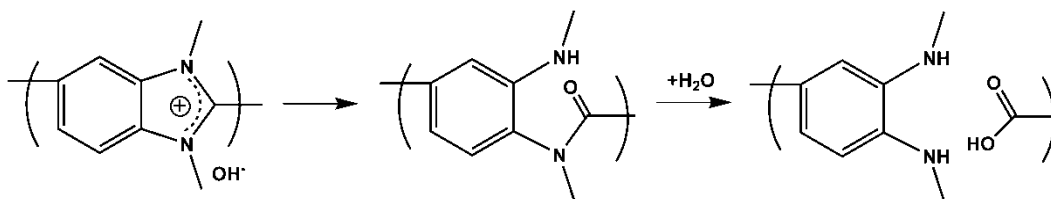
Figure 51: Possible reaction pathway for the decomposition of the benzimidazole ring in the presence of OH$^-$.

Evidence for the decomposition of **11-OH$^-$** was found using FTIR, which indicated a reduction in absorbance at 1590 cm^{-1} (imidazole) and a new absorbance at 1680 cm^{-1}, around the wavelength expected for amide C=O stretches (Figure 52b).
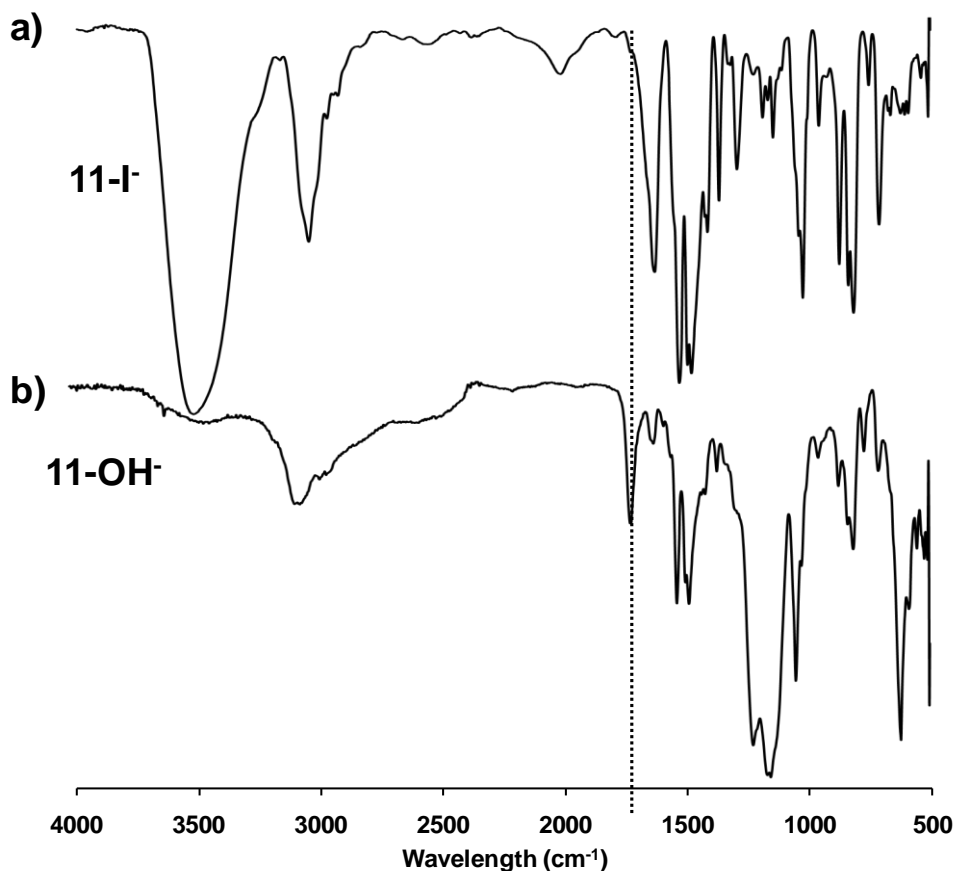
Figure 52: FTIR spectrum of a) **11-I⁻** and b) the resulting material after **11-I⁻** is exposed to OH⁻ (dashed line highlights increased absorbance ~1700 cm⁻¹ inferring a new C=O stretch)

3.3.5 Synthesis and decomposition of **12-OH⁻**

A small molecule analogue of compound **11** was synthesized to examine its stability in basic solutions. This compound, 1,3-dimethylbenzimidazolium (**12**) was synthesized by deprotonating benzimidazole and reacting it with iodomethane according to literature procedures.[110] This yielded the iodide form (**12-I⁻**). ¹H NMR showed the expected spectrum (Figure 53).[110] A singlet with an integral of six protons at ~4 ppm representing the methyl groups attached at the

nitrogen groups. The two peaks found in the aromatic region are expected in this symmetrical molecule.
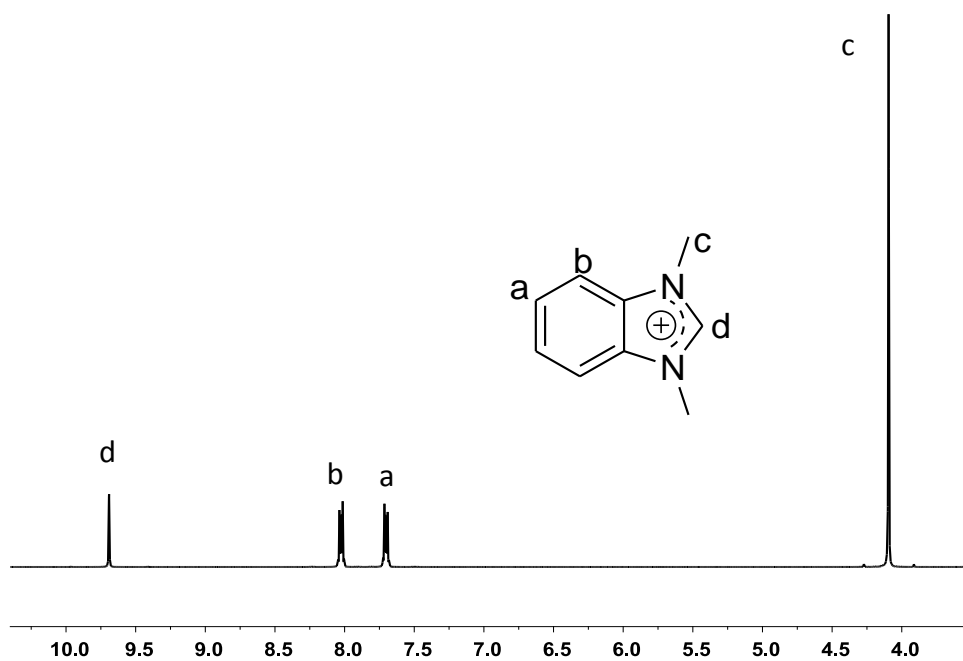
Figure 53: ^{1}H NMR spectrum of **12-I⁻** showing proton assignments.

Upon exposure to strongly basic solution (4 M KOH$_{(aq)}$), **12-I⁻** decomposes through an opening of the imidazole ring. Evidence for this decomposition product (N-methyl-N-(2-methylamino-phenyl)-formamide, **13**) is found in the FTIR (Figure 54) and ^{1}H NMR (Figure 55) spectra.
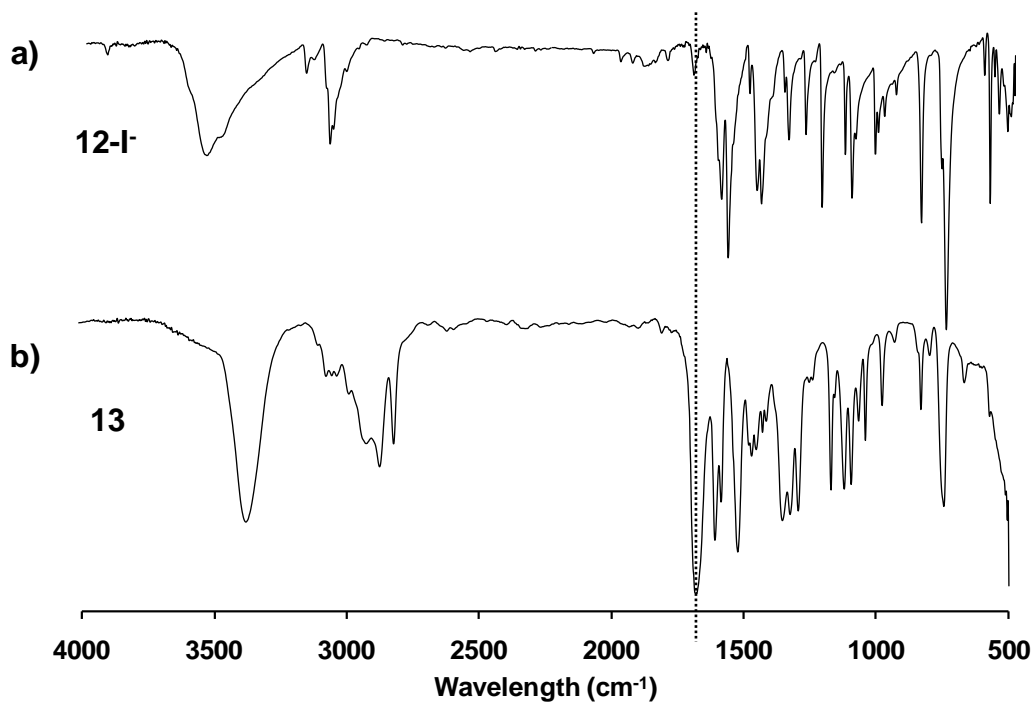
Figure 54: FTIR spectrum **12-I⁻** and **13** showing evidence of a carbonyl group after exposure to OH⁻ solution (C=O, 1680 cm⁻¹).

The ^{1}H NMR shows an increase in peaks expected due to the reduced symmetry in the molecule. In addition, there are new peaks corresponding to aldehyde and amine protons. This spectrum is in agreement with those found in the literature.[109]
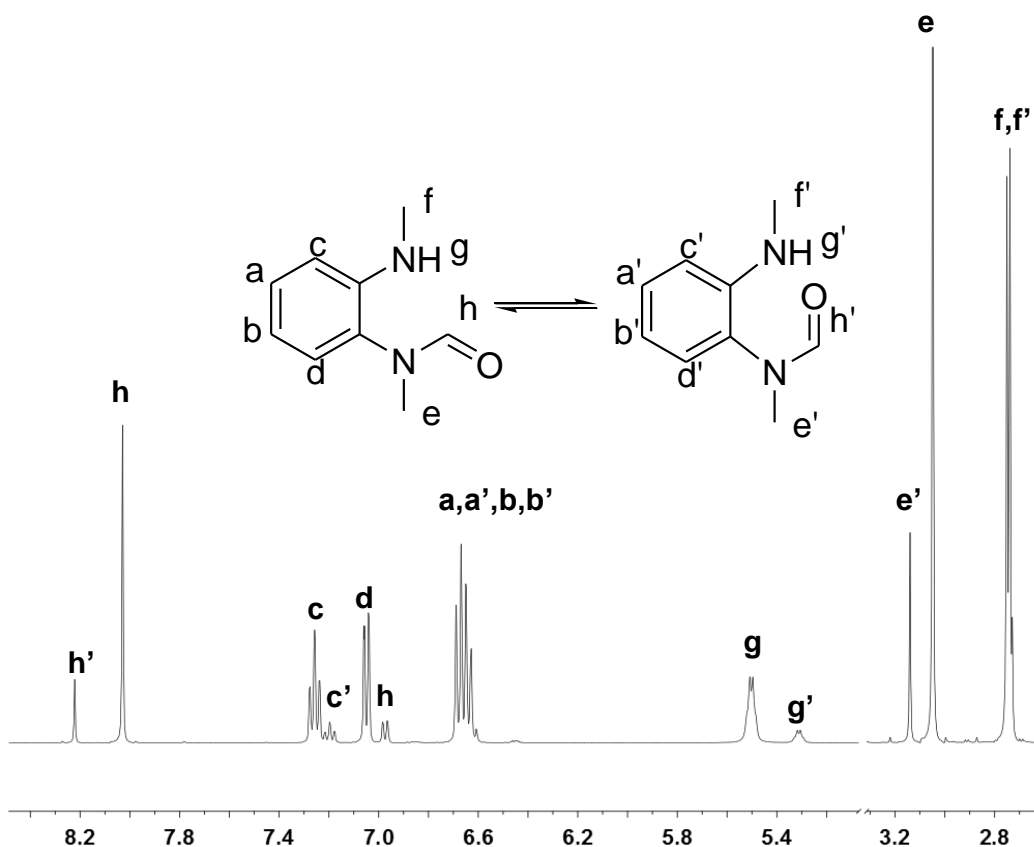
Figure 55: ^{1}H NMR spectrum of compound **13**.

The ^{1}H NMR spectrum found for **13** also shows a series of smaller peaks. These peaks are a result of there being two possible conformations of this molecule caused by of the lack of free rotation around the C-N bond of the amide group (Figure 56). Rotation about this bond is possible, however it is sufficiently slow to not be averaged out on the NMR time scale. As such, the ratio of conformational peaks (E:Z) is dependent on the sterics of each conformation. The ratio found for this compound using the integrals found in the ^{1}H NMR spectrum is 5:1, suggesting a preference for the E conformation about the C-N bond of the amide.

E-conformation   Z-conformation
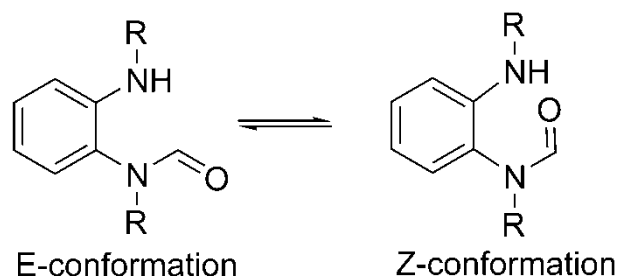
Figure 56: **Diagram illustrating the E and Z conformations possible due to the slow rotation about the amide C-N bond in compound 13.**

3.3.6 Stabilization of benzimidazolium ring

The mechanism for opening the imidazolium ring in basic solution relies on the C2 carbon being at least partially cationic for the OH⁻ to attack. In an effort to stabilize the ring, a more strongly electron-donating group was attached to one of the nitrogens in an attempt to localize the positive charge on that nitrogen and thus, away from the C2 position.

3.3.7 Synthesis and decomposition of 14-OH⁻

1,3-diisopropylbenzimidazolium iodide (**14-I⁻**) was synthesized according to the procedures described by Huynh et al.[111,112] The branched alkyl groups are expected to donate to the ring by induction, thereby stabilizing the ring. The ^{1}H NMR for this compound has the appropriate peaks according to the literature (Figure 57).[112]
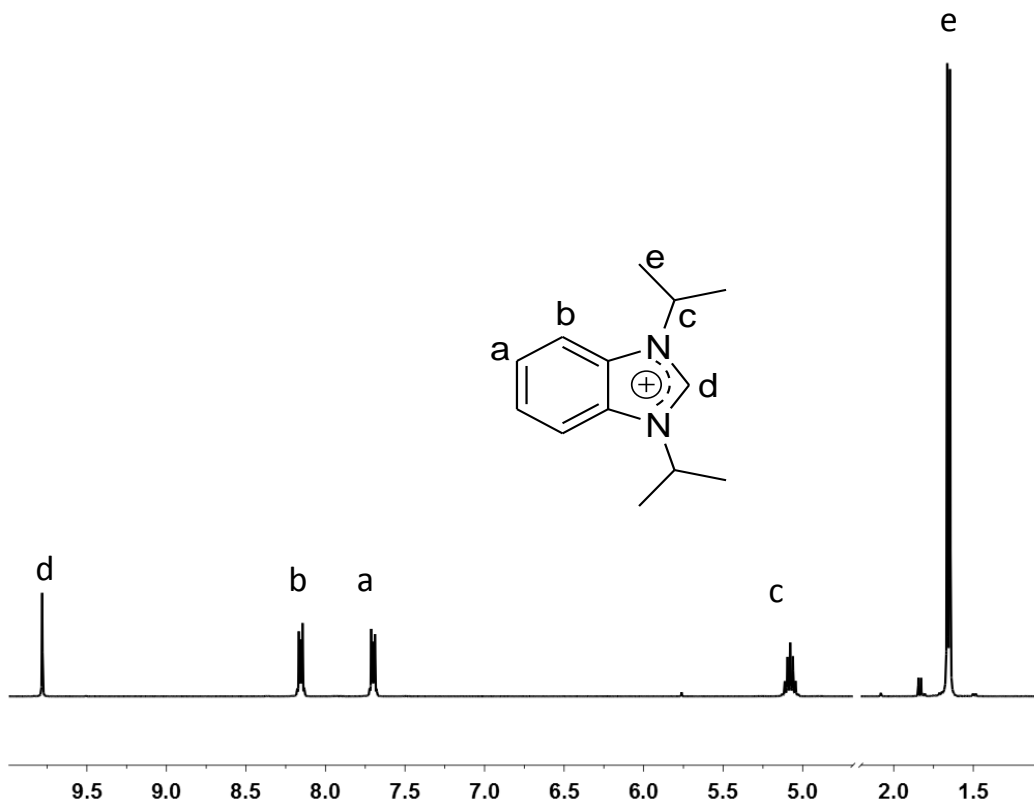
Figure 57: ^{1}H NMR spectrum of compound **14-I⁻**.
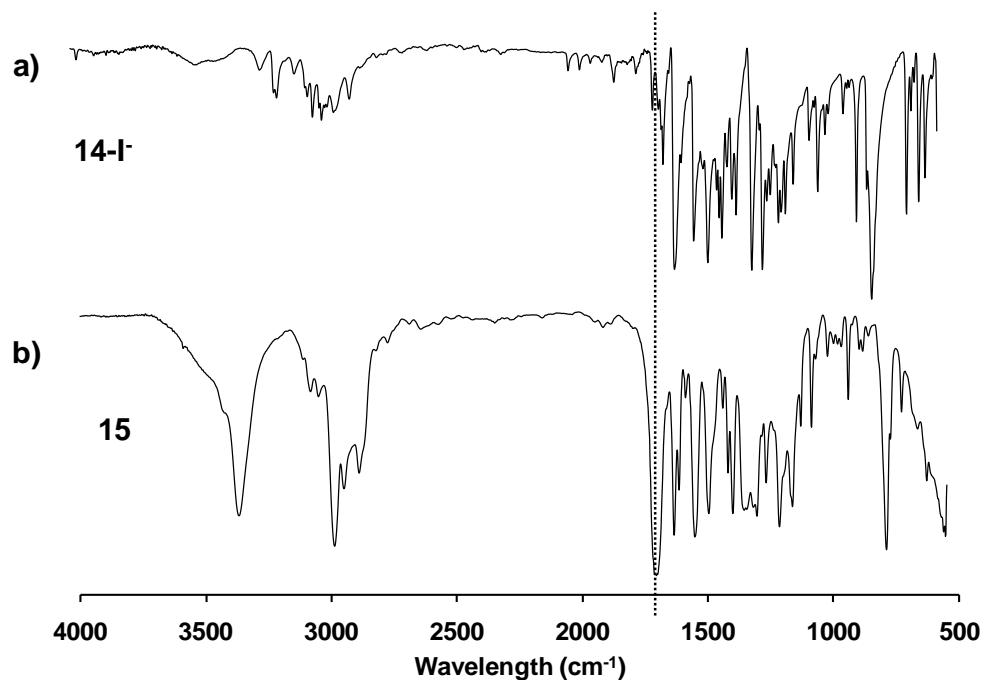
Figure 58: FTIR spectra of a) compound **14-I⁻** and b) the decomposition product (**15**) showing the emergence of a peak at 1690 cm⁻¹.

Upon exposure to concentrated basic solutions, **14** also decomposes. Similarly to the decomposition of **12**, FTIR shows a new absorbance in the range for an amide C=O stretch (1690 cm⁻¹) (Figure 58). In addition, the ^{1}H NMR showed appropriate peaks for the suspected decomposition product, N-*iso*-propyl-N-(2-*iso*-propylamino-phenyl)-formamide, **15** (Figure 59). The addition of the isopropyl groups results in a more even ratio between the E and Z conformations (E:Z = 5:2), likely as a result of their larger size.
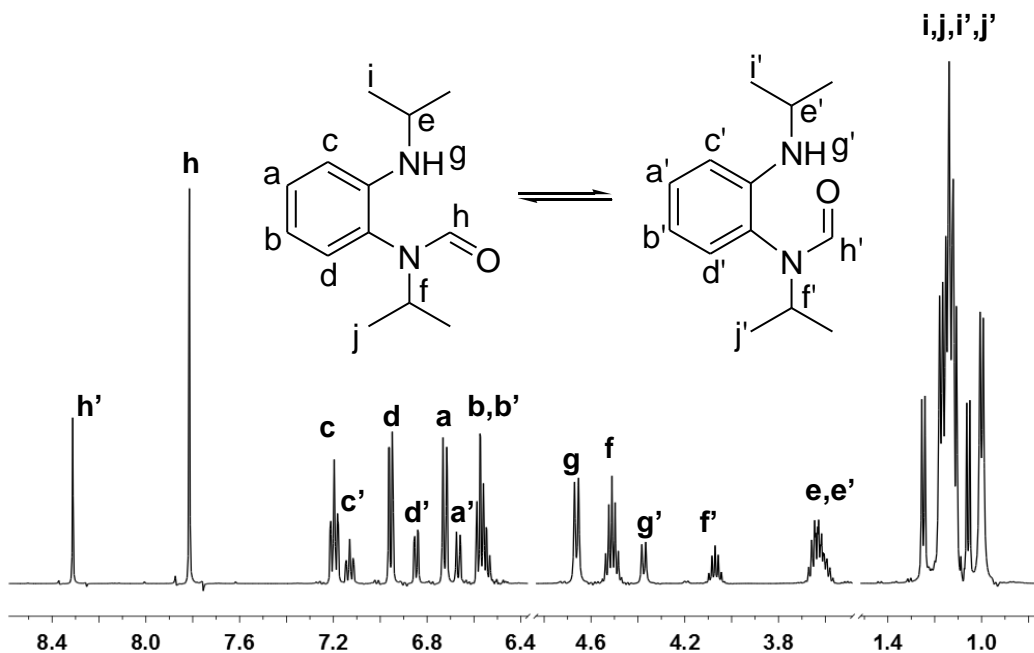
Figure 59: ¹H NMR spectrum of **15**.

The relative rates of decomposition of the small molecule benzimidazoles (**12**, **14**) over time were determined using NMR taken at intervals over 144 hours (Figure 60). The results of this study show significantly less degradation over the course of the experiment for compound **14**. This indicates an increase in stability for the isopropyl substituted benzimidazolium molecule, when exposed to hydroxide containing solutions.
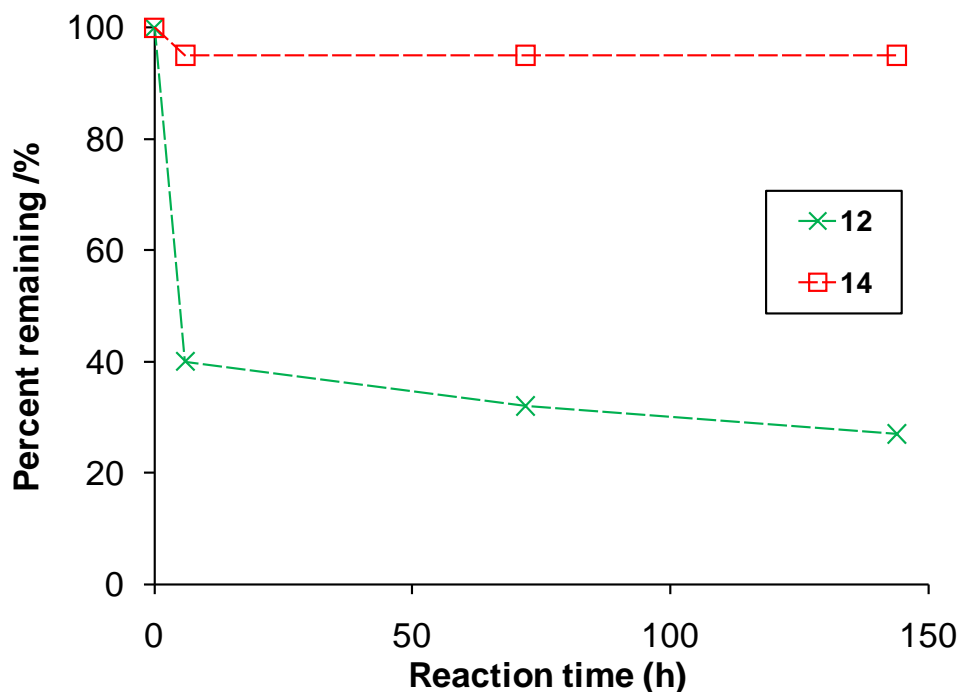
Figure 60: Percent of dialkylbenzimidazolium salt (**12** or **14**) remaining after treatment in KOH solution over a period of 144 hours.

3.4 Conclusion and Future work

In this work, an anion exchange membrane was synthesized by methylating PBI. This material was found to display different physical properties dependent on the anion present. Water content (λ) and anion conductivity (σ'_{X-}) were measured and found lambda values ranging from 2 for the iodide and bromide forms to 167 for the chloride. It is thought that anionic size plays a role in the water content; however no definitive trend could be observed. Conductivity of these membranes was in the range of 3.3 to 8.5 mS/cm, with the chloride and bicarbonate membrane showing the highest values. Attempts to convert this polymer to the hydroxide form were unsuccessful due to the instability of the polymer in alkaline solutions.

Further study on the stability of small molecule analogues led to a greater understanding of the processes involved in the benzimidazolium degradation in this material. It was thought that through stabilization of the positive charge on the nitrogen atoms, the C2 carbon (the site of the OH$^-$ attack) would be less reactive. When this hypothesis was tested, it was found that the ring became more stable when inductively donating groups were added to the nitrogens (i.e., compound **14**).

Future work in this area could be done by investigating other electron-donating groups (e.g., *t*-butyl, etc.) to be used to stabilize the benzimidazolium. This could result in rings that are more stable due to better electron donation. Furthermore, the stabilization method used on the small molecule analogues could be transferred to the polymer. This could produce a polymer that may have greater hydroxide stability.
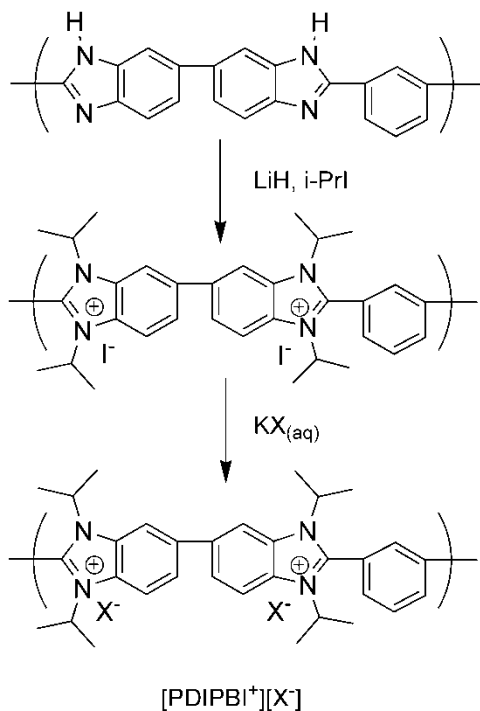
Figure 61:   Scheme showing the synthesis of a diisopropylated PBI.

The mechanism whereby the imidazolium ring is attacked by OH^- relies on the C2 carbon being somewhat positive. In this work, we attempted to reduce the positive charge on C2 by making it more favourable for the charge to reside on the nitrogens and thus, away from C2. An alternative approach could be to add an electron-withdrawing group to the C2 position. This would reduce the stability of the resonance structure containing the positively charged C2 and thus, lessen its prevalence. Adapting this to a polymer system could be done by creating a PBI with a nitro group on the m-phenylene unit (Figure 62).
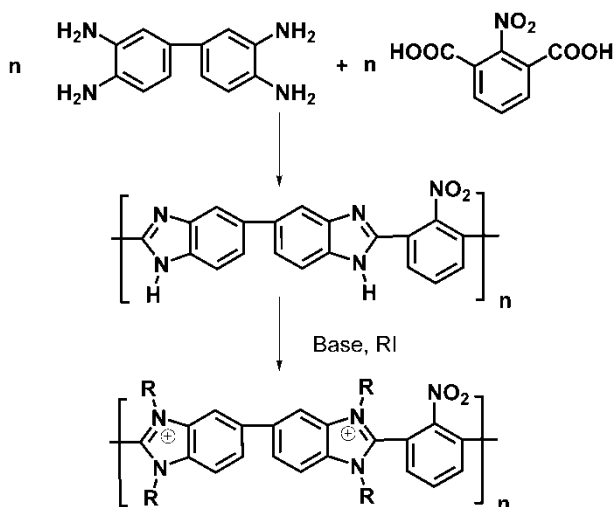
Figure 62: Scheme showing the synthesis of a dialkylated PBI containing nitro groups on the m-phenylene rings.

3.5 Experimental

3.5.1 Synthesis

3.5.1.1 Materials

All chemicals were obtained from Sigma-Aldrich Canada Ltd. unless stated otherwise. 3,3'-diaminobenzidine and isophthalic acid were purified according to literature procedures. Potassium salts were obtained from Caladon Laboratory Chemicals Inc. Deionized H_2O was purified using a Millipore Gradient Milli-Q® water purification system.

3.5.1.2 Synthesis of PBI (**10**)

Polymer **10** was produced according to literature procedures[82] to produce a high molecular weight polymer. 3,3'-Diaminobenzidine **(6)** (10.00 g, 0.582 mmol), isophthalic acid **(8)** (0.0931 g, 0.407 mmol), and poly(phosphoric acid) (PPA) (4 mL) were placed in a 500 mL flask. The flask was placed under vacuum

97

and refilled with Ar. After this process was repeated three times, the contents of the flask were heated to 120 ºC for 48 h and then to 200 ºC for 24 h. The hot solution was poured slowly into Millipore water in order to precipitate the polymer into long fine fibres to maximize surface area. The product (brown solid) wa soaked in a 2 M $K_2CO_{3(aq)}$ solution to neutralize the PPA and washed with Millipore water. The fibres were then powdered by cooling them with liquid N_2 and grinding them with a mortar and pestle. This powder was then washed repeatedly to remove any trace of K_2CO_3 or PPA. The powder was then dried under vacuum. Yield: 17.03 g (90%) of a brown solid.

Polymer **10**: ^{1}H NMR (500 Hz, DMSO-d_6, δ, ppm) (Figure 47): 13.30 (2H, s, H_F), 9.18 (1H, s, H_D), 8.35 (2H, d, 1 Hz, H_A), 8.06 (1H, s, H_F), 7.70 (6H, m, $H_{B,C,E}$). FTIR (DMSO solution cast onto NaCl plate) (Figure 50): 3200 v.br (N-H stretch), 1606 (C=N stretch), 1440 (benzimidazole ring deformation).

3.5.1.3 Synthesis of P(DMBI⁺I⁻) (**11-I⁻**)

11-I⁻ was made by treating **10** with LiH followed by a methylation using iodomethane based on a procedure by Hu et al.[105]

In a 250 mL round bottom flask, **10** (2 g, 6.5 mmol) was dissolved in dry N-methylpyrolidone (NMP) (100 mL). The flask was fitted with a condenser and was put under argon to reduce exposure to moisture. While stirring, the flask was heated to 80 ºC for 2 h until the solid had dissolved and was then allowed to cool to room temperature. Next, LiH (0.3 g, 38 mmol) was added slowly to the stirring solution. The temperature was then increased to 80 ºC and stirred for 15 h. The

remaining LiH solid was removed by centrifuge and the solution was allowed to cool back to room temperature in the round bottom flask. Iodomethane (excess, 9 mL, 144 mmol) was added drop-wise over 15 min to the stirring solution and the temperature was raised to 80 ºC for 6 h. The light brown solid that precipitated was separated by vacuum filtration. The solid was then dissolved in DMSO (60 mL) and another 9 mL of iodomethane was added. The mixture was heated to 80 ºC for 15 h to increase the degree of methylation. The polymer was precipitated in acetone and residual DMSO was removed using Soxlet purification for 16 h.

Polymer **11-I⁻**: ^{1}H NMR (500 Hz, DMSO-d_6, δ, ppm) (Figure 49): 8.84 – 8.26 (10H, aromatic protons, H_{A-E}), 4.23, 4.15 (11.89H, methyl protons $H_{G,H}$). FTIR (DMSO solution cast onto NaCl plate) (Figure 52a): 3060 (aromatic C-H stretch), 1606 (C=N stretch), 1440 (benzimidazole ring deformation).

3.5.1.4 Synthesis of 1,3-dimethylbenzimidazolium iodide (12-I⁻)

12-I⁻ was made by dissolving 1.0 g (8 mmol) benzimidazole in 30 mL acetone. Powdered KOH (2.5 g, 44 mmol) was added to the solution and stirred rapidly. Iodomethane (5 mL, 11 g, 77 mmol) was added dropwise to the stirring solution and the mixture remained stirring at room temperature for 2 days. The solid was filtered and washed with cold acetone and dried under vacuum.

12-I⁻: ^{1}H NMR (500 Hz, DMSO-d_6, δ, ppm) (Figure 53): 9.71 (1H, H_D), 8.03 (2H, m, 3 Hz, H_B), 7.70 (2H, m, 3 Hz, H_A), 4.09 (6H, s, methyl protons, H_C). FTIR (KBr Disk) (Figure 54): 3053 (aromatic C-H stretch) 1577 (C=N stretch), 1444 (benzimidazole ring deformation).

3.5.1.5 Decomposition product of 12-I⁻ in presence of OH⁻ (13)

12-I⁻ (0.5 g, 1.8 mmol) was dissolved in water (2 mL), to this 6 mL of 5 M KOH$_{(aq)}$ was added. The solution was stirred for 24 h and two layers formed. The mixture was extracted with ether (5 mL) and the aqueous layer was separated and dried over MgSO$_4$. The ether was removed by evaporation yielding the decomposition product **13** (clear oil, 0.2 g 1.2 mmol, 70% yield).

13: ^{1}H NMR (500 Hz, DMSO-d$_6$, δ, ppm) (Figure 55): 7.98 (1H, s, H$_H$), 7.21 (1H, m, H$_C$), 6.99 (1H, m, H$_D$), 6.62 (2H, m, H$_{A,B}$), 5.45 (1H, q, 4 Hz, H$_G$), 3.00 (3H, s, H$_E$), 2.70 (3H, d, 4 Hz, H$_F$). FTIR (NaCl disk) (Figure 54): 3355 (N-H stretch secondary amine), 2858 (aldehyde C-H stretch), 1668 (C=O stretch, amide).

3.5.1.6 Synthesis of 1,3-diisopropylbenzimidazolium iodide(14-I⁻)

1.15 g (0.01 mol) of benzimidazole was dissolved in 6 mL of acetonitrile. To this 1.5 g (0.011 mol) of K$_2$CO$_3$ was added and mixture was stirred for 2 h. Next, 3.6 mL (0.036 mol) of 2-iodopropane was added and the mixture refluxed for 24 h. Then an additional 3.6 mL (0.036 mol) of 2-iodopropane was added and refluxed for 72 h. Next, the mixture was dried under vacuum and triturated in 10 mL of dichloromethane. This mixture was filtered through celite and the solid washed with 4 x 10 mL dichloromethane. The filtrate was collected and the solvent was removed under vacuum, producing a light brown solid. This solid was washed thoroughly with ethyl acetate to produce a white powder, **14-I⁻**, in 90% yield.

14-I⁻: ^1H NMR (500 Hz, DMSO-d_6, δ, ppm) (Figure 57): 9.78 (1H, s, H_D), 8.15 (2H, m, H_B), 7.70 (2H, m, H_A), 5.08 (2H, septet, 7 Hz H_C), 1.66 (12H, d, 7 Hz H_E). FTIR (KBr Disk) (Figure 58): 3011 (aromatic C-H stretch), 1552 (C=N stretch).

3.5.1.7 Decomposition product of **14-I⁻** in presence of OH⁻ **(15)**

Reaction conditions adapted from decomposition of **12-I⁻**, reaction time increased from 24 h to 72 h. Yield: clear oil, 20% yield.

15: ^1H NMR (500 MHz, DMSO-d_6, δ, ppm) (Figure 55): 7.81 (1H, s, H), 7.21 (1H, td, 7 Hz, 1 Hz, H), 6.97 (1H, dd, 7 Hz, 1 Hz, H), 6.73 (2H, d, 7Hz, H), 5.58 (1H, td, 7 Hz, 1 Hz, H_G), 4.65 (1H, d, 8 Hz, H), 4.50 (1H, septet, 7 Hz, H), 3.63 (1H, septet, 7 Hz, H), 1.14 (3H, d, 7 Hz, H).

^{13}C NMR (500 MHz, DMSO-d_6, δ, ppm): 163.4 (C_{11}), 146.9 (C_5), 131.9 (C_3), 129.9 (C_4), 123.0 (C_6), 115.3 (C_1), 111.8 (C_2), 51.2 (C_8), 43.5 (C_7), 24-19 ($C_{9,10}$)

FTIR (DMSO cast on NaCl Disk) (Figure 54): 3348 (N-H stretch secondary amine), 2862 (aldehyde C-H stretch), 1668 (C=O stretch, amide).

3.5.2 Characterization Procedures

3.5.2.1 Nuclear Magnetic Resonance (NMR)

^1H and ^{13}C NMR spectra were obtained using a Varian Unity Spectrometer operating at 500 MHz. The compounds were dissolved in DMSO-d_6 at a concentration of ~30 mg/mL.

3.5.2.2 Fourier Transform Infrared Spectroscopy (FTIR)

Polymer films for FTIR analysis were drop-cast from dilute DMSO solution on to a glass slide and dried under vacuum at 80 °C for 2 h. Small molecules were analyzed either by depositing DMSO solutions of the desired compound onto NaCl disks and drying in the oven for 1 h or incorporated into KBr disks. All samples were analyzed using a Bomem® FTLA2000-154 FTIR system.

3.5.2.3 Membrane Preparation

Membranes of **11-I⁻** were cast from DMSO solutions flat bottom petri dishes, heated to 60 ºC for 6 h and dried under vacuum overnight at 50 ºC. The films were removed easily from the petri dishes.

3.5.2.4 Anion Conversion

Films of **11-I⁻** were soaked in solutions of 2 M potassium salts of the desired anion (KX, where X= Cl⁻, Br⁻, NO_3^- or HCO_3^-) for 24 h. The films were then soaked in deionized water for 4 h, refreshing the water frequently. Then the membranes were soaked in deionized water overnight, removed and dried at room temperature.

3.5.2.5 Water mass uptake (WU)/ Water volume uptake (VU)

See Section 2.5.3 for similar procedure.

3.5.2.6 Degree of methylation/dimethylation

The degree of methylation was determined using ^{1}H NMR. The integral of the methyl peaks (Figure 49) was divided by integral of the aromatic peaks as shown in Equation 17.

$$\text{Degree of methylation} = \frac{\text{integral of methyl H} \times 10 \text{ aromatic H per repeat unit}}{\text{integral of aromatic H} \times 12 \text{ methyl H per repeat unit}} \qquad (17)$$

The extent to which the imidazole rings became dimethylated is determined assuming all of the imidazoles are at least monomethylated. Thus the number of dimethylated rings is determined using Equation 18.

$$\text{Degree of dimethylation} = 2(\text{degree of methylation}) - 1 \qquad (18)$$

3.5.2.7 Ion exchange capacity (IEC)

IEC was determined by dividing the number of cationic sites in the polymer by the molecular weight of the polymer as shown in Equation 19. The number of cationic sites is determined using the degree of dimethylation and the number of cationic sites found in fully methylated repeat unit (Equation 20). The IEC varies depending on the weight of the counter ion.

$$\text{IEC} = \frac{\text{\# cationic sites per repeat unit}}{\text{Molecule weight of repeat unit}} \qquad (19)$$

$$\text{\# cationic sites per repeat unit} = (\text{degree of dimethylation}) \times (\text{\# cationic sites in fully methylated unit}) \qquad (20)$$

3.5.2.8 Lambda (λ)

This value represents the average number of H_2O molecules per cationic site in the polymer. These were calculated using water uptake (WU) the molecular weight of water (MW_{water}) and IEC using Equation 21:

$$\lambda = 10 \frac{WU}{(MW_{water})(IEC)} \qquad (21)$$

The multiplier 10 takes into account that WU is a percentage and IEC is in meq·g^{-1}

3.5.2.9 Ion concentration ([X$^-$])

Ion concentrations of the hydrated membranes are determined as shown in Equation 22 using IEC, membrane dry weight (W_{Dry}) and wet volume (V_{Wet}). Results in concentration in mol·L^{-1}, when IEC in meq·g^{-1}, W_{Dry} in g and V_{Wet} in mL.

$$[X^-] = \frac{IEC \times W_{Dry}}{V_{Wet}} \qquad (22)$$

3.5.2.10 Exchange percentage

200 mg films of **11-X$^-$** were repeatedly soaked in 150 mL solutions of 2 M potassium nitrate, replacing the solutions every 8 hours to ensure exchange. The solutions were combined and titrated using the Mohr method. In this, the solutions were titrated with a standardized silver nitrate ($AgNO_3$) solution, using potassium chromate (K_2CrO_4) as the indicator. The end point is reached when all of the X$^-$ leached from the membrane is precipitated as a silver salt (AgX), any additional titrant added reacts with the CrO_4^{2-} resulting in a colour change from yellow to red. The moles of X$^-$ found through titration (moles X$^-_{titr}$) is determined from the volume of $AgNO_3$ titrant (V_{titr}) added and its concentration ([$AgNO_3$] according to Equation 23.

$$\text{moles } X^-_{titr} = V_{titr} \times [AgNO_3] \qquad (23)$$

The moles of X$^-$ expected (moles X$^-_{exp}$) in the solution are determined by the IEC of the membrane titrated and the mass used (Equation 24). From this and the moles of X$^-$ titrated, the anion exchange percent can be calculated (Equation 25).

$$\text{moles X}^-_{exp} = \text{IEC of the membrane} \times \text{mass of the membrane} \qquad (24)$$

$$\text{Anion exchange \%} = \frac{\text{moles X}^-_{titr}}{\text{moles X}^-_{exp}} \times 100\% \qquad (25)$$

3.5.2.11 Anion conductivity

Anion conductivity was measured by AC impedance spectroscopy with a Solartron 1260 frequency response analyzer (FRA) employing a transverse two-electrode configuration. Membrane samples were soaked in deionized water overnight, cut to required dimensions (0.5 cm $\times$ 1.0 cm), and laid across two Pt electrodes (1 cm $\times$ 1.5 cm) 0.5 cm apart, fixed on a PTFE block. A second PTFE block was placed on top and two clamps were used to hold the assembly together during measurement. Both PTFE blocks were vented with rectangular cut-aways to allow for membrane hydration. Membranes were kept hydrated by periodically wetting them with deionized water.

Ionic resistance was extracted from impedance data and fitting was performed by non-linear least squares regression analysis to a standard Randles equivalent circuit model. The data from a sample measurement is shown in Figure 63. The ionic resistance was used to calculate anion conductivity, σ_{X^-}, according to Equation 26:

$$\sigma_{X^-} = \frac{L}{R_m A} \qquad (26)$$

where L is the spacing between the Pt electrodes (0.5 cm), A is the cross sectional area of the membrane (w × h), and R_m is the ionic resistance of the membrane.
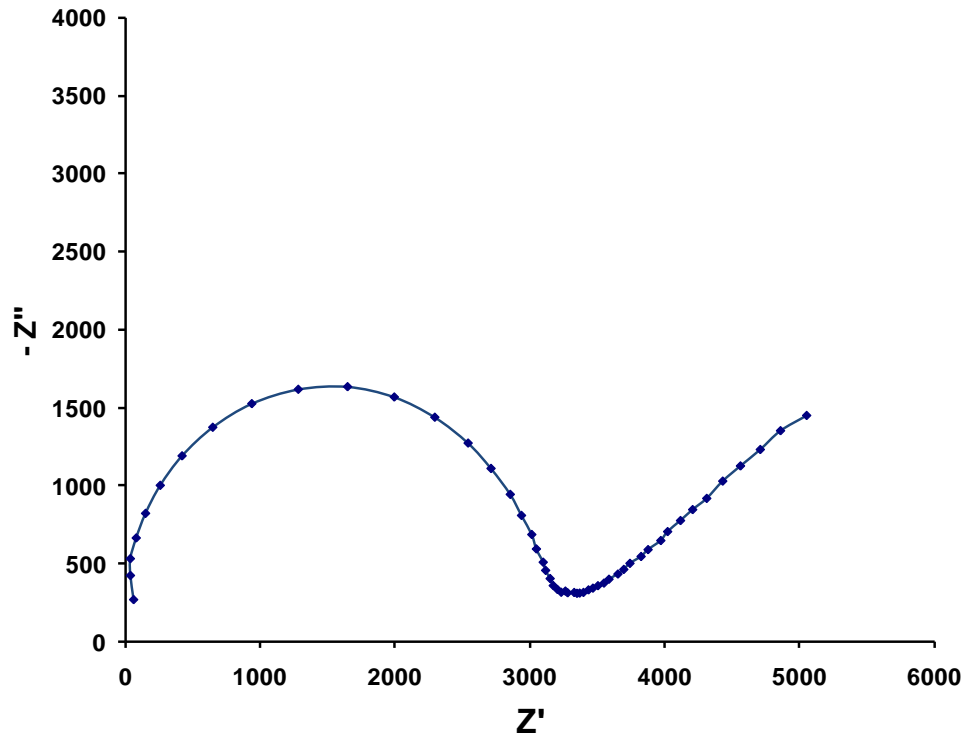

Figure 63: **Typical Nyquist plot for AC impedance spectroscopy measurement of 11-I⁻**

3.5.2.12 Anion Mobility (μ'_{X^-})

The effective anion mobility was calculated using the anion conductivity (σ_{X^-}) and anion concentration ([X⁻]) from Equation 27:

$$\mu'_{X^-} = \frac{\sigma_{X^-}}{F[X^-]} \qquad (27)$$

where F is Faraday's constant.

3.5.2.13 Measurement of decomposition over time for small molecule analogues

Example given for decomposition over time procedure for **12-X⁻**, a similar procedure was followed for the decomposition **14-X⁻**. A solution of 50 mg of **12-I⁻** was prepared using 1.000 mL of D_2O. 0.500 mL of d_6-DMSO was added to this and mixed thoroughly. A 0.500 ml sample was taken and analyzed using ^1H NMR to collect an initial (t = 0) spectrum. To the remaining solution, 0.400 ml of 5 M KOH solution (also in D_2O) was added. After thorough mixing, this solution was deposited into NMR tubes and the samples were analyzed periodically by ^1H NMR to determine the percentage of **12-X⁻** remaining.

The amount of **12-X⁻** remaining was determined from the aromatic peaks in the ^1H NMR. By dividing the peaks found for the aromatic protons in **12-I⁻** (multiplets at δ 7.74 ppm and 7.58 ppm) with the entire aromatic region (δ 8.00 – 6.50 ppm), the percentage of **12-X⁻** remaining was found.

REFERENCES

(1)   Grove, W. Philosophical Magazine and Journal of Science 1839; 14: 127-130.

(2)   Grove, W. Philosophical Magazine and Journal of Science 1842; 21: 417-420.

(3)   Whittingham, M. S.; Savinell, R. F.; Zawodzinski, T. Chemical Reviews 2004; 104(10): 4243-4244.

(4)   von Helmolt, R.; Eberle, U. Journal of Power Sources 2007; 165(2): 833-843.

(5)   Multiyear Program Plan FreedomCAR and Vehicle Technologies:U.S. Department of Energy, Office of Energy Efficiency and Renewable Energy, 2004.

(6)   Carle, G.; Axhausen, K. W.; Wokaun, A.; Keller, P. Transport Reviews 2005; 25(6): 739-760.

(7)   Cleghorn, S. J. C.; Ren, X.; Springer, T. E.; Wilson, M. S.; Zawodzinski, C.; Zawodzinski, T. A.; Gottesfeld, S. International Journal of Hydrogen Energy 1997; 22(12): 1137-1144.

(8)   Burke, K. A. Fuel Cells For Space Science Applications Cleveland, Ohio:National Aeronautics and Space Administration, Glenn Research Center, 2002.

(9)   Carrette, L.; Friedrich, K. A.; Stimming, U. ChemPhysChem 2000; 1(4): 162-193.

(10)   Perry, M. L.; Fuller, T. F. Journal of the Electrochemical Society 2002; 149(7): S59-S67.

(11)   The State of Hydrogen and Fuel Cell Commercialization and Technical Development:U.S Department of Energy, Hydrogen and Fuel Cell Technical Advisory Committee, 2009.

(12)   National Hydrogen Energy Roadmap:United States Department of Energy, Energy Efficiency and Renewable Energy, 2002.

(13)   Carrette, L.; Friedrich, K. A.; Stimming, U. Fuel Cells 2001; 1(1): 5-39.

(14)   Teagan, W. P.; Bentley, J.; Barnett, B. Journal of Power Sources 1998; 71(1-2): 80-85.

(15)   Steele, B. C. H.; Heinzel, A. Nature 2001; 414(6861): 345-352.

(16)   Smitha, B.; Sridhar, S.; Khan, A. A. Journal of Membrane Science 2005; 259(1-2): 10-26.

(17)   Starz, K. A.; Auer, E.; Lehmann, T.; Zuber, R. Journal of Power Sources 1999; 84(2): 167-172.

(18)   Hickner, M. A.; Ghassemi, H.; Kim, Y. S.; Einsla, B. R.; McGrath, J. E. Chemical Reviews 2004; 104(10): 4587-4611.

(19)   Rikukawa, M.; Sanui, K. Progress in Polymer Science 2000; 25(10): 1463-1502.

(20)   Hsueh, K. L.; Chin, D. T.; Srinivasan, S. Journal of Electroanalytical Chemistry 1983; 153(1-2): 79-95.

(21)   Damjanovic, A.; Brusic, V. Electrochimica Acta 1967; 12(6): 615-628.

(22)   Damjanovic, A.; Dey, A.; Bockris, J. O. M. Electrochimica Acta 1966; 11(7): 791-814.

(23)   Damjanovic, A. Journal of The Electrochemical Society 1991; 138(8): 2315-2320.

(24)   Gebel, G. Polymer 2000; 41(15): 5829-5838.

(25)   Kreuer, K. D.; Paddison, S. J.; Spohr, E.; Schuster, M. Chemical Reviews 2004; 104(10): 4637-4678.

(26)   Yang, Y.; Holdcroft, S. Fuel Cells 2005; 5(2): 171-186.

(27)   Wang, L.; Husar, A.; Zhou, T. H.; Liu, H. T. International Journal of Hydrogen Energy 2003; 28(11): 1263-1272.

(28)   Agmon, N. Chem. Phys. Lett. 1995; 244(5-6): 456-462.

(29)   Hickner, M. A.; Pivovar, B. S. Fuel Cells 2005; 5(2): 213-229.

(30)   Yu, J.; Yi, B.; Xing, D.; Liu, F.; Shao, Z.; Fu, Y.; Zhang, H. Physical Chemistry Chemical Physics 2003; 5(3): 611-615.

(31)   Inaba, M.; Kinumoto, T.; Kiriake, M.; Umebayashi, R.; Tasaka, A.; Ogumi, Z. Electrochimica Acta 2006; 51(26): 5746-5753.

(32)   Curtin, D. E.; Lousenberg, R. D.; Henry, T. J.; Tangeman, P. C.; Tisack, M. E. Journal of Power Sources 2004; 131: 41-48.

(33)   Mauritz, K. A.; Moore, R. B. Chemical Reviews 2004; 104(10): 4535-4585.

(34)   Ralph, T. R.; Hards, G. A.; Keating, J. E.; Campbell, S. A.; Wilkinson, D. P.; Davis, M.; StPierre, J.; Johnson, M. C. Journal of the Electrochemical Society 1997; 144(11): 3845-3857.

(35)   Safe Handling and Use of Perfluorsulfonic Acid Products:DuPont Company, 2005.

(36)   Zhang, J. L.; Xie, Z.; Zhang, J. J.; Tanga, Y. H.; Song, C. J.; Navessin, T.; Shi, Z. Q.; Song, D. T.; Wang, H. J.; Wilkinson, D. P.; Liu, Z. S.; Holdcroft, S. Journal of Power Sources 2006; 160(2): 872-891.

(37)   Kerres, J. A. Journal of Membrane Science 2001; 185(1): 3-27.

(38)   Kreuer, K. D. Journal of Membrane Science 2001; 185(1): 29-39.

(39)   Yang, Y.; Siu, A.; Peckham, T.; Holdcroft, S. Advances in Polymer Science 2008; 215: 55-126.

(40)   Zhang, H. W.; Zhou, Z. T. Progress in Chemistry 2008; 20(4): 602-619.

(41)   Hubner, G.; Roduner, E. Journal of Materials Chemistry 1999; 9(2): 409-418.

(42)   Wang, C.; Mao, Z. Q.; Xu, J. M.; Xie, X. F. Key Engineering Materials 2003; 247: 397-400.

(43)   Zhang, Y.; Zhang, H. M.; Zhu, X. B.; Bi, C. Journal of Physical Chemistry B 2007; 111(23): 6391-6399.

(44)   Ye, H.; Huang, J.; Xu, J. J.; Kodiweera, N.; Jayakody, J. R. P.; Greenbaum, S. G. Journal of Power Sources 2008; 178(2): 651-660.

(45)   He, R. H.; Li, Q. F.; Jensen, J. O.; Bjerrum, N. J. Journal of Polymer Science Part a-Polymer Chemistry 2007; 45(14): 2989-2997.

(46)   Ma, Y. L.; Wainright, J. S.; Litt, M. H.; Savinell, R. F. Journal of The Electrochemical Society 2004; 151(1): A8-A16.

(47)   Lobato, J.; Canizares, P.; Rodrigo, M. A.; Linares, J. J.; Aguilar, J. A. Journal of Membrane Science 2007; 306(1-2): 47-55.

(48)   Steininger, H.; Schuster, M.; Kreuer, K. D.; Kaltbeitzel, A.; Bingol, B.; Meyer, W. H.; Schauff, S.; Brunklaus, G.; Maier, J.; Spiess, H. W. Physical Chemistry Chemical Physics 2007; 9(15): 1764-1773.

(49)   Zhang, J. L.; Tang, Y. H.; Song, C. J.; Zhang, J. J. Journal of Power Sources 2007; 172: 163-171.

(50)   Wainright, J. S.; Wang, J. T.; Weng, D.; Savinell, R. F.; Litt, M.; ECS: 1995; Vol. 142, p L121-L123.

(51)   Smitha, B.; Sridhar, S.; Khan, A. A. Journal of Membrane Science 2003; 225(1-2): 63-76.

(52)   Muthu, L.; Choudhary, V.; Varma, I. K. Journal of Materials Science 2005; 40(3): 629-636.

(53)   Lufrano, F.; Gatto, I.; Staiti, P.; Antonucci, V.; Passalacqua, E. Solid State Ionics 2001; 145(1-4): 47-51.

(54)   Schuster, M.; de Araujo, C. C.; Atanasov, V.; Andersen, H. T.; Kreuer, K. D.; Maier, J. Macromolecules 2009; 42(8): 3129-3137.

(55)   Eikerling, M.; Kornyshev, A. A. Journal of Electroanalytical Chemistry 2002; 528(1-2): 196-197.

(56)   Eikerling, M.; Kornyshev, A. A.; Kucernak, A. R. Physics Today 2006; 59(10): 38-44.

(57)   Yin, Y.; Fang, J. H.; Watari, T.; Tanaka, K.; Kita, H.; Okamoto, K. Journal of Materials Chemistry 2004; 14(6): 1062-1070.

(58)   Peckham, T. J.; Schmeisser, J.; Rodgers, M.; Holdcroft, S. Journal of Materials Chemistry 2007; 17(30): 3255-3268.

(59)   Chen, W. F.; Kuo, P. L. Macromolecules 2007; 40(6): 1987-1994.

(60)   Mikhailenko, S. D.; Robertson, G. P.; Guiver, M. D.; Kaliaguine, S. Journal of Membrane Science 2006; 285(1-2): 306-316.

(61)   Mikhailenko, S. U. D.; Wang, K. P.; Kaliaguine, S.; Xing, P. X.; Robertson, G. P.; Guiver, M. D. Journal of Membrane Science 2004; 233(1-2): 93-99.

(62)   Kerres, J.; Cui, W.; Junginger, M. Journal of Membrane Science 1998; 139(2): 227-241.

(63)   Zhang, W.; Dai, G.; Kerres, J. Acta Polymerica Sinica 1998(5): 608-611.

(64)   Gasa, J. V.; Weiss, R. A.; Shaw, M. T. Journal of Membrane Science 2007; 304(1-2): 173-180.

(65)   Tang, C. M.; Zhang, W.; Kerres, J. Journal of New Materials for Electrochemical Systems 2004; 7(4): 287-298.

(66)   Hong, Y. T.; Lee, C. H.; Park, H. N. S.; Min, K. A.; Kim, H. J.; Nam, S. Y.; Lee, Y. M. Journal of Power Sources 2008; 175(2): 724-731.

(67)   Wang, J. L.; Song, Y. L.; Zhang, C.; Ye, Z. B.; Liu, H.; Lee, M. H.; Wang, D. H.; Ji, J. B. Macromolecular Chemistry and Physics 2008; 209(14): 1495-1502.
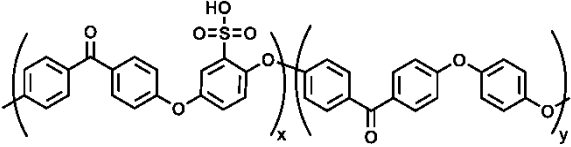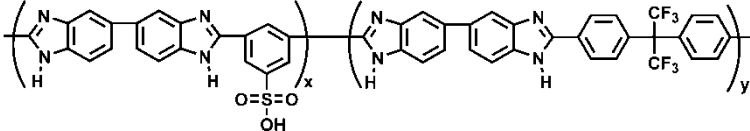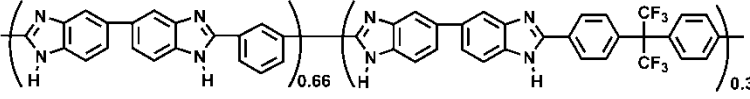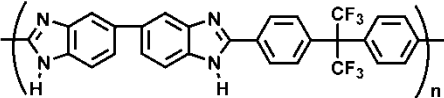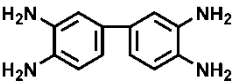
(68) Schonberger, F.; Hein, M.; Kerres, J. Solid State Ionics 2007; 178(7-10): 547-554.

(69) Xu, H. J.; Chen, K. C.; Guo, X. X.; Fang, J. H.; Yin, J. Polymer 2007; 48: 5556-5564.

(70) Kerres, J.; Ullrich, A.; Meier, F.; Haring, T. Solid State Ionics 1999; 125(1-4): 243-249.

(71) Kerres, J. A. Fuel Cells 2005; 5(2): 230-247.

(72) Kerres, J.; Cui, W.; Patent, U. S., Ed. USA, 2001.

(73) Hasiotis, C.; Qingfend, L.; Deimede, V.; Kallitsis, J. K.; Kontoyannis, C. G.; Bjerrum, N. J. Journal of the Electrochemical Society 2001; 148(5): A513-A519.

(74) Zhang, H. Q.; Li, X. F.; Zhao, C. J.; Fu, T. Z.; Shi, Y. H.; Na, H. Journal of Membrane Science 2008; 308(1-2): 66-74.

(75) Cui, W.; Kerres, J.; Eigenberger, G. Separation and Purification Technology 1998; 14(1-3): 145-154.

(76) Lee, J. K.; Kerres, J. Journal of Membrane Science 2007; 294: 75-83.

(77) Rogers, M.; Long, T. Synthetic methods in step-growth polymers:John Wiley & Sons, Inc., 2003.

(78) Makowski, H. S.; Lundberg, R. D.; Singhal, G. H.; Patent, U. S., Ed. USA, 1975.

(79) Wang, F.; Hickner, M.; Kim, Y. S.; Zawodzinski, T. A.; McGrath, J. E. Journal of Membrane Science 2002; 197(1-2): 231-242.

(80) Guiver, M. D.; Robertson, G. P.; Foley, S. Macromolecules 1995; 28(23): 7612-7621.

(81) Robertson, G. P.; Guiver, M. D.; Bilodeau, F.; Yoshikawa, M. Journal of Polymer Science Part a-Polymer Chemistry 2003; 41(9): 1316-1329.

(82) Iwakura, Y.; Uno, K.; Chau, N. Die Makromolekulare Chemie 1975; 176(1): 23-36.

(83) Peron, J.; Ng, F.; Ruiz, E.; Jones, D.; Roziere, J. ECS Transactions 2008; 16(2): 1415-1421.

(84) Ueda, M.; Sato, M.; Mochizuki, A. Macromolecules 1985; 18(12): 2723-2726.

(85) Tully, P. S. Kirk-Othmer Encyclopedia of Chemical Technology New York:John Wiley & Sons, Inc., 1996.

(86) Patai, S.; Rappoport, Z.; Stirling, C. J. M. The Chemistry of Sulphones and Sulphoxides New York:John Wiley & Sons, Inc, 1988.

(87) Jerez, G.; Kaufman, G.; Prystai, M.; Schenkeveld, S.; Donkor, K. K. Journal of Separation Science 2009; 32(7): 1087-1095.

(88) Wainright, J. S.; Wang, J. T.; Weng, D.; Savinell, R. F.; Litt, M. J. Electrochem. Soc. 1995; 142(7): L121-L123.

(89) Blachot, J. F.; Diat, O.; Putaux, J.-L.; Rollet, A.-L.; Rubatat, L.; Vallois, C.; Müller, M.; Gebel, G. Journal of Membrane Science 2003; 214(1): 31-42.

(90) Brown, T. N.; Mora-Diez, N. The Journal of Physical Chemistry B 2006; 110(18): 9270-9279.

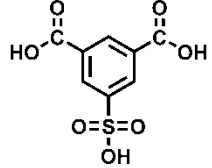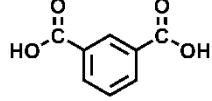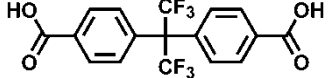(91) Huang, R. Y. M.; Shao, P. H.; Burns, C. M.; Feng, X. Journal of Applied Polymer Science 2001; 82(11): 2651-2660.

(92)   Kojima, T. J. Polym. Sci. Part B: Polym. Phys. 1980**;** 18(8): 1791-1800.
(93)   Xu, T. Journal of Membrane Science 2005**;** 263(1-2): 1-29.
(94)   Agmon, N. Chem. Phys. Lett. 2000**;** 319(3-4): 247-252.
(95)   Sadrzadeh, M.; Razmi, A.; Mohammadi, T. Sep. Purif. Technol. 2007**;** 54(2): 147-156.
(96)   Varcoe, J. R.; Slade, R. C. T.; Yee, E. L. H.; Poynton, S. D.; Driscoll, D. J.; Apperley, D. C. Chem. Mat. 2007**;** 19(10): 2686-2693.
(97)   Hibbs, M. R.; Fujimoto, C. H.; Cornelius, C. J. Macromolecules 2009**;** 42(21): 8316-8321.
(98)   Varcoe, J. R.; Slade, R. C. T. Fuel Cells 2005**;** 5(2): 187-200.
(99)   Wang, G.; Weng, Y.; Chu, D.; Xie, D.; Chen, R. Journal of Membrane Science 2009**;** 326(1): 4-8.
(100) Vega, J. A.; Chartier, C.; Mustain, W. E. Journal of Power Sources**;** 195(21): 7176-7180.
(101) Bauer, B.; Strathmann, H.; Effenberger, F. Desalination 1990**;** 79(2-3): 125-144.
(102) Komkova, E. N.; Stamatialis, D. F.; Strathmann, H.; Wessling, M. Journal of Membrane Science 2004**;** 244(1-2): 25-34.
(103) Sata, T.; Tsujimoto, M.; Yamaguchi, T.; Matsusaki, K. Journal of Membrane Science 1996**;** 112(2): 161-170.
(104) Wang, J.; Li, S.; Zhang, S. Macromolecules 2010**;** 43(8): 3890-3896.
(105) Hu, M.; Pearce, E. M.; Kwei, T. K. Journal of Polymer Science Part a-Polymer Chemistry 1993**;** 31(2): 553-561.
(106) Atkins, P. W. Physical Chemistry, 4th ed. New York, 1990.
(107) Schwarz, D. E.; Cameron, T. M.; Hay, P. J.; Scott, B. L.; Tumas, W.; Thorn, D. L. Chem. Comm. 2005(47): 5919-5921.
(108) Hofmann, K. Imidazole and Its Derivatives London:Interscience, 1953.
(109) Bai, Y.-j.; Li, C.-y.; Sun, W.; Zhao, G.-f.; Shi, Z. Huaxue Shiji 2008**;** 30(6): 409-411.
(110) Bostai, B.; Novak, Z.; Benyei, A. C.; Kotschy, A. Organic Letters 2007**;** 9(17): 3437-3439.
(111) Huynh, H. V.; Han, Y.; Ho, J. H. H.; Tan, G. K. Organometallics 2006**;** 25(13): 3267-3274.
(112) Han, Y.; Huynh, H. V.; Koh, L. L. Journal of Organometallic Chemistry 2007**;** 692(17): 3606-3613.
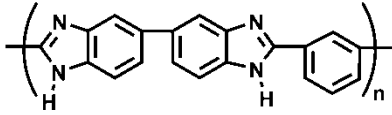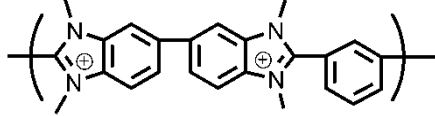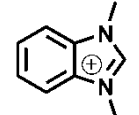
APPENDIX
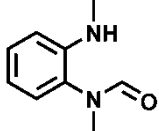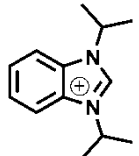
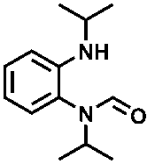**Table A1:   Identification of numbered compounds used Chapter 2 of this work.**

Number	Name	Structure
2	Sulfonated poly(ether ether ketone) (SPEEK)	
3	Sulfonated polybenzimidazole[a] (SuPBI)	
4	Angled non-sulfonated polybenzimidazole [a]	
5	Linear non-sulfonated polybenzimidazole [a]	
6	3,3'-Diaminobenzidine	

Number	Name	Structure
7	5-Sulfoisophthalic acid	
8	Isophthalic acid	
9	2,2-bis(4-carboxyphenyl)-hexafluoropropane	

[a] The term polybenzimidazole and its abbreviation PBI is used to refer to both: a class of polymers containing repeating benzimidazole units, or the polymer, poly(2,2'-(m-phenylene)-5,5'-dibenzimidazole)).

Table A2:   Identification of numbered compounds used in Chapter 3 of this work.

Number	Name	Structure
10	Polybenzimidazole [a]	
11	Poly(dimethylbenzimidazolium)	
12	1,3-Dimethylbenzimidazolium	
13	N-Methyl-N-(2-methylamino-phenyl)formamide	
14	1,3-Diisopropylbenzimidazolium	

Number	Name	Structure
15	N-isopropyl-N-(2-isopropylamino-phenyl)formamide	

[a] The term polybenzimidazole and its abbreviation PBI is used to refer to both: the class of polymers containing repeating benzimidazole

units, or the polymer, poly(2,2'-(m-phenylene)-5,5'-dibenzimidazole))